OPEN ACCESS Freely available online

PLoS one

Wnt4 and LAP2alpha as Pacemakers of Thymic Epithelial Senescence

Krisztian Kvell[1], Zoltan Varecza[1], Domokos Bartis[1], Sebastian Hesse[1], Sonia Parnell[2], Graham Anderson[2], Eric J. Jenkinson[2], Judit E. Pongracz[1,2]*

1 Department of Medical Biotechnology, Institute for Immunology and Biotechnology, University of Pecs, Pecs, Hungary, **2** Division of Immunity and Infection, Department of Anatomy, Institute for Biomedical Research, University of Birmingham, Birmingham, United Kingdom

Abstract

Age-associated thymic involution has considerable physiological impact by inhibiting *de novo* T-cell selection. This impaired T-cell production leads to weakened immune responses. Yet the molecular mechanisms of thymic stromal adipose involution are not clear. Age-related alterations also occur in the murine thymus providing an excellent model system. In the present work structural and molecular changes of the murine thymic stroma were investigated during aging. We show that thymic epithelial senescence correlates with significant destruction of epithelial network followed by adipose involution. We also show in purified thymic epithelial cells the age-related down-regulation of Wnt4 (and subsequently FoxN1), and the prominent increase in LAP2α expression. These senescence-related changes of gene expression are strikingly similar to those observed during mesenchymal to pre-adipocyte differentiation of fibroblast cells suggesting similar molecular background in epithelial cells. For molecular level proof-of-principle stable LAP2α and Wnt4-over-expressing thymic epithelial cell lines were established. LAP2α over-expression provoked a surge of PPARγ expression, a transcription factor expressed in pre-adipocytes. In contrast, additional Wnt4 decreased the mRNA level of ADRP, a target gene of PPARγ. Murine embryonic thymic lobes have also been transfected with LAP2α- or Wnt4-encoding lentiviral vectors. As expected LAP2α over-expression increased, while additional Wnt4 secretion suppressed PPARγ expression. Based on these pioneer experiments we propose that decreased Wnt activity and increased LAP2α expression provide the molecular basis during thymic senescence. We suggest that these molecular changes trigger thymic epithelial senescence accompanied by adipose involution. This process may either occur directly where epithelium can trans-differentiate into pre-adipocytes; or indirectly where first epithelial to mesenchymal transition (EMT) occurs followed by subsequent pre-adipocyte differentiation. The latter version fits better with literature data and is supported by the observed histological and molecular level changes.

Citation: Kvell K, Varecza Z, Bartis D, Hesse S, Parnell S, et al. (2010) Wnt4 and LAP2alpha as Pacemakers of Thymic Epithelial Senescence. PLoS ONE 5(5): e10701. doi:10.1371/journal.pone.0010701

Editor: Immo A. Hansen, New Mexico State University, United States of America

Received February 4, 2010; **Accepted** April 27, 2010; **Published** May 18, 2010

Copyright: © 2010 Kvell et al. This is an open-access article distributed under the terms of the Creative Commons Attribution License, which permits unrestricted use, distribution, and reproduction in any medium, provided the original author and source are credited.

Funding: Research was supported by the following grants: The Wellcome Trust grant No.: 079415 (grant-holders: J.E.P., G.A. and E.J.J.), 'Science Please' Research Team on Innovation grant No.: SROP-4.2.2/08/1/2008-0011 (grant holder: J.E.P.) and OTKA (Hungarian Scientific Research Fund) type: PD (post-doctoral) grant No.: 78310 (grant-holder: K.K.). The funders had no role in study design, data collection and analysis, decision to publish, or preparation of the manuscript.

Competing Interests: The authors have declared that no competing interests exist.

* E-mail: judit.e.pongracz@aok.pte.hu

Introduction

Thymic senescence

Thymic senescence begins early, around late puberty. This process is called adipose involution, as the thymus is invaded by adipose tissue [1]. Due to decrease in thymic epithelial tissue mass, the thymus can no longer support the same output of T-cell production [2]. Therefore peripheral blood T lymphocyte composition exhibits the dominance of memory T lymphocytes resulting in impaired responses towards novel, particularly viral infections [3,4,5]. Since the thymic epithelium has a key role in deleting auto-reactive T-cell clones, functional impairment increases the chances of developing auto-immune disease [6]. If we were able to slow down or even stop the loss of thymic epithelium the elderly would have a better chance to address late-onset autoimmune diseases and viral infections. However, despite studies of thymic senescence, the molecular mechanism of thymic aging remains elusive.

Signaling pathways of thymic epithelial cell development and maintenance

Understanding signaling mechanisms that regulate tissue development and maintenance of thymic epithelial cells might reveal the process of adipose involution. Certainly, maintenance and functional integrity of the thymic stroma requires stimuli through Notch, BMP, and Wnt signaling pathways [7,8,9,10,11]. Undoubtedly, the Wnt family of secreted glycoproteins is one of the best analyzed among the required ligands [12]. Most members of the nineteen known Wnt glycoproteins have been implicated in both the development of embryonic thymus and the maintenance of adult thymic epithelium [13]. In the thymus, Wnt ligands originate primarily from thymic epithelial cells and activate a highly complex signaling network via ten G-protein dependent receptors called Frizzleds (Fz), and their co-receptors of low-density lipoprotein receptor-related proteins 5/6 called LRP5/6 [14,15]. The actual constellation of ligands, receptors, co-receptors and further regulatory molecules define Wnt-mediated effects.

Recent studies have highlighted Wnt4 as responsible for the direct up-regulation of FoxN1, a key transcription factor responsible for the differentiation of thymic epithelial cells and the subsequent maintenance of thymic epithelial identity [13]. Interestingly, the Wnt/β-catenin pathway is known to efficiently block the adipocyte differentiation program in mesenchymal elements like fibroblasts [16,17,18,19].

Trans-differentiation of fibroblasts into adipocytes

Studies with fibroblast cells have also revealed that fibroblast to pre-adipocyte transformation is strongly connected to LAP2α, the member of the LAP2 protein family [17]. To date there are 7 classified intranuclear LAP2 polypeptides marked by the Greek alphabet. They are all splice variants of the same LAP2 gene previously called thymopoietin. While most splice variants associate with the nuclear envelope, LAP2α is involved in several nucleoplasmic activities including cell-cycle control and differentiation [20,21]. LAP2α is synthesized in the cytoplasm and is then transported into the nucleus by a PKC-dependent mechanism [22]. The mere over-expression of LAP2α in fibroblasts is known to directly up-regulate PPARγ expression, an acknowledged marker and key transcription factor of pre-adipocyte differentiation [17]. In pre-adipocytes PPARγ expression is followed by an increase of ADRP expression (adipose differentiation-related protein) a known direct target gene of PPARγ. Although LAP2α over-expression alone initiates pre-adipocyte differentiation in fibroblasts, it is not sufficient to complete the adipocyte differentiation program in the absence of additional stimuli [17].

Results and Discussion

Disintegration of epithelial network

Senescence exhibits characteristic histological changes in both the human and mouse thymus [1,23]. In order to demonstrate this process the thymic lobes of 1 month and 1 year old BALB/c mice were analyzed (see Figures 1A and 1B). In young adult mice, histology revealed strict segregation of epithelial cell compartments by staining for medullary ($EpCAM1^{++}$, $Ly51^{-}$) and cortical ($EpCAM1^{+}$, $Ly51^{++}$) epithelial cellular subsets (Figure 1A). This shows high level of morphological integrity just preceding puberty/early adulthood. However, the highly organized structure disintegrates and becomes chaotic by the age of 1 year (Figure 1B). By this age the previously shown strict cortico-medullary delineation becomes disintegrated, degenerative vacuoles appear surrounded by areas showing strong co-staining with both epithelial markers. There are also other large cellular areas that lack staining with either epithelial marker, a pattern completely absent at the young adult age.

Staining of extracellular matrix components of fibroblast origin ($ER\text{-}TR7^{++}$) was also performed on cryostate thymic sections of 2

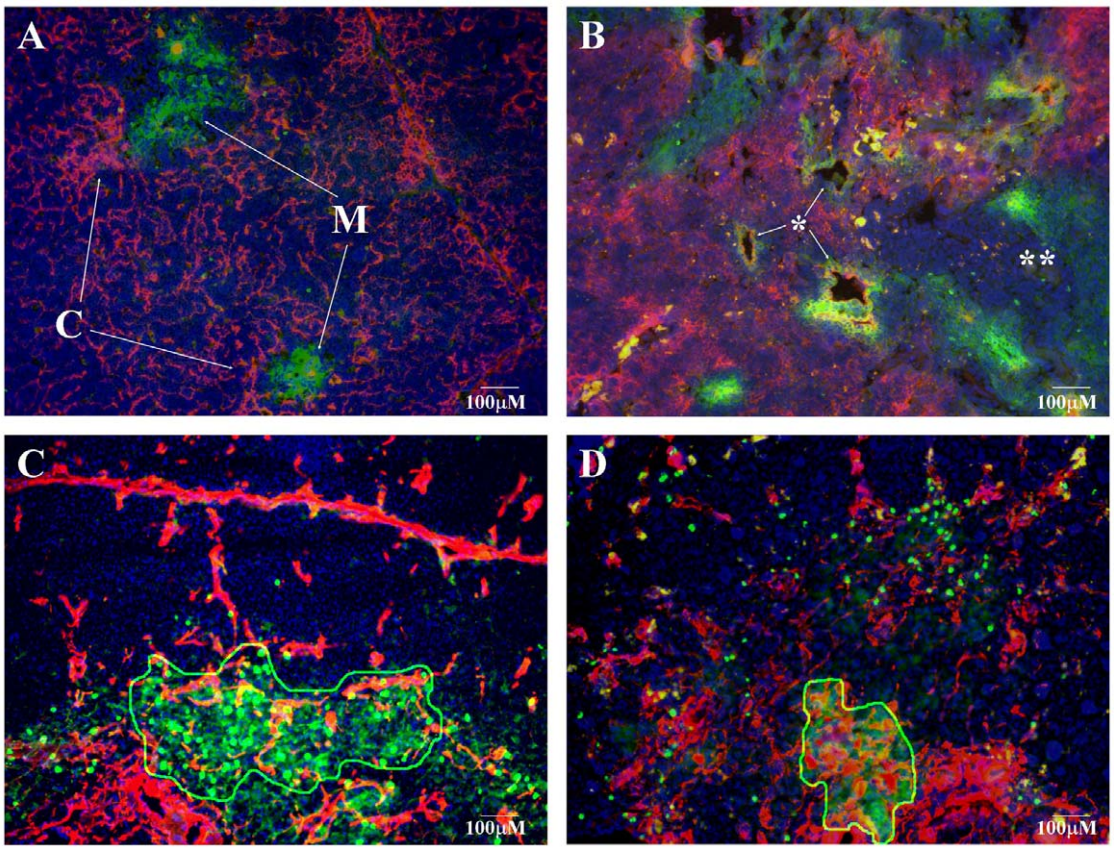

Figure 1. Disintegration of epithelial network. Figure 1A demonstrates cryostat section of 1 month, whereas figure 1B presents cryostat section of 1 year old BALB/c mouse thymus. Staining pattern: anti-EpCAM1-FITC (green), anti-Ly51-PE (red), DAPI (blue). 'M' marks medullary ($EpCAM1^{++}$, $Ly51^{-}$), while 'C' marks cortical ($EpCAM1^{+}$, $Ly51^{++}$) epithelial compartments on Figure 1A. Single asterisk (*) marks degenerative vacuoles, while double asterisk (**) mark the loss of epithelial staining on Figure 1B. Figure 1C (lower left) shows cryostate section of 2 month, whereas figure 1D (lower right) demonstrates cryostate section of 9 month old BALB/c mouse thymus. Staining pattern: anti-EpCAM1-FITC, ER-TR7-PE, DAPI (blue). The $EpCAM1^{++}$ thymic medulla is outlined by continuous line on Figures 1C and 1D for easier visualization.
doi:10.1371/journal.pone.0010701.g001

month and 9 month old BALB/c mice to identify epithelial and mesenchymal elements in young adult and aging thymic lobes. The above ages were selected to check additional time points and more precisely map the timeframe of thymic physiological senescence (see Figures 1C and 1D). The staining patterns are strikingly different at the two ages examined. In the 2 month old thymic tissue section a-EpCAM1 and ER-TR7-staining show little tendency for co-localization. In stark contrast, by the age of 9 months a-EpCAM1 and ER-TR7-staining show significant overlap within the thymic medulla, a phenomenon completely absent at earlier ages.

Adipose involution

To demonstrate how the disorganization of thymic epithelial network is followed by the emergence of adipocytes, thymic sections of 1.5 year old GFP-transgenic BALB/c mice were analyzed. This mouse strain develops and reproduces exactly like control BALB/c mice, and the thymic epithelial function and thymocyte maturation is indistinguishable from wild type controls [24]. However, due to the ubiquitous and strong EF1 promoter-driven transgene transcription, bright GFP expression offers a native, green-colored, cytoplasmic staining for all the cells in these mice. Thymic sections of senescent GFP-transgenic mice were co-stained with LipidTox Red to identify adipocytes. Histology shows the presence of relatively large, inflated cells in which the green-colored (GFP-containing) cytoplasm is pushed to the periphery by red-staining neutral lipid deposits, a pattern characteristic of adipose cells (see Figure 2).

Molecular changes of thymic epithelium

Having presented structural changes of thymic epithelial senescence, we set out to investigate the underlying molecular events. In order to detect gene expression changes, thymic epithelial cells were purified from 1 month and 1 year old BALB/c mice based on EpCAM1 expression (MACS separation). Following cDNA synthesis, quantitative RT-PCR analysis was performed. Several genes including Wnt4, FoxN1, PPARγ, ADRP, lamin1 and LAP2α were tested (Table 1 lists primer sequences and characteristics, see Figures 3A–D for changes in gene expression). Figure 3A shows that the expression of both Wnt4 and FoxN1 decreases in thymic epithelial cells. Highly decreased level (or total absence in some cases) of FoxN1 could be the consequence of strong Wnt4 down-regulation by the age of 1 year, indicating that thymic epithelial cells can down-regulate FoxN1 expression while maintaining that of epithelial cell surface markers like EpCAM1 [13]. At the same time, mRNA levels of pre-adipocyte differentiation markers PPARγ and ADRP rise with age in the same, EpCAM1-positive cell population (Figure 3C). This finding is in harmony with histological data demonstrating the emergence of adipocytes in the thymic lobes of senescent mice (Figure 2). The expression of lamin1, a key component of the nuclear lamina remains unaffected during senescence in thymic epithelial cells; whereas, the expression of LAP2α increases significantly (see Figure 3B). This degree of dissociation between lamin1 and LAP2α expression is of note and suggests functional differences despite conventionally anticipated association of lamin1 and LAP2 molecular family members. The measured LAP2α up-regulation associated with age-related adipose involution is, however, in perfect agreement with other literature data suggesting the pre-adipocyte differentiation-promoting effect of LAP2α in fibroblasts [17]. This is the first report to show that such, normally fibroblast associated molecular changes occur in purified thymic epithelial cells. In the literature, epithelial-mesenchymal transition is associated with differential expression of E- and N-cadherin [25]. While E-cadherin decreases, N-cadherin normally compensates for the loss of E-cadherin expression. To investigate whether the first step towards pre-adipocyte differentiation is the epithelial-mesenchymal transition of epithelial cells, gene expression changes of E-cadherin and N-cadherin were measured (Figure 3D). While E-cadherin mRNA levels significantly decreased, N-cadherin gene expression showed a slight increase, indicating that EMT might be the initial step in epithelial cell transition to become pre-adipocytes.

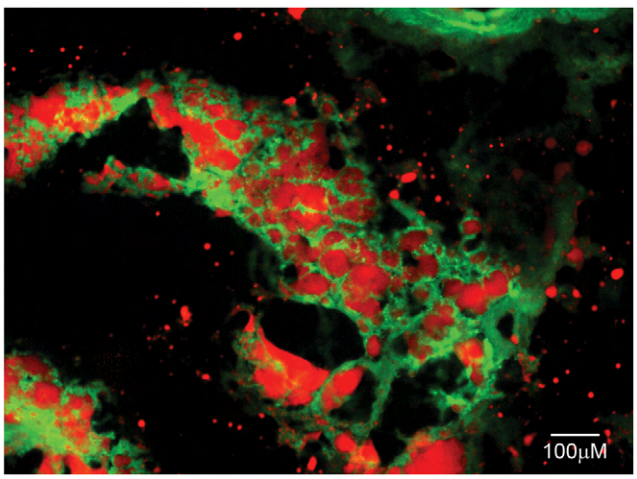

Figure 2. Adipose involution. Figure 2 shows adipose involution over cryostat section of 1.5 year old GFP-transgenic BALB/c mouse thymus. Staining pattern: GFP (green), LipidTox Red (red).
doi:10.1371/journal.pone.0010701.g002

Transgenic cell lines

Stable LAP2α over-expressing or Wnt4-secreting transgenic TEP1 cell lines were established using lentiviral transgenesis. The use of a primary-derived model cell line provides the advantage of absolute purity, the complete lack of other cell types that could potentially affect the gene expression profile of epithelial cells [26]. The established transgenic cell lines proliferated normally and did not show obvious signs of phenotypic changes (data not shown). In contrast to morphology, quantitative RT-PCR analysis revealed that LAP2α over-expression triggers an immense surge of PPARγ expression (Figure 4). Such an increase in mRNA level suggests that this is not a plain quantitative, but rather a qualitative change. ADRP a direct target gene of PPARγ was also up-regulated albeit to a lesser extent (Figure 4). On the other hand in Wnt4-secreting TEP1 cells the mRNA level of both PPARγ and ADRP was decreased (Figure 4). In the TEP1 cell line the expression of FoxN1 could not be addressed as it is very low/undetectable and remains as such with all the tested treatments (data not shown).

Transfected embryonic thymic organ cultures

To confirm the involvement of LAP2α and Wnt4 during adipogenesis through their direct effect on PPARγ expression in primary cells, murine thymic lobes were isolated from timed pregnancies at E12. Thymic lobes at the age of E12 provide an excellent experimental setting where the thymus has just been formed and there is no sign of aging. Furthermore, thymic lobes at this stage are also small enough to be both cultured and transfected as a whole, nutrients and virions have free access to most of the cells in the lobe without the need of disrupting any intercellular connection or tissue matrix [8,27]. The isolated lobes were therefore transfected with lentiviral vectors encoding GFP (mock), Wnt4 or LAP2α and were cultured for 4 days *in vitro*. Q-PCR was

Table 1. List of gene specific PCR primers.

Gene	Forward primer	Reverse primer
β-actin	5′-TGG CGC TTT TGA CTC AGG A -3′	5′-GGG AGG GTG AGG GAC TTC C - 3′
Wnt4	5′-CTC AAA GGC CTG ATC CAG AG - 3′	5′-TCA CAG CCA CAC TTC TCC AG - 3′
LAP2α	5′-TGA ACT GCA GGC AGC TAA GA-3′	5′-TCA TAG CTA GAC TCT GAG G-3′
Lamin1	5′ - TGA GTA CAA CCT GCG CTC AC -3′	5′ - TGA CTA GGT TGT CCC CGA AG -3′
PPARγ	5′ - CCC AAT GGT TGC TGA TTA CAA A -3′	5′ - AAT AAT AAG GTG GAG ATG CAG GTT CT -3′
ADRP	5′ - CGC CAT CGG ACA CTT CCT TA -3′	5′ - GTG ATG GCA GGC GAC ATC T -3′
E-cadherin	5′- AAG TGA CCG ATG ATG ATG CC -3′	5′- CTT CAT TCA CGT CTA CCA CGT -3′
N-cadherin	5′ - GTG GAG GCT TCT GGT GAA AT - 3′	5′ - CTG CTG GCT CGC TGC TT - 3′
FoxN1	Applied Biosystems TaqMan probe PN4351272 (Mm00477457_m1)	

doi:10.1371/journal.pone.0010701.t001

performed to confirm over-expression of LAP2α and Wnt4 in the embryonic thymic lobes as a result of lentiviral transgenesis (Figure 5A) and their effect on PPARγ expression was also analyzed (Figure 5B). The level of over-expression was confirmed following transfection with both LAP2α- and Wnt4-encoding viral vectors. Q-PCR analysis revealed that LAP2α over-expression triggers an increase of PPARγ expression, whereas additional Wnt4 secretion suppresses PPARγ level (Figure 5B). The latter Wnt4-mediated suppression of PPARγ expression in cultures of E12 thymic embryonic lobes was also confirmed by treatment with Wnt4-containing supernatants of Wnt4 over-expressing TEP1 cell line (data not shown). Interestingly, the expression of FoxN1 did not decrease in LAP2α over-expressing thymic lobes (data not shown), possibly due to high levels of Wnt4 in the embryonic thymic tissue preserving FoxN1 status. Our molecular studies using E12 thymic lobes confirmed our data obtained with the TEP1 cell lines, that even in embryonic thymic tissue pre-adipocyte differentiation markers can be up-regulated in the presence of LAP2α, indicating that the process can be dissected and controlled at a molecular level.

Conclusion

Here we show that with senescence, thymic epithelial Wnt4 secretion decreases, possibly below a threshold level that is required to maintain the identity of established thymic epithelial cells. This is measured by the loss of FoxN1 expression, a key transcription factor defining thymic epithelial cell identity. However, these epithelial cells still express cell surface markers

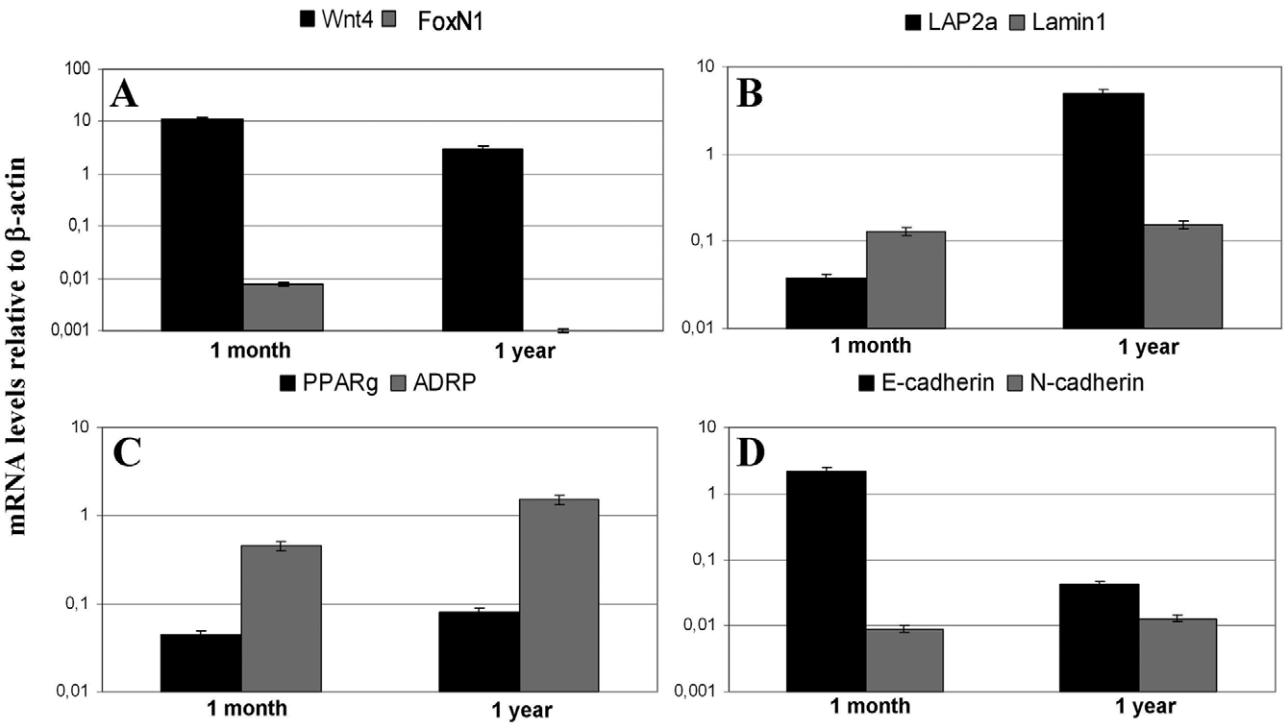

Figure 3. Molecular changes in thymic epithelium. Figures 3A–D demonstrate gene expression changes of MACS purified thymic epithelial cells measured by Q-PCR. Please note that the Y-axis scale is logarithmic. Error bars show ±1 SD.
doi:10.1371/journal.pone.0010701.g003

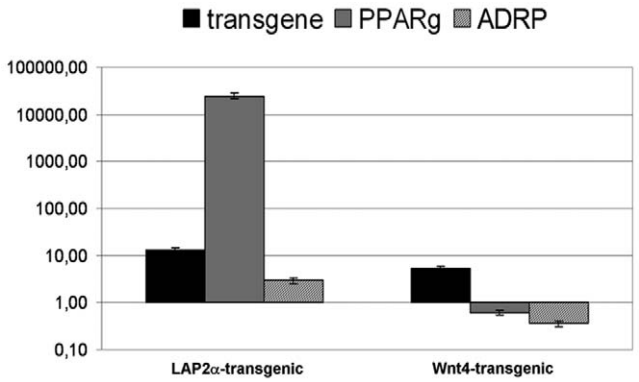

Figure 4. Confirmation in transgenic thymic cell lines. Figure 4 shows gene expression changes of LAP2α and Wnt4 over-expressing transgenic TEP1 cells measured by Q-PCR. Please note that Y-axis scale is logarithmic. Error bars show ±1 SD.
doi:10.1371/journal.pone.0010701.g004

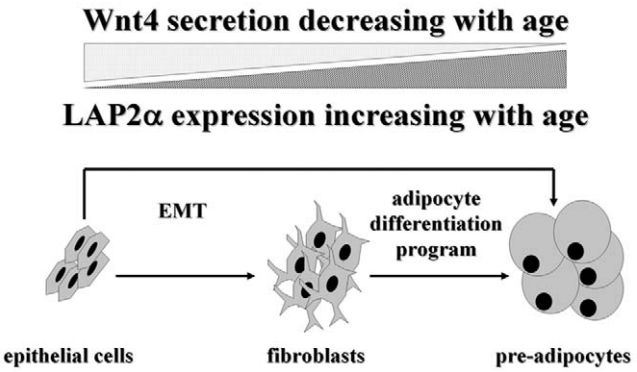

Figure 6. Model for thymic epithelial senescence. Figure 6 demonstrates our molecular level model of thymic adipose involution. Decreasing Wnt4 and increasing LAP2α levels promote epithelial cells to differentiate into pre-adipocytes either directly or indirectly via EMT.
doi:10.1371/journal.pone.0010701.g006

characteristic for thymic epithelial cells – i.e. EpCAM1. Wnt4 deprivation opens up an opportunity for trans-differentiation into pre-adipocytes. The simultaneous increase in LAP2α expression provides the necessary signal that pushes de-differentiated thymic epithelial cells to differentiate into pre-adipocytes, as detected by increased mRNA levels of PPARγ and ADRP.

We propose two different mechanisms for the process of adipose involution (see Figure 6). The first allows for the direct initiation of pre-adipocyte differentiation from de-differentiated thymic epithelial cells due to the down-regulation of Wnt4 and up-regulation of LAP2α. Although we cannot rule out this first model, we favor the second model where the process occurs indirectly: de-differentiation of thymic epithelial cells triggers EMT first, and then the resulting fibroblasts undergo the conventional route of differentiation program towards adipocyte-lineage commitment. The latter model certainly fits better with current literature of EMT [28] and is also supported by our histological and molecular results. Co-localization of a-EpCAM1 and ER-TR7-staining in the aging thymic medulla (Figure 1D) confirms that in the 9 month old thymus there are cells expressing the EpCAM1 marker as a legacy of their primary origin, and also secreting ER-TR7-positive extracellular matrix components, a function conventionally attributed to fibroblast cells. Moreover, Q-PCR data obtained with cDNA samples of MACS-purified thymic epithelial cells also demonstrate an age-related shift in cadherin expression levels characteristic for EMT (Figure 3D) providing additional evidence for the active process of EMT during thymic epithelial senescence.

Our model of thymic epithelial senescence is based on data obtained with mice undergoing physiological senescence. This is the first model for the molecular basis of the thymic epithelium to undergo adipose involution. This model withstands molecular level proof-of-principle using both a model cell line and primary embryonic thymic organ cultures rendered transgenic by lentiviral transgenesis.

Perspectives

Further experiments, however, are required. We plan using inducible, LAP2α-transgenic mice to allow us precise temporal-spatial over-expression of LAP2α in adult thymic epithelium to model and decisively verify the role of LAP2α in pre-adipocyte trans-differentiation *in vivo* exploiting our experience in establishing transgenic animals [24,29]. If LAP2α proves to be a master regulator of thymic adipose involution *in vivo* too, this knowledge appoints LAP2α as target molecule for directed rejuvenation of the thymic epithelial structure and function. This rejuvenation process could theoretically reinforce naïve T-cell output to reach young adult levels that could ameliorate senescence-related immunological disorders like impaired antiviral defense and late-onset autoimmune diseases.

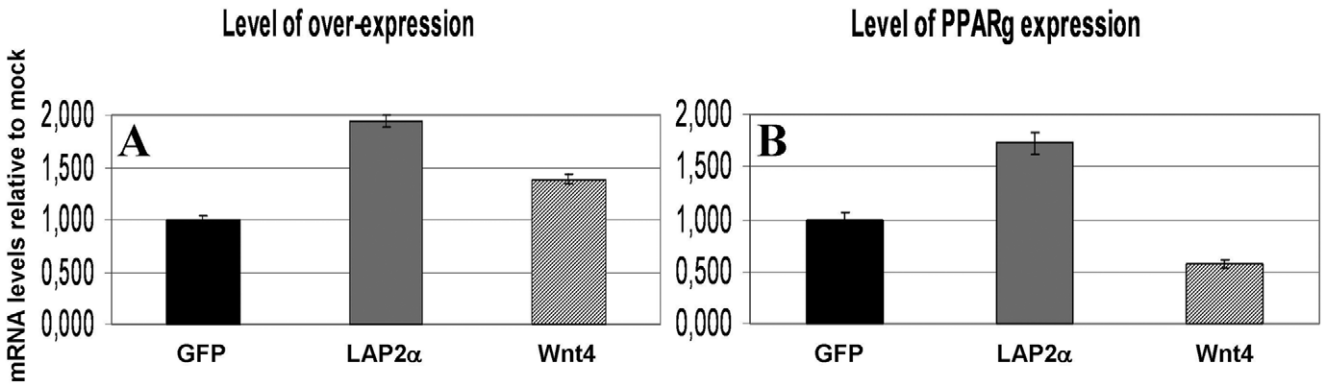

Figure 5. Confirmation in transfected thymic lobes. Figures 5A–B present gene expression changes measured by Q-PCR from cDNA of murine thymic lobes transfected at E12 and cultured for 4 days *in vitro*. Please note that Y-axis scale is linear. Error bars show ±1 SD.
doi:10.1371/journal.pone.0010701.g005

Methods

Cell lines and mice

The 293T (ATCC: CRL-11268) and TEP1 [26] cell lines were cultured in DMEM supplemented with 10% FCS, penicillin, streptomycin and β-mercapto-ethanol (Lonza Walkersville). For the experiments we used thymic lobes from timed pregnancies at E12, and also from adult BALB/c mice at 4 week and 1 year of age, and from 1.5 year old GFP-transgenic BALB/c-mice. Mice were bred in our animal facility; all animal work has been conducted according to relevant national and international guidelines following approval of ethics committee of the University of Pecs. Senescent animals developed and aged normally, without any treatment.

Transgenic cell, organ and animal models

The GFP-transgenic BALB/c model was created using lentiviral transgenesis as published by our group [24]. The Wnt4 sequence was purchased and subcloned from an Origene (Origene) vector containing human full-length Wnt4 cDNA. The full-length murine LAP2α cDNA containing plasmid was a kind gift of Dr. Simon Amos. The GFP (mock), LAP2α or Wnt4 over-expressing TEP1 cell lines or E12 thymic lobes were generated using lentiviral vectors that were prepared as described previously [30]. Following overnight lentiviral transfection the thymic lobes were transferred over Nucleopore Track-Etch Membranes (Whatman) and were cultured in DMEM supplemented with 20% FCS, penicillin, streptomycin, ciprofloxacin, amphotericin-B and β-mercapto-ethanol (Lonza Walkersville).

Histology using fluorescent antibodies, proteins and dyes

Sections (9 μm) of frozen thymic lobes of BALB/c mice were fixed in cold acetone, then dried and blocked using 5% BSA in PBS for 20 min before staining with a-Ly51-PE (clone 6C3), a-EpCAM-FITC (clone G8.8), ER-TR7-PE antibodies and DAPI. Thymic sections of GFP-transgenic mice were fixed in 4% paraformaldehyde before staining with LipidTOX Red following the manufacturer's instructions (Invitrogen). The sections were analyzed using an Olympus BX61 microscope equipped with a CCD camera and AnalySIS software.

Separation and enrichment of thymic epithelial cells

Thymic lobes were digested with type F collagenase from *C. hystolyticum* (Sigma) for 30 min, then washed with DMEM 10% FCS. Cell suspensions were then labeled with anti-EpCAM1-FITC (clone G8.8) and washed with MACS-buffer followed by incubation with anti-FITC micro-beads (Miltenyi Biotec), the $EpCAM^{+}$-cells were used for total RNA isolation and subsequent quantitative PCR analysis. The cells were purified using MACS LS separation columns (Miltenyi Biotec).

RNA isolation, preparation of cDNA, Q-PCR analysis

Total RNA was isolated the RNAII kit (Macherey-Nagel), including an on column DNA digestion step. cDNA was constructed using the high capacity RNA to cDNA kit (Applied Biosystems). For Q- PCR analysis, we used an AB7500 platform and either SYBR green or TaqMan PCR master mix (Applied Biosystems). Gene expression was normalized to β-actin. The sequences and data of primers are listed in Table 1.

Statistical analysis

All experiments were performed on three occasions, representative experiments are shown. Measures were obtained in triplicates; data are presented as mean ±1 SD by error bars.

Acknowledgments

The supernatant of ER-TR7 hybridoma clone was originally donated by Dr. Willem van Ewijk to Dr. Peter Balogh, who provided it for the authors. The authors are grateful to Prof. S. Amos (Institute of Hematology, Chaim Sheba Medical Center, Tel-Hashomer, Israel) for providing the murine LAP2α construct and Prof. E. L. Cooper (Laboratory of Comparative Neuroimmunology, Department of Neurobiology, David Geffen School of Medicine at UCLA, University of California, Los Angeles, USA) for critically and carefully reading the manuscript.

Author Contributions

Conceived and designed the experiments: KK GA EJJ JEP. Performed the experiments: KK ZV DB SH SP. Analyzed the data: KK ZV DB SH SP GA EJJ JEP. Contributed reagents/materials/analysis tools: KK GA EJJ JEP. Wrote the paper: KK JEP.

References

1. Marinova TT (2005) Epithelial framework reorganization during human thymus involution. Gerontology 51: 14–18.
2. Ribeiro RM, Perelson AS (2007) Determining thymic output quantitatively: using models to interpret experimental T-cell receptor excision circle (TREC) data. Immunol Rev 216: 21–34.
3. Grubeck-Loebenstein B (2009) Fading Immune Protection in Old Age: Vaccination in the Elderly. J Comp Pathol.
4. Chidgey A, Dudakov J, Seach N, Boyd R (2007) Impact of niche aging on thymic regeneration and immune reconstitution. Semin Immunol 19: 331–340.
5. Gui J, Zhu X, Dohkan J, Cheng L, Barnes PF, et al. (2007) The aged thymus shows normal recruitment of lymphohematopoietic progenitors but has defects in thymic epithelial cells. Int Immunol 19: 1201–1211.
6. Hsu HC, Mountz JD (2003) Origin of late-onset autoimmune disease. Immunol Allergy Clin North Am 23: 65–82, vi.
7. Bleul C, Boehm T (2005) BMP signaling is required for normal thymus development. J Immunol 175: 5213–5221.
8. Pongracz J, Hare K, Harman B, Anderson G, Jenkinson E (2003) Thymic epithelial cells provide Wnt signals. Eur J Immunol 33: 1949–1956.
9. Osada M, Ito E, Fermin HA, Vazquez-Cintron E, Venkatesh T, et al. (2006) The Wnt signaling antagonist Kremen1 is required for development of thymic architecture. Clin Dev Immunol 13: 299–319.
10. Kuraguchi M, Wang XP, Bronson RT, Rothenberg R, Ohene-Baah NY, et al. (2006) Adenomatous polyposis coli (APC) is required for normal development of skin and thymus. PLoS Genet 2: e146.
11. Anderson G, Pongracz J, Parnell S, Jenkinson EJ (2001) Notch ligand-bearing thymic epithelial cells initiate and sustain Notch signaling in thymocytes independently of T cell receptor signaling. Eur J Immunol 31: 3349–3354.
12. Mikels AJ, Nusse R (2006) Wnts as ligands: processing, secretion and reception. Oncogene 25: 7461–7468.
13. Balciunaite G, Keller M, Balciunaite E, Piali L, Zuklys S, et al. (2002) Wnt glycoproteins regulate the expression of FoxN1, the gene defective in nude mice. Nat Immunol 3: 1102–1108.
14. Gordon MD, Nusse R (2006) Wnt signaling: multiple pathways, multiple receptors, and multiple transcription factors. J Biol Chem 281: 22429–22433.
15. Schweizer L, Varmus H (2003) Wnt/Wingless signaling through beta-catenin requires the function of both LRP/Arrow and frizzled classes of receptors. BMC Cell Biol 4: 4.
16. Torday JS, Rehan VK (2006) Up-regulation of fetal rat lung parathyroid hormone-related protein gene regulatory network down-regulates the Sonic Hedgehog/Wnt/betacatenin gene regulatory network. Pediatr Res 60: 382–388.
17. Dorner D, Vlcek S, Foeger N, Gajewski A, Makolm C, et al. (2006) Lamina-associated polypeptide 2alpha regulates cell cycle progression and differentiation via the retinoblastoma-E2F pathway. J Cell Biol 173: 83–93.
18. Christodoulides C, Lagathu C, Sethi JK, Vidal-Puig A (2009) Adipogenesis and WNT signalling. Trends Endocrinol Metab 20: 16–24.
19. Moldes M, Zuo Y, Morrison RF, Silva D, Park BH, et al. (2003) Peroxisome-proliferator-activated receptor gamma suppresses Wnt/beta-catenin signalling during adipogenesis. Biochem J 376: 607–613.
20. Berger R, Theodor L, Shoham J, Gokkel E, Brok-Simoni F, et al. (1996) The characterization and localization of the mouse thymopoietin/lamina-associated polypeptide 2 gene and its alternatively spliced products. Genome Res 6: 361–370.
21. Hutchison CJ, Alvarez-Reyes M, Vaughan OA (2001) Lamins in disease: why do ubiquitously expressed nuclear envelope proteins give rise to tissue-specific disease phenotypes? J Cell Sci 114: 9–19.

22. Dreger M, Otto H, Neubauer G, Mann M, Hucho F (1999) Identification of phosphorylation sites in native lamina-associated polypeptide 2 beta. Biochemistry 38: 9426–9434.
23. Oksanen A (1971) Multilocular fat in thymuses of rats and mice associated with thymus involution: a light- and electron-microscope and histochemical study. J Pathol 105: 223–226.
24. Kvell K, Czompoly T, Hiripi L, Balogh P, Kobor J, et al. Characterisation of eGFP-transgenic BALB/c mouse strain established by lentiviral transgenesis. Transgenic Res 19: 105–112.
25. Seike M, Mizutani H, Sudoh J, Gemma A (2009) Epithelial to mesenchymal transition of lung cancer cells. J Nippon Med Sch 76: 181.
26. Beardsley TR, Pierschbacher M, Wetzel GD, Hays EF (1983) Induction of T-Cell Maturation by a Cloned Line of Thymic Epithelium (TEPI) 10.1073/pnas.80.19.6005. Proceedings of the National Academy of Sciences 80: 6005–6009.
27. Pongracz JE, Parnell SM, Jones T, Anderson G, EJ. J (2006) Overexpression of ICAT highlights a role for catenin-mediated canonical Wnt signalling in early T cell development. Eur J Immunol 36: 2376–2383.
28. Friedl P, Gilmour D (2009) Collective cell migration in morphogenesis, regeneration and cancer. Nat Rev Mol Cell Biol 10: 445–457.
29. Hiripi L, Negre D, Cosset FL, Kvell K, Czompoly T, et al. Transgenic rabbit production with simian immunodeficiency virus-derived lentiviral vector. Transgenic Res.
30. Kvell K, Nguyen TH, Salmon P, Glauser F, Werner-Favre C, et al. (2005) Transduction of CpG DNA-stimulated primary human B cells with bicistronic lentivectors. Mol Ther 12: 892–899.

Hindawi Publishing Corporation
Clinical and Developmental Immunology
Volume 2007, Article ID 83671, 10 pages
doi:10.1155/2007/83671

Review Article

Blurring Borders: Innate Immunity with Adaptive Features

K. Kvell,[1] EL. Cooper,[2] P. Engelmann,[1] J. Bovari,[1] and P. Nemeth[1]

[1] *Department of Immunology and Biotechnology, Faculty of Medicine, University of Pécs, 7624 Pécs, Hungary*
[2] *Laboratory of Comparative Neuroimmunology, Department of Neurobiology, David Geffen School of Medicine at UCLA, University of California, Los Angeles, CA 90095-1763, USA*

Correspondence should be addressed to P. Nemeth, peter.nemeth@aok.pte.hu

Received 26 June 2007; Accepted 5 November 2007

Recommended by Yasunobu Yoshikai

Adaptive immunity has often been considered the penultimate of immune capacities. That system is now being deconstructed to encompass less stringent rules that govern its initiation, actual effector activity, and ambivalent results. Expanding the repertoire of innate immunity found in all invertebrates has greatly facilitated the relaxation of convictions concerning what actually constitutes innate and adaptive immunity. Two animal models, incidentally not on the line of chordate evolution (*C. elegans* and *Drosophila*), have contributed enormously to defining homology. The characteristics of specificity and memory and whether the antigen is pathogenic or nonpathogenic reveal considerable information on homology, thus deconstructing the more fundamentalist view. Senescence, cancer, and immunosuppression often associated with mammals that possess both innate and adaptive immunity also exist in invertebrates that only possess innate immunity. Strict definitions become blurred casting skepticism on the utility of creating rigid definitions of what innate and adaptive immunity are without considering overlaps.

Copyright © 2007 K. Kvell et al. This is an open access article distributed under the Creative Commons Attribution License, which permits unrestricted use, distribution, and reproduction in any medium, provided the original work is properly cited.

1. INTRODUCTION: WHERE INNATE AND ADAPTIVE IMMUNITY CONVERGE

All multicellular animals (invertebrates and vertebrates) manage to keep self-integrity. Any attempt to answer questions concerning immune recognition must consider the universality of receptor-mediated responses. These may designate two forms: (1) rearranging clonally distributed antigen-specific receptors that distinguish between self and nonself according to classical Burnet hypothesis; and/or (2) pattern recognition receptors introduced by Janeway [1, 2]. The ideal immune system provides rapid and efficient responses, diverse repertoire of recognition, and effector molecules as well as specific memory on an individual level. In the self and nonself discrimination theory, the recognition receptors are central to immunity. However, a recently advanced hypothesis emphasizes that alarm signals have priority and initiate immune responses. These alarm danger signals released from the body's own cells are explained by the danger model of immunity. According to this model, immune cells must "decide" what poses harm to the body among self and nonself structures [3, 4]. The two branches of vertebrate immunity (innate and adaptive) are dependent on each other. The innate immune system, responsible for the first encounter with a pathogen, can trigger adaptive immunity in case the initial response is ineffective. Both arms interact with each other, via cell-cell interactions and soluble factors maintaining a physiological steady state [5].

With this in mind, we felt compelled to clarify and extend what seems to be the blurring or masking of certain immunological characteristics of invertebrates and vertebrates [6–8]. To do this, we first define the general features of innate and adaptive immunities. Innate immunity is considered to be natural, nonspecific, nonanticipatory, and nonclonal but germ-line encoded; whereas adaptive immunity is indeed specific, anticipatory, clonal, and somatic. Then, we discuss the blurring of vertebrate and invertebrate immunological characteristics in the following sections: (1) a preface to adaptive immunity; (2) senescence, cancer, and immunosuppressive viruses; (3) invertebrate immunological memory triggered by nonpathogenic stimuli; (4) the dawn of adaptive immunity; and (5) perspectives on innate and adaptive immunity.

2. A PREFACE TO ADAPTIVE IMMUNITY

2.1. Products of eons

Ancient innate immunity-related functions like phagocytosis and cytokine production (i.e., IL-1 and TNF) were already developed 700 million years ago in sponges and higher aquatic invertebrates (i.e., starfish). These fundamental functions remained unaltered during phylogenesis. A major evolutionary step happened 500 million years ago when fish developed jaws accompanied by evolution of the gut associated immune system. This system was fundamental to providing the genetic material required for recombination and mutation to produce variability and diversity of proteins (i.e., immunoglobulins). This system also enabled the occurrence of a wide spectrum of antigen-presenting proteins like the major histocompatibility complex (MHC). These MHC molecules developed from a primordial molecule over 300 million years ago [9].

2.2. Interspecies borders

A genetically colorful background is generally considered to be advantageous for species in their constant adaptation to the neighboring environment. On the other hand, for a suddenly emerging costly macroscopic function like adaptive immunity, working with clonally distributed receptors, intraspecies genetic backcrosses can make survival difficult. Therefore, in such cases, interspecies borders may help the genetic solidification of evolutionarily novel characteristics. However, drawing interspecies borders is not always easy as often seen in cases of hybridogenesis with certain invertebrate arthropods or even with vertebrate fish and amphibian species [10–12].

2.3. Lymphocyte receptors: survival of the fittest molecule

In the case of invertebrate organisms, species survival is maintained at the population level, which is risky for individuals. Whenever a new pathogen takes its toll, the remaining individuals are spared because they are more resistant than others. Such differences are genetically encoded [13]. However, for vertebrates, the surviving strategy is quite different. Vertebrates have a more complex immune system that generates a practically indefinite pool of recognition molecules, each present as a single cell clone. From this array of cells, those that provide better adaptation to various environments are selected in a fashion quite similar to macroscopic evolution. Cells that meet the requirements in this tough selection survive and proliferate. Such selection occurs every time a new pathogen attacks a vertebrate and the winners of this quick intercellular evolution are selected and propagated quickly enough to hunt down and neutralize the pathogen in the host organism [14].

2.4. Aspects of immunological ecology and evolution

Ecological immunology is a young but increasing science that examines causes and consequences of changes in immune function in the context of evolution and of ecology. Millions of invertebrate species depend exclusively on using innate immunity, in contrast to the only 45 000 vertebrate species that employ an additional acquired immune system. Regardless of this major distinction, most studies of ecological immunology discuss only vertebrates. Nevertheless, insect immunity might be more specific and similar to vertebrate immunity than previously thought [15–17].

An explanation to why an anticipatory immune system employing clonally distributed receptors has not developed in invertebrates may be provided by immunological ecology. Highly developed organisms tend to be large in size. Since the size of individual cells does not show significant interspecies variances, being larger means having more cells. Adaptive immunity works with a huge number of recognition molecules distributed in a clonal pattern. Therefore, only highly developed organisms can afford to run such a costly immune system; otherwise costs would always outweigh benefits. It seems that having huge and complex communities of cells not only demands a highly effective adaptive immune system, but actually provides its basic framework in order to exist [18, 19].

3. SENESCENCE, CANCER, AND IMMUNOSUPPRESSIVE VIRUSES

3.1. Is senescence relevant to understanding immunity?

Senescence and age-related research isa promising approach that discovers revolutionary data. Immunological senescence of vertebrate adaptive immunity is a process widely accepted by most immunologists. This is, however, less evident when thinking in terms of invertebrate innate immunity. However, this will likely change in the near future as there is accumulating evidence of senescence and more specifically immunological senescence in invertebrate species.

Morphological features of the aging process (senescence) have been recognized for many years in invertebrates. For example, when earthworms are maintained for long periods in the laboratory, a progressive decrease in size reminiscent of degeneration and a kind of wasting syndrome occur [20]. Congo red staining indicates the presence of amyloid in every organ-system as a diagnostic feature of aging [21]. With invertebrates and from a comparative viewpoint, there are examples of (1) rapid senescence and sudden death (progeria); (2) gradual senescence with definite life span; (3) negligible senescence; and (4) genetic influence on life span, mortality rates, and age-related diseases [22]. Increased activation of the immune system is a general characteristic that accompanies senescence in animals, including mammals and certain invertebrates. Gene expression analyses show that some of the most remarkable transcriptional changes that happen during aging are related to immunity. As a consequence, the use of invertebrate model organisms is highly desirable.

During senescence, *Drosophila melanogaster* expresses increasing levels of numerous antimicrobial peptides if exposed to septic bacterial infections, but not in response to bacterial extracts [23]. Mortality factor on chromosome 4 (MORF4)

is known to initiate senescence in a number of cell lines. MORF-related gene on chromosome 15 (MRG15 expressed from yeast to humans) has been shown to be extremely conserved. The significant effect of MRG1 (the *Caenorhabditis elegans* ortholog of the above MRG15) in the aging process has also been demonstrated [24]. The DAF family of transcription factors supports its critical importance in the control of aging (immunosenescence) in this nematode model. The DAF-2 mediated insulin signaling pathway is a key cascade that influences senescence in *Caenorhabditis elegans* and this function seems to be evolutionarily conserved: the DAF pathway also affects aging in *Drosophila melanogaster* and rodents [25]. Innate immune functions in *Caenorhabditis elegans* are also regulated by the TGFβ-like and the p38 MAPK pathways. The requirement of the DAF-2 cascade in regulating senescence and immunity raises molecular-level linkage of these processes [26].

3.2. Cancer and immunosuppressive viruses in invertebrates

3.2.1. Cancer development

Cancer development has often been addressed in vertebrate species especially its relation with adaptive immunity. However, invertebrates also develop tumors in response to environmental carcinogens. Studying cancer development in species possessing innate immunity alone is a very promising field of research and may highlight adaptivelike functions present in invertebrates.

Mussels are vulnerable to several environmental toxicants and carcinogens. DNA sequence alignment of the *Mytilus edulis* homologue of vertebrate *ras* and p53 demonstrates extreme evolutionary conservatism in active domains, including four mutational hot spots [27]. Cases of transmissible sarcoma caused by environmental carcinogens (i.e., chlordane) in the soft-shell clam *Mya arenaria* have also been reported [28–30].

Drosophila offers a unique platform for the rapid identification and characterization of tumor suppressor genes, many of which have mammalian homologues. Genomewide microarray analysis of *Drosophila* brain tumor caused by the disfunction of the *Brat* tumor suppressor gene has identified over three hundred associated genes. Sixty of these sequences show homology to existing mammalian genes involved in tumor development [31]. As in human cancers, loss of heterozygosity can lead to tumor formation as reported in the case of the warts (*wts*) sequence. The *wts* sequence was identified by the massive overgrowth of clones homozygous for *wts* deletion [32, 33]. Similarly, mutations of the fat locus cause hyperplastic overgrowth of the imaginal discs. The affected protein product is a relative of cadherins, which are known to play an important role in human tumor suppression [34].

3.2.2. Immunosuppressive viruses

For those who believe in the orthodox split between innate and adaptive immunities in terms of characteristics, it is perhaps difficult to accept the existence of viruses that specifically suppress the cellular components of innate immunity. Nevertheless, as proved by experimental data, innate immunity-specific immunosuppressive viruses exist. *Cotesia congregata* is a wasp that injects its eggs into the host caterpillar *Manduca sexta*. However, in this particular host-parasite relation, the presence of a third partner is necessary for successful parasitism: a bracovirus. The *C. congregata* bracovirus (CcBV) is injected simultaneously with the wasp eggs. Expression of viral genes hijacks the caterpillar's immune defense responses, which favors the survival and development of adult parasitoid wasps [63, 64]. This parasitoid wasp is known to take advantage of yet another virus in a similar fashion, a polydnavirus. Polydnaviruses (PDVs) also suppress the immune system of the host and allow the juvenile parasitoids to develop without being encapsulated by host hemocytes [65]. In invertebrates, the ambivalent relation of viruses and their hosts is further complicated by presence of both specific (RNA interference-mediated) and nonspecific (interferon-mediated) antiviral responses supporting the *blurring* of immunological functions [66].

4. INVERTEBRATE IMMUNOLOGICAL MEMORY TRIGGERED BY NONPATHOGENIC STIMULI

4.1. Protostomes

Numerous examples have been presented of animal immune responses that may develop following challenge by pathogenic organisms or nonpathogenic stimuli [8]. Here, we refer to reports previously neglected thus widening the scope of definitions of what may trigger invertebrate memory and further adaptive immunity-related features (Table 1). Most evidence concerning the evolution of innate immunity has been derived from two ecdysozoan species: *C. elegans* and *Drosophila*. In contrast, the lophotrochozoan systems share some distinct differences; mollusks may have managed immunological defense in a special manner similar to the annelids including earthworms [67] (Figure 1).

Early invertebrates present numerous examples of nonself recognition. Two classes of receptors with Ig-like domains have been identified in marine sponges: receptor tyrosine kinases and adhesion molecules. The expression of these molecules is known to be upregulated following a grafting process [35, 36, 68].

Various worm species have been used in tissue transplantation experiments. The marine nemertean ribbon worm *Lineus* readily rejects xenogeneic grafts revealing a memory component that lasts for three months [39–42]. In annelids (earthworms and leeches), accelerated rejection, weak specificity and short-term "memory" mediated by the cellular immune system have been reported [43–45, 69–74]. Molluscs are also capable of recognizing tissue alloantigens as demonstrated in the terrestrial slug *Incilaria fruhstorferi* after exchanging dorsal skin-allografts: immune cells infiltrated the grafts [46].

Recent knowledge of invertebrate innate immunity is mainly based on molecular data of dipteran insect species; however there is no recent information available about tissue

Table 1: Invertebrates exhibiting induction, specificity, and/or immunological memory in the nonpathogenic context of first and second challenges with transplants (n.a.: not analyzed).

Species	Challenge	Specifity	Memory	References
Porifera				
C. diffusa	Tissue (allograft) transplantation	+	+	Smith and Hildemann,1986 [35]
G. cydonium		+	n.a.	Müller et al., 1999 [36]
Cnidaria				
E. stricta	Colonial contact/allograft, xenograft	+	n.a.	Theodor, 1970 [37]
M. verrucosa		+	+	Hildemann et al., 1977 [38]
Nemertea				
L. ruber	Tissue (allograft, xenograft) transplantation	+	+	Bierne and Langlet, 1974 [39];
L. lacteus				Langlet and Bierne,1975 [40]; 1982 [41]; 1984 [42]
Annelida				
Earthworms *L. terrestris E. fetida*	Tissue (allograft, xenograft) transplantation	+	+	Cooper, 1969 [43]; Cooper and Roch, 1986 [44]
Leeches *H. medicinalis G. complanata*	Tissue (allograft, xenograft) transplantation	+	+	Tettamanti et al., 2003 [45]
Mollusca				
I. fruhstorferi	Tissue (allograft) Transplantation	+	n.a.	Yamaguchi et al., 1999 [46]
Arthropoda				
P. americana B. orientalis	Tissue (allograft, xenograft) transplantation	+	+	Hartmann and Karp, 1989 [47]; Karp and Meade, 1993 [48]
Echinodermata				
S. purpuratus L. pictus	Tissue (allograft) transplantation	+	−	Coffaro and Hinegardner, 1977 [49]
D. imbricata		+	+	Karp and Hildemann, 1976 [50]
Tunicata				
B. schlosseri	Colonial contact/allograft	+	n.a.	Rinkevich et al., 1998 [51]; Scofield et al., 1982 [52];
S. plicata		+	+	Raftos et al., 1987 [53]; 1988 [54]

allorecognition in these model organisms. However, several studies have indicated that the cockroach can respond to integumentary xenografts and effectively discriminate between self and allogeneic tissues [47, 48].

4.2. Deuterostomes

Sea urchins and sea stars exhibit immune responses against grafted tissues similar to those found in vertebrates [49, 50]. The responses of the urochordates *Styela plicata* and *Botryllus schlosseri* to tunic grafts confirm the existence of a sensitive histocompatibility system. Screening for genes differentially expressed during allorecognition in *Botryllus schlosseri* has identified a gene encoding a transmembrane protein showing close similarity to CD94/NKR-P1. The allorecognition of *B. schlosseri* is controlled by an ancient MHC-like system (called Fu/HC) [51, 53, 54, 75–78].

Since the complete genome of the urochordate *Ciona intestinalis* has been sequenced, it allows for the rapid identification of early evolutionary roots of adaptive immunity. In the hemocytes of *C. intestinalis,* certain adaptive-immunity homologous ESTs have been identified including vWF-like (von Willebrand factor-like), distant homologues of type I interferon (IFN) receptors, and C6-like (complement 6-like) elements [79, 80]. Moreover, genes that encode molecules with membrane receptor features of the immunoglobulin superfamily (IgSf) have also been reported [81].

5. THE DAWN OF ADAPTIVE IMMUNITY

The emergence of adaptive immunity was not a sudden event; its far-reaching evolutionary roots are currently under investigation by modern molecular biological methods. Genomewide sequence analysis of invertebrates has focused on the genes of innate immunity including complement components, Toll-like receptors, and those involved in intracellular signal transduction of immune responses. Assessment of extracellular C-type lectins, immunoglobulin domains, intracellular immunoreceptor tyrosine-based inhibitory motifs (ITIMs), and immunoreceptor tyrosine-based activation motifs (ITAMs) (together with their associated signal transduction molecules) suggests that activating and inhibitory receptors have an early evolutionary origin [82].

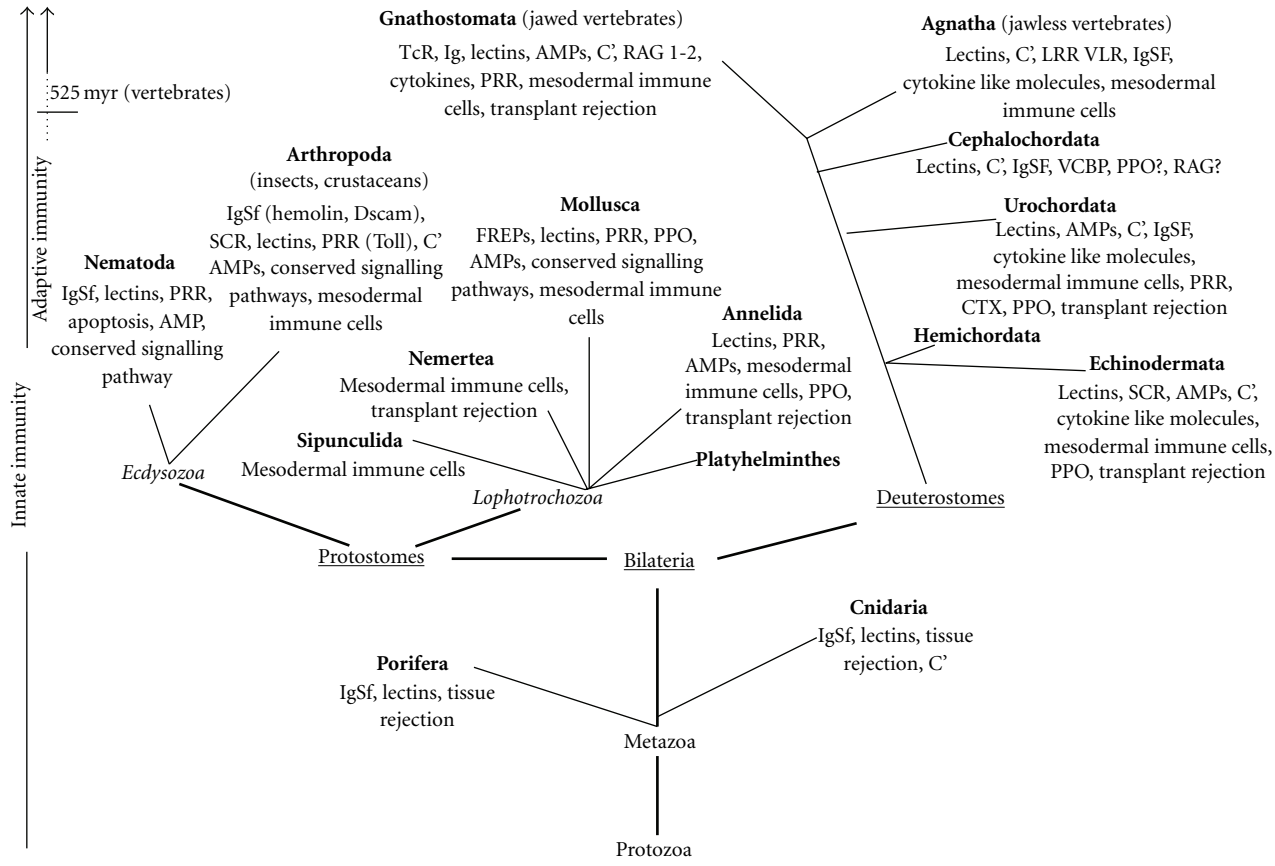

AMP: antimicrobial peptides
C': complement pathway elements
CTX: cortical thymocytemarker in *Xenopus*
Dscam: drosophila homolog for Down syndrome cell adhesion molecule
FREPs: fibrinogen related peptides
IgSF: immunoglobulin superfamily
LRR VLR: variable lymphocyte receptors with leucine rich repeats
PPO: prophenoloxidase cascade
PRR: pattern recognition receptors
RAG: recombination-activating genes
SCR: scavenger receptors
VCBP: variable chitin binding proteins
TCR: T cell receptor

Figure 1: *Phylogenetic tree of the animal kingdom highlighting the evolution of key immunological elements.* Two arrows on the left side of Figure 1 indicate possible appearance of the two branches of immunity. Innate immunity may be observed along the entire animal kingdom. Traditionally accepted adaptive immunity appeared only in vertebrates, while certain adaptive immune mechanisms may have appeared early at the level of arthropods and molluscs illustrated by dots (below the arrow).

After decades of anticipation, the ancestors of some cytokines—soluble intercellular signaling molecules that form a complex network for the regulation of immunity—have recently been identified. In vertebrates, helical cytokines inlude IL2, IL6, INF $\alpha-1$, and GM-CSF. Malagoli et al. have identified a putative helical cytokine in *Drosophila melanogaster* by elaborate bioinformatics transcriptome analysis. It is very promising that transcription from this homologue is upregulated in parallel with the known antimicobial factors defensin and cecropin A1 following Gram− or Gram+ challenge [83, 84]. Similarly, Söderhäll et al. have identified a prokineticin (PK) domain in astakine, an endogenous cytokine-like factor from the freshwater crayfish *Pacifastacus leniusculus* by mass spectrometry and PCR using degenerate primers. An astakine homologue has also been identified in the shrimp *Penaeus monodon*. In vertebrates, PK domains direct angiogenic growth. It has been demonstrated that injections of recombinant astakine actively influence differentiation and growth of hemopoietic stem cells in vivo [85].

It is a notable observation that even our most distant vertebrate relatives, jawless fish (hagfish, lamprey), have an adaptivelike immune system. It operates by means of clonally distributed leucine-rich repeat (LRR) receptors (similar to Toll-like receptors) using a novel mechanism of gene rearrangement other than RAG. These LRR modules constitute the variable lymphocyte receptors (VLRs). Computer-assisted prediction suggests a repertoire of approximately 10^{14} unique VLR receptors [86–89]. In response to the results described above, one suggestion involves the use of a different terminology for vertebrates instead of "adaptive" or "acquired" immune system: AIS or antibody-based immune

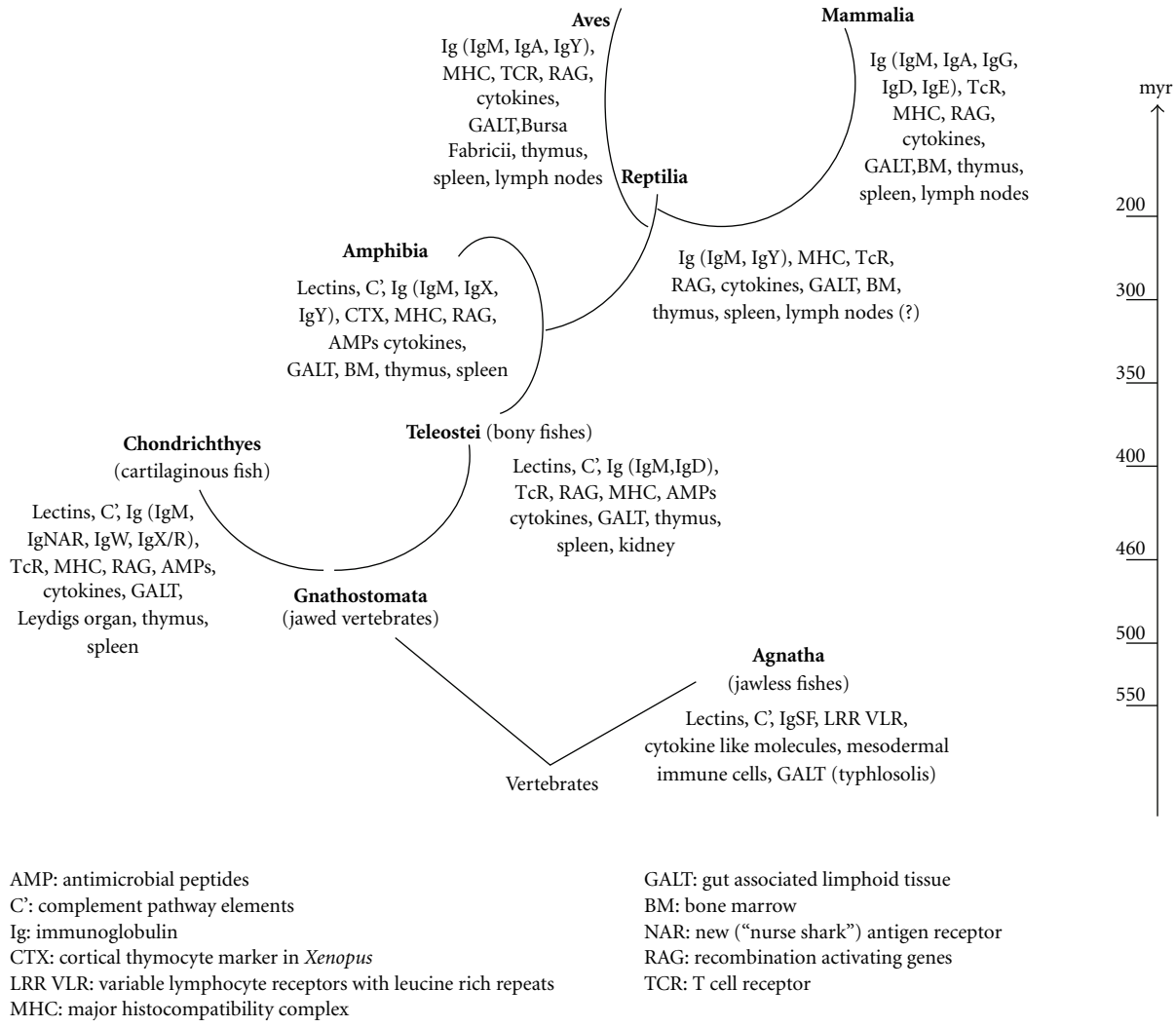

AMP: antimicrobial peptides
C': complement pathway elements
Ig: immunoglobulin
CTX: cortical thymocyte marker in *Xenopus*
LRR VLR: variable lymphocyte receptors with leucine rich repeats
MHC: major histocompatibility complex
GALT: gut associated limphoid tissue
BM: bone marrow
NAR: new ("nurse shark") antigen receptor
RAG: recombination activating genes
TCR: T cell receptor

Figure 2: *Evolution of molecular and histological structures of the vertebrate immune system.* Regarding lymphatic tissues, the thymus, and spleen appeared early in fishes, while lymph-filtering lymph nodes are observed only in birds and mammals. Among the development of various immunoglobulin isotypes, IgD is expressed in bony fishes, later only mammals are using this B-cell receptor [55].

system [90]. Recent studies performed in noncanonic invertebrate model-species indicate that the tracks of adaptive immunity may be much deeper than previously suggested, referring to adaptivelike immunological functions present in invertebrates [91].

6. PERSPECTIVES ON INNATE AND ADAPTIVE IMMUNITY

According to the orthodox view of phylogenetic development, immunity has reached its zenith with the emergence of the adaptive immune system (or AIS) (Figure 2). Consequently, we tend to be influenced by anthropocentric views and overlook how other highly developed organisms manage to live in hostile environments [61]. As more recent data have become available regarding nontraditional animal models, it has been suggested that the emergence of adaptive immunity is perhaps not the culmination of the evolution of immunity, but simply a successful alternative to using innate immunity alone [92]. For millions of years, many species could keep up in the continuous arms race between pathogen and host called coevolution without the surveillance of adaptive immunity [93]. The complexity of biology should never be underestimated as it turns out that those animals lacking RAG-dependent adaptive immunity can make up for an equal amount of diversity using highly variable elements of innate immunity (FREPs, DsCAM, SRCRs) finally exhibiting adaptive features [59, 92–94]. On the other hand, in vertebrates, adaptive immunity often simply serves as a sophisticated targeting device that recognizes and then processes the antigen but finally leaves the messy job of actually clearing up pathogens to the immense capacity of innate immunity. Therefore, once again we see that borders are *blurring* and the strict distinction between innate and adaptive immunities might need revision (Figure 3).

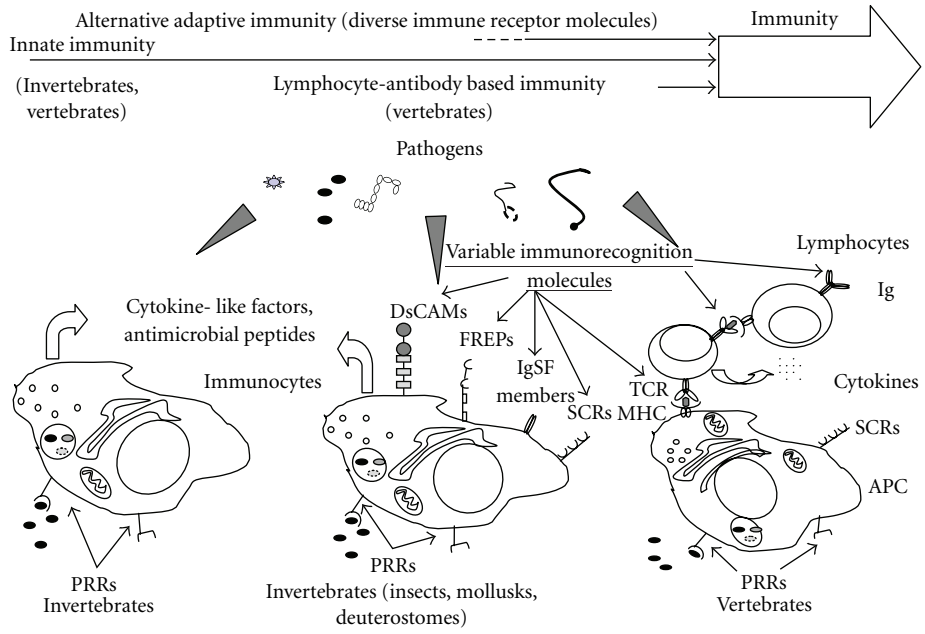

Figure 3: *Schematic representation of innate and adaptive immune feature development in animals.* All immune cells express nonspecific receptors, for example, pattern recognition receptors that recognize pathogen associated molecular patterns (PAMPs). Several clusters of innate receptors are conserved from plants to humans and are essential components in the defense of self-integrity. Immune cells of invertebrates also express various scavenger receptorlike proteins (Croquemort, SCRs) [37, 38, 52, 56, 57], immunglobulin superfamily members (hemolin, DsCAM) [58, 59], and fibrinogen-related peptides (FREPs) [60]; all involved in immune functions (eliminating apoptotic cells, parasites, etc.). Invertebrate immune systems also exhibit receptors with high diversity involved in immune functions: FREPs, SCRs, and DsCAMs have extreme individual variability [60–62] like vertebrate adaptive immune recognition molecules (Ig, TcR).

REFERENCES

[1] F. M. Burnet, *The Clonal Selection Theory of Acquired Immunity*, Vanderbilt University Press, Nashville, Tenn, USA, 1959.

[2] C. A. Janeway Jr., "The immune system evolved to discriminate infectious nonself from noninfectious self," *Immunology Today*, vol. 13, no. 1, pp. 11–16, 1992.

[3] P. Matzinger, "The danger model in its historical context," *Scandinavian Journal of Immunology*, vol. 54, no. 1-2, pp. 4–9, 2001.

[4] P. Matzinger, "Tolerance, danger, and the extended family," *Annual Review of Immunology*, vol. 12, pp. 991–1045, 1994.

[5] C. Hörner, A. Bouchon, A. Bierhaus, et al., "Role of the innate immune response in sepsis," *Der Anaesthesist*, vol. 53, no. 1, pp. 10–28, 2004.

[6] E. L. Cooper, B. Rinkevich, G. Uhlenbruck, and P. Valembois, "Invertebrate immunity: another viewpoint," *Scandinavian Journal of Immunology*, vol. 35, no. 3, pp. 247–266, 1992.

[7] T. J. Little, D. Hultmark, and A. F. Read, "Invertebrate immunity and the limits of mechanistic immunology," *Nature Immunology*, vol. 6, no. 7, pp. 651–654, 2005.

[8] J. Kurtz, "Specific memory within innate immune systems," *Trends in Immunology*, vol. 26, no. 4, pp. 186–192, 2005.

[9] G. G. Petrányi, "The complexity of immune and alloimmune response," *Transplant Immunology*, vol. 10, no. 2-3, pp. 91–100, 2002.

[10] S. H. Cahan and S. B. Vinson, "Reproductive division of labor between hybrid and nonhybrid offspring in a fire ant hybrid zone," *Evolution*, vol. 57, no. 7, pp. 1562–1570, 2003.

[11] K. Saitoh, I.-S. Kim, and E.-H. Lee, "Mitochondrial gene introgression between spined loaches via hybridogenesis," *Zoological Science*, vol. 21, no. 7, pp. 795–798, 2004.

[12] D. S. Schmeller, A. Seitz, A. Crivelli, and M. Veith, "Crossing species' range borders: interspecies gene exchange mediated by hybridogenesis," *Proceedings of the Royal Society B*, vol. 272, no. 1572, pp. 1625–1631, 2005.

[13] A. L. Hughes, "Genomic catastrophism and the origin of vertebrate immunity," *Archivum Immunologiae et Therapiae Experimentalis*, vol. 47, no. 6, pp. 347–353, 1999.

[14] A. L. Hughes, "Natural selection and the diversification of vertebrate immune effectors," *Immunological Reviews*, vol. 190, no. 1, pp. 161–168, 2002.

[15] J. Rolff and M. T. Siva-Jothy, "Invertebrate ecological immunology," *Science*, vol. 301, no. 5632, pp. 472–475, 2003.

[16] J. Kurtz, I. T. van der Veen, and J. J. Ryder, "Ecological immunity of arthropods-a thread of Ariadne?" *Trends in Ecology & Evolution*, vol. 17, no. 5, pp. 204–205, 2002.

[17] P. Schmid-Hempel, "Evolutionary ecology of insect immune defenses," *Annual Review of Entomology*, vol. 50, pp. 529–551, 2005.

[18] J. Klein, "Homology between immune responses in vertebrates and invertebrates: does it exist?" *Scandinavian Journal of Immunology*, vol. 46, no. 6, pp. 558–564, 1997.

[19] C. Vogel and C. Chothia, "Protein family expansions and biological complexity," *PLoS Computational Biology*, vol. 2, no. 5, p. e48, 2006.

[20] E. L. Cooper and B. S. Baculi, "Degenerative changes in the annelid, *Lumbricus terrestris*," *Journals of Gerontology*, vol. 23, no. 3, pp. 375–381, 1968.

[21] G. Romhányi, "Selective differentiation between amyloid and connective tissue structures based on the collagen specific topo-optical staining reaction with Congo red," *Virchows Archiv*, vol. 354, no. 3, pp. 209–222, 1971.

[22] E. L. Cooper, "Invertebrates can tell us something about senescence," *Aging Clinical and Experimental Research*, vol. 6, no. 1, pp. 5–23, 1994.

[23] B. DeVeale, T. Brummel, and L. Seroude, "Immunity and aging: the enemy within?" *Aging Cell*, vol. 3, no. 4, pp. 195–208, 2004.

[24] A. Olgun, T. Aleksenko, O. M. Pereira-Smith, and D. K. Vassilatis, "Functional analysis of MRG-1: the ortholog of human MRG15 in *Caenorhabditis elegans*," *Journals of Gerontology A*, vol. 60, no. 5, pp. 543–548, 2005.

[25] M. E. Giannakou, M. Goss, J. Jacobson, G. Vinti, S. J. Leevers, and L. Partridge, "Dynamics of the action of *dFOXO* on adult mortality in *Drosophila*," *Aging Cell*, vol. 6, no. 4, pp. 429–438, 2007.

[26] C. L. Kurz and M.-W. Tan, "Regulation of aging and innate immunity in *C. elegans*," *Aging Cell*, vol. 3, no. 4, pp. 185–193, 2004.

[27] C. M. Ciocan and J. M. Rotchell, "Conservation of cancer genes in the marine invertebrate *Mytilus edulis*," *Environmental Science and Technology*, vol. 39, no. 9, pp. 3029–3033, 2005.

[28] D. J. Christensen, C. A. Farley, and F. G. Kern, "Epizootic neoplasms in the clam *Macoma balthica* (L.) from Chesapeake Bay," *Journal of the National Cancer Institute*, vol. 52, no. 6, pp. 1739–1749, 1974.

[29] C. A. Farley, D. L. Plutschak, and R. F. Scott, "Epizootiology and distribution of transmissible sarcoma in Maryland soft-shell clams, *Mya arenaria*, 1984–1988," *Environmental Health Perspectives*, vol. 90, pp. 35–41, 1991.

[30] C. F. Dungan, R. M. Hamilton, K. L. Hudson, C. B. McCollough, and K. S. Reece, "Two epizootic diseases in Chesapeake Bay commercial clams, *Mya arenaria* and *Tagelus plebeius*," *Diseases of Aquatic Organisms*, vol. 50, no. 1, pp. 67–78, 2002.

[31] T. Loop, R. Leemans, U. Stiefel, et al., "Transcriptional signature of an adult brain tumor in *Drosophila*," *BMC Genomics*, vol. 5, no. 1, p. 24, 2004.

[32] P. J. Bryant, K. L. Watson, R. W. Justice, and D. F. Woods, "Tumor suppressor genes encoding proteins required for cell interactions and signal transduction in *Drosophila*," *Development*, vol. 119, pp. 239–249, 1993.

[33] E. Gateff, J. Wismar, N. Habtemichael, et al., "Functional analysis of *Drosophila* developmental genes instrumental in tumor suppression," *In Vivo*, vol. 10, no. 2, pp. 211–216, 1996.

[34] K. L. Watson, R. W. Justice, and P. J. Bryant, "*Drosophila* in cancer research: the first fifty tumor suppressor genes," *Journal of Cell Science*, vol. 18, pp. 19–33, 1994.

[35] L. C. Smith and W. H. Hildemann, "Allograft rejection, autograft fusion and inflammatory responses to injury in *Callyspongia diffusa* (Porifera; Demospongia)," *Proceedings of the Royal Society of London Series B*, vol. 226, no. 1245, pp. 445–464, 1986.

[36] W. E. G. Müller, B. Blumbach, and I. M. Müller, "Evolution of the innate and adaptive immune systems: relationships between potential immune molecules in the lowest metazoan phylum (Porifera) and those in vertebrates," *Transplantation*, vol. 68, no. 9, pp. 1215–1227, 1999.

[37] J. L. Theodor, "Distinction between "self" and "not-self" in lower invertebrates," *Nature*, vol. 227, no. 259, pp. 690–692, 1970.

[38] W. H. Hildemann, R. L. Raison, G. Cheung, C. J. Hull, L. Akaka, J. Okamoto, et al., "Immunological specificity and memory in a scleractinian coral," *Nature*, vol. 270, no. 5634, pp. 219–223, 1977.

[39] J. Bierne and C. Langlet, "Studies on graft immunity in nemerteans of the genus *Lineus* Study of the primary reaction to heterospecies transplantation," *Comptes Rendus Hebdomadaires Des Seances De L'Academie Des Sciences. Serie D: Sciences Naturelles*, vol. 278, no. 10, pp. 1445–1447, 1974.

[40] C. Langlet and J. Bierne, "Transplantation immunity in nemerteans of the genus *lineus* Accelerated rejection of second heterospecific incompatible grafts," *Comptes Rendus Hebdomadaires Des Seances De L'Academie Des Sciences. Serie D: Sciences Naturelles*, vol. 281, no. 9, pp. 595–598, 1975.

[41] C. Langlet and J. Bierne, "Immune characteristics of graft rejection in nemerteans of the genus *Lineus*," *European Journal of Immunology*, vol. 12, no. 9, pp. 705–708, 1982.

[42] C. Langlet and J. Bierne, "Immunocompetent cells requisite for graft rejection in *Lineus* (invertebrata, nemertea)," *Developmental & Comparative Immunology*, vol. 8, no. 3, pp. 547–557, 1984.

[43] E. L. Cooper, "Specific tissue graft rejection in earthworms," *Science*, vol. 166, no. 3911, pp. 1414–1415, 1969.

[44] E. L. Cooper and P. Roch, "Earthworm leukocyte interactions during early stages of graft rejection," *Journal of Experimental Zoology*, vol. 232, no. 1, pp. 67–72, 1984.

[45] G. Tettamanti, A. Grimaldi, R. Ferrarese, et al., "Leech responses to tissue transplantation," *Tissue and Cell*, vol. 35, no. 3, pp. 199–212, 2003.

[46] K. Yamaguchi, E. Furuta, and H. Nakamura, "Chronic skin allograft rejection in terrestrial slugs," *Zoological Science*, vol. 16, no. 3, pp. 485–495, 1999.

[47] R. S. Hartman and R. D. Karp, "Short-term immunologic memory in the allograft response of the American cockroach, *Periplaneta americana*," *Transplantation*, vol. 47, no. 5, pp. 920–922, 1989.

[48] R. D. Karp and C. C. Meade, "Transplantation immunity in the American cockroach, *Periplaneta americana* the rejection of integumentary grafts from *Blatta orientalis*," *Developmental & Comparative Immunology*, vol. 17, no. 4, pp. 301–307, 1993.

[49] K. A. Coffaro and R. T. Hinegardner, "Immune response in the sea urchin *Lytechinus pictus*," *Science*, vol. 197, no. 4311, pp. 1389–1390, 1977.

[50] R. D. Karp and W. H. Hildemann, "Specific allograft reactivity in the sea star *Dermasterias imbricata*," *Transplantation*, vol. 22, no. 5, pp. 434–439, 1976.

[51] B. Rinkevich, I. L. Weissman, and A. W. De Tomaso, "Transplantation of Fu/HC-incompatible zooids in *Botryllus schlosseri* results in chimerism," *Biological Bulletin*, vol. 195, no. 2, pp. 98–106, 1998.

[52] V. L. Scofield, J. M. Schlumpberger, L. A. West, and I. L. Weissman, "Protochordate allorecognition is controlled by a MHC-like gene system," *Nature*, vol. 295, no. 5849, pp. 499–502, 1982.

[53] D. A. Raftos, N. N. Tait, and D. A. Briscoe, "Allograft rejection and alloimmune memory in the solitary urochordate, *Styela plicata*," *Developmental & Comparative Immunology*, vol. 11, no. 2, pp. 343–351, 1987.

[54] D. A. Raftos, D. A. Briscoe, and N. N. Tait, "The mode of recognition of allogeneic tissue in the solitary urochordate *Styela plicata*," *Transplantation*, vol. 45, no. 6, pp. 1123–1126, 1988.

[55] L. Du Pasquier and G. W. Litman, Eds., *Origin and Evolution of the Vertebrate Immune System*, Current Topics in Microbiology and Immunology, Springer, Heidelberg, Germany, 2000.

[56] N. C. Franc, J.-L. Dimarcq, M. Lagueux, J. Hoffmann, and R. A. B. Ezekowitz, "Croquemort, a novel *Drosophila* hemocyte/macrophage receptor that recognizes apoptotic cells," *Immunity*, vol. 4, no. 5, pp. 431–443, 1996.

[57] Z. Pancer, "Dynamic expression of multiple scavenger receptor cysteine-rich genes in coelomocytes of the purple sea urchin," *Proceedings of the National Academy of Sciences of the United States of America*, vol. 97, no. 24, pp. 13156–13161, 2000.

[58] F. L. Watson, R. Püttmann-Holgado, F. Thomas, et al., "Immunology: extensive diversity of Ig-superfamily proteins in the immune system of insects," *Science*, vol. 309, no. 5742, pp. 1874–1878, 2005.

[59] S.-C. Sun, I. Lindstrom, H. G. Boman, I. Faye, and O. Schmidt, "Hemolin: an insect-immune protein belonging to the immunoglobulin superfamily," *Science*, vol. 250, no. 4988, pp. 1729–1732, 1990.

[60] S.-M. Zhang and E. S. Loker, "The *FREP* gene family in the snail *Biomphalaria glabrata* additional members, and evidence consistent with alternative splicing and *FREP* retrosequences," *Developmental & Comparative Immunology*, vol. 27, no. 3, pp. 175–187, 2003.

[61] M. F. Flajnik and L. Du Pasquier, "Evolution of innate and adaptive immunity: can we draw a line?" *Trends in Immunology*, vol. 25, no. 12, pp. 640–644, 2004.

[62] S.-M. Zhang, C. M. Adema, T. B. Kepler, and E. S. Loker, "Diversification of Ig superfamily genes in an invertebrate," *Science*, vol. 305, no. 5681, pp. 251–254, 2004.

[63] E. Espagne, V. Douris, G. Lalmanach, et al., "A virus essential for insect host-parasite interactions encodes cystatins," *Journal of Virology*, vol. 79, no. 15, pp. 9765–9776, 2005.

[64] K. E. Amaya, S. Asgari, R. Jung, M. Hongskula, and N. E. Beckage, "Parasitization of *Manduca sexta* larvae by the parasitoid wasp *Cotesia congregata* induces an impaired host immune response," *Journal of Insect Physiology*, vol. 51, no. 5, pp. 505–512, 2005.

[65] M. Bonvin, D. Marti, S. Wyder, D. Kojic, M. Annaheim, and B. Lanzrein, "Cloning, characterization and analysis by RNA interference of various genes of the *Chelonus inanitus* polydnavirus," *Journal of General Virology*, vol. 86, no. 4, pp. 973–983, 2005.

[66] J. Robalino, T. C. Bartlett, R. W. Chapman, P. S. Gross, C. L. Browdy, and G. W. Warr, "Double-stranded RNA and antiviral immunity in marine shrimp: inducible host mechanisms and evidence for the evolution of viral counter-responses," *Developmental & Comparative Immunology*, vol. 31, no. 6, pp. 539–547, 2007.

[67] E. S. Loker and C. J. Bayne, "Molecular studies of the molluskan response to digenean infection," in *Phylogenetic Perspectives on the Vertebrate Immune Systems*, G. Beck, M. Sungumaran, and E. L. Cooper, Eds., pp. 209–222, Kluwer Academic/Plenum, New York, NY, USA, 2001.

[68] W. H. Hildemann, P. L. Jokiel, C. H. Bigger, and I. S. Johnston, "Allogeneic polymorphism and alloimmune memory in the coral, *Montipora verrucosa*," *Transplantation*, vol. 30, no. 4, pp. 297–301, 1980.

[69] E. L. Cooper and P. Roch, "Second-set allograft responses in the earthworm *Lumbricus terrestris*. Kinetics and characteristics," *Transplantation*, vol. 41, no. 4, pp. 514–520, 1986.

[70] R. K. Hostetter and E. L. Cooper, "Coelomocytes as effector cells in earthworm immunity," *Immunological Communications*, vol. 1, no. 2, pp. 155–183, 1972.

[71] R. K. Hostetter and E. L. Cooper, "Cellular anamnesis in earthworms," *Cellular Immunology*, vol. 9, no. 3, pp. 384–392, 1973.

[72] E. A. Stein and E. L. Cooper, "In vitro agglutinin production by earthworm leukocytes," *Developmental & Comparative Immunology*, vol. 12, no. 3, pp. 531–547, 1988.

[73] E. L. Cooper, A. Cossarizza, M. M. Suzuki, et al., "Autogeneic but not allogeneic earthworm effector coelomocytes kill the mammalian tumor cell target K562," *Cellular Immunology*, vol. 166, no. 1, pp. 113–122, 1995.

[74] A. Cossarizza, E. L. Cooper, M. M. Suzuki, et al., "Earthworm leukocytes that are not phagocytic and cross-react with several human epitopes can kill human tumor cell lines," *Experimental Cell Research*, vol. 224, no. 1, pp. 174–182, 1996.

[75] D. A. Raftos, N. N. Tait, and D. A. Briscoe, "Cellular basis of allograft rejection in the solitary urochordate, *Styela plicata*," *Developmental & Comparative Immunology*, vol. 11, no. 4, pp. 713–725, 1987.

[76] D. A. Raftos and E. L. Cooper, "Proliferation of lymphocyte-like cells from the solitary tunicate, *Styela clava*, in response to allogeneic stimuli," *Journal of Experimental Zoology*, vol. 260, no. 3, pp. 391–400, 1991.

[77] Z. Pancer, E. L. Cooper, and W. E. G. Müller, "A tunicate (*Botryllus schlosseri*) cDNA reveals similarity to vertebrate antigen receptors," *Immunogenetics*, vol. 45, no. 1, pp. 69–72, 1996.

[78] K. Khalturin, M. Becker, B. Rinkevich, and T. C. G. Bosch, "Urochordates and the origin of natural killer cells: identification of a CD94/NKR-P1-related receptor in blood cells of *Botryllus*," *Proceedings of the National Academy of Sciences of the United States of America*, vol. 100, no. 2, pp. 622–627, 2003.

[79] T. Wakoh, M. Ikeda, R. Uchino, et al., "Identification of transcripts expressed preferentially in hemocytes of *Ciona intestinalis* that can be used as molecular markers," *DNA Research*, vol. 11, no. 5, pp. 345–352, 2004.

[80] C. D. Krause and S. Pestka, "Evolution of the class 2 cytokines and receptors, and discovery of new friends and relatives," *Pharmacology & Therapeutics*, vol. 106, no. 3, pp. 299–346, 2005.

[81] L. Du Pasquier, I. Zucchetti, and R. De Santis, "Immunoglobulin superfamily receptors in protochordates: before RAG time," *Immunological Reviews*, vol. 198, no. 1, pp. 233–248, 2004.

[82] K. Azumi, R. De Santis, A. De Tomaso, et al., "Genomic analysis of immunity in a Urochordate and the emergence of the vertebrate immune system: "waiting for Godot"," *Immunogenetics*, vol. 55, no. 8, pp. 570–581, 2003.

[83] D. Malagoli and E. Ottaviani, "Helical cytokines and invertebrate immunity: a new field of research," *Scandinavian Journal of Immunology*, vol. 66, no. 4, pp. 484–485, 2007.

[84] D. Malagoli, D. Conklin, S. Sacchi, M. Mandrioli, and E. Ottaviani, "A putative helical cytokine functioning in innate immune signalling in *Drosophila melanogaster*," *Biochimica et Biophysica Acta (BBA)*, vol. 1770, no. 6, pp. 974–978, 2007.

[85] I. Söderhäll, Y.-A. Kim, P. Jiravanichpaisal, S.-Y. Lee, and K. Söderhäll, "An ancient role for a prokineticin domain in invertebrate hematopoiesis," *Journal of Immunology*, vol. 174, no. 10, pp. 6153–6160, 2005.

[86] Z. Pamcer, C. T. Amemiya, G. R. A. Ehrhardt, J. Coitlin, G. L. Gartland, and M. D. Cooper, "Somatic diversification of variable lymphocyte receptors in the agnathan sea lamprey," *Nature*, vol. 430, no. 6996, pp. 174–180, 2004.

[87] Z. Pancer, N. R. Saha, J. Kasamatsu, et al., "Variable lymphocyte receptors in hagfish," *Proceedings of the National Academy of Sciences of the United States of America*, vol. 102, no. 26, pp. 9224–9229, 2005.

[88] J. P. Cannon, R. N. Haire, Z. Pancer, et al., "Variable domains and a VpreB-like molecule are present in a jawless vertebrate," *Immunogenetics*, vol. 56, no. 12, pp. 924–929, 2005.

[89] M. N. Alder, I. B. Rogozin, L. M. Iyer, G. V. Glazko, M. D. Cooper, and Z. Pancer, "Diversity and function of adaptive immune receptors in a jawless vertebrate," *Science*, vol. 310, no. 5756, pp. 1970–1973, 2005.

[90] J. Klein and N. Nikolaidis, "The descent of the antibody-based immune system by gradual evolution," *Proceedings of the National Academy of Sciences of the United States of America*, vol. 102, no. 1, pp. 169–174, 2005.

[91] J. J. Marchalonis, S. F. Schluter, R. M. Bernstein, and V. S. Hohman, "Antibodies of sharks: revolution and evolution," *Immunological Reviews*, vol. 166, pp. 103–122, 1998.

[92] G. W. Litman, J. P. Cannon, and L. J. Dishaw, "Reconstructing immune phylogeny: new perspectives," *Nature Reviews Immunology*, vol. 5, no. 11, pp. 866–879, 2005.

[93] E. L. Cooper, E. Kauschke, and A. Cossarizza, "Digging for innate immunity since Darwin and Metchnikoff," *BioEssays*, vol. 24, no. 4, pp. 319–333, 2002.

[94] K. Khalturin, U. Kürn, N. Pinnow, and T. C. G. Bosch, "Towards a molecular code for individuality in the absence of MHC: screening for individually variable genes in the urochordate *Ciona intestinalis*," *Developmental & Comparative Immunology*, vol. 29, no. 9, pp. 759–773, 2005.

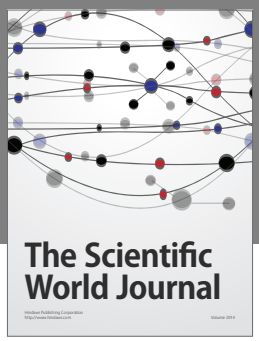

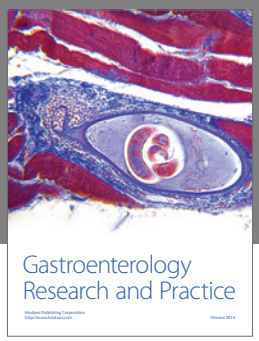

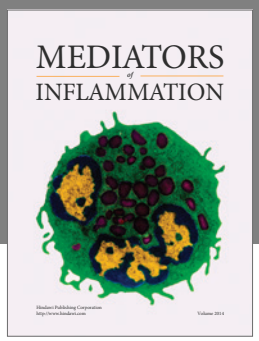

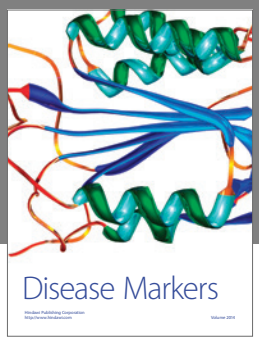

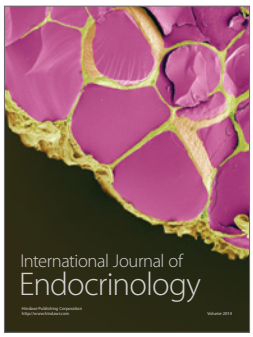

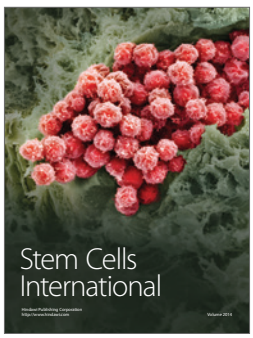

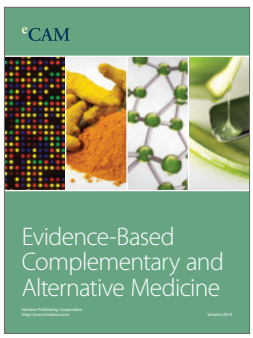

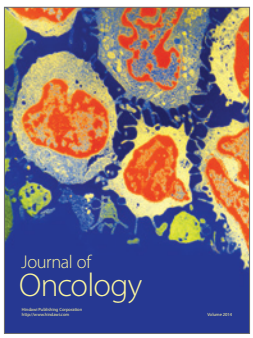

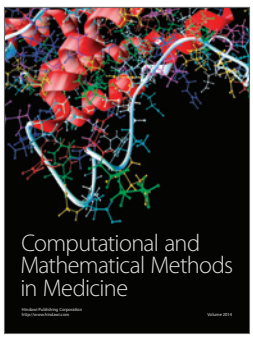

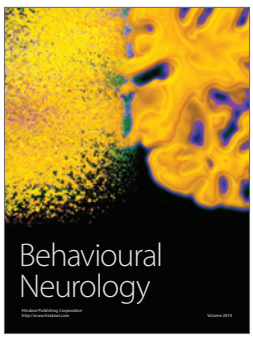

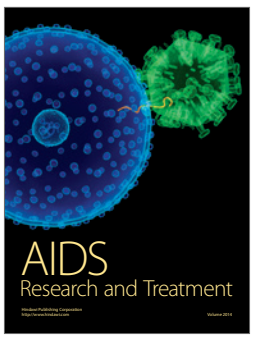

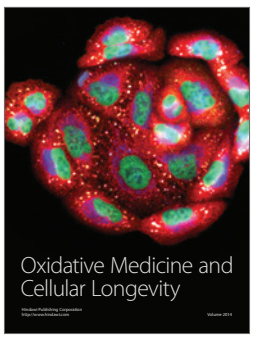

Hindawi

Submit your manuscripts at
http://www.hindawi.com

PLOS | ONE

RESEARCH ARTICLE

Thymic Atrophy and Apoptosis of $CD4^+CD8^+$ Thymocytes in the Cuprizone Model of Multiple Sclerosis

Izabella Solti[1☯], Krisztian Kvell[2☯], Gergely Talaber[3], Sara Veto[1], Peter Acs[4], Ferenc Gallyas, Jr.[1,5,6], Zsolt Illes[7], Katalin Fekete[1], Petra Zalan[1], Arpad Szanto[8], Zita Bognar[1]*

1 Department of Biochemistry and Medical Chemistry, University of Pecs, Pecs, Hungary, **2** Department of Pharmaceutical Biotechnology, University of Pecs, Pecs, Hungary, **3** Karolinska Institutet, Department of Biosciences and Nutrition, NOVUM, Huddinge, Sweden, **4** Department of Neurology, University of Pecs, Pecs, Hungary, **5** MTA-PTE Nuclear-Mitochondrial Research Group, Pecs, Hungary, **6** Szentagothai Research Center, University of Pecs, Pecs, Hungary, **7** Department of Neurology, Odense University Hospital, Institute of Clinical Research, University of Southern Denmark, Odense, Denmark, **8** Department of Urology, University of Pecs, Pecs, Hungary

☯ These authors contributed equally to this work.
* zita.bognar@aok.pte.hu

CrossMark
click for updates

OPEN ACCESS

Citation: Solti I, Kvell K, Talaber G, Veto S, Acs P, Gallyas F, Jr., et al. (2015) Thymic Atrophy and Apoptosis of $CD4^+CD8^+$ Thymocytes in the Cuprizone Model of Multiple Sclerosis. PLoS ONE 10(6): e0129217. doi:10.1371/journal.pone.0129217

Academic Editor: Arun Rishi, Wayne State University, UNITED STATES

Received: February 24, 2015

Accepted: May 6, 2015

Published: June 8, 2015

Copyright: © 2015 Solti et al. This is an open access article distributed under the terms of the Creative Commons Attribution License, which permits unrestricted use, distribution, and reproduction in any medium, provided the original author and source are credited.

Data Availability Statement: All relevant data are within the paper.

Funding: This work was supported by Hungarian grants OTKA NN109841 (FG) and PTE AOK KA 2013/4 (ZB). The funders had no role in study design, data collection and analysis, decision to publish, or preparation of the manuscript.

Competing Interests: The authors have declared that no competing interests exist.

Abstract

Previous studies on the degenerative animal model of multiple sclerosis suggested that the copper-chelator cuprizone might directly suppress T-cell functions. Peripheral T-cell function in the cuprizone model has already been explored; therefore, in the present study, we investigated, for the first time, how cuprizone feeding affects the thymus, the organ of T-cell maturation and selection. We found that even one week of cuprizone treatment induced significant thymic atrophy, affecting the cortex over the medulla. Fluorescent microscopy and flow-cytometric analyses of thymi from cuprizone- and vehicle-treated mice indicated that eradication of the cluster of the differentiation-4 (CD4)-CD8 double-positive T-cell subset was behind the substantial cell loss. This result was confirmed with CD3-CD4-CD8 triple-staining experiments. Ultrastructurally, we observed degraded as well as enlarged mitochondria, myelin-bodies, large lipid droplets, and large lysosomes in the thymi of cuprizone-treated mice. Some of these features were similar to those in physiological and steroid-induced accelerated aging. According to our results, apoptosis was mainly of mitochondrial origin mediated by both caspase-3- and apoptosis inducing factor-mediated mechanisms. Additionally, mitogen activated protein kinase activation and increased pro-apoptotic B cell lymphoma-2 family protein expression were the major underlying processes. Our results do not indicate a functional relationship between cuprizone-induced thymus involution and the absence of inflammatory responses or the selective demyelination observed in the cuprizone model. On the other hand, due to the reversible nature of cuprizone's deleterious effects, the cuprizone model could be valuable in studying thymus regeneration as well as remyelination processes.

Introduction

Administration of the copper chelator cuprizone to young adult C57BL/6 mice induces multifocal demyelination mainly in the corpus callosum and superior cerebellar peduncle [1] without significant T-cell activation in the affected areas [2]. According to histopathological studies [3], the pattern of cuprizone-induced demyelination resembles that of type III multiple sclerosis (MS) lesions characterised by oligodendrocyte degeneration and minor inflammation [4]. Therefore, the cuprizone model was extensively used for studying the degenerative aspects of MS [5]. The mechanism of the oligodendrocyte loss and demyelination in the cuprizone model is not well understood. Mature oligodendrocytes seem to be the primary targets, which are eliminated by apoptosis inducing factor (AIF)-mediated apoptosis [6]. Cuprizone-induced early formation of mega-mitoachondria in the liver [7] and oligodendrocytes [8], and expressional and functional changes of mitochondrial enzymes [9,10] indicate mitochondrial dysfunction behind the oligodendrocyte loss. However, there is no explanation for the preferential regional distribution of cuprizone-induced demyelination, and the exclusivity of the cell death toward oligodendrocytes.

Unlike the cuprizone model, experimental allergic encephalomyelitis (EAE) reflects the autoimmune feature of MS [11,12]. In this model, after immunising the animals with myelin antigens, myelin-specific $CD4^+$ T-cells are initially activated in the peripheral immune organs and migrate to the central nervous system (CNS) [13] where they encounter their cognate antigen on CNS antigen presenting cells and produce immune mediators such as pro-inflammatory cytokines and chemokines. These immune mediators locally activate the second cascade of the autoimmune response involving microglia, the resident macrophage [14,15]. In contrast, demyelinating areas in the cuprizone model, were reported to lack B and T-cells, and the blood brain barrier was found to be intact [2,16]. Additionally, with respect to the cuprizone model, RAG-1(1/1) mice, which lack mature B and T lymphocytes are indistinguishable from controls, indicating that T-cells may not play a role in cuprizone-induced demyelination [16]. The major difference between type III MS lesions and cuprizone-induced demyelination is the presence of perivascular inflammation and $CD3^+$ T-cells in the former [4]. This difference, along with the down-regulation of EAE by cuprizone-treatment [16–18] suggests that cuprizone may directly suppress T-cell functions [19]. A previous study [17] has already explored peripheral T-cell function in the cuprizone model. However there is no data regarding the thymus, the organ of T-cell maturation and selection. To elaborate on the suggested suppressive effect of cuprizone on T-cell function, in the present study, we investigated how cuprizone feeding affects the thymus.

Materials and Methods

Ethics Statement

The investigation conforms to the Guide for the Care and Use of Laboratory Animals published by the U.S. National Institutes of Health (NIH Publication No. 85–23, revised 1996), and was approved by the Animal Research Review Committee of the University of Pecs, Medical School.

Animals and cuprizone administration

C57BL/6 male mice were purchased from Charles River Laboratories Hungary Ltd (Isaszeg, Hungary) and kept under standardised, specific pathogen free circumstances. Starting at four weeks of age, mice received a diet of powdered rodent chow containing 0.2% cuprizone (bis-cyclohexanone oxaldihydrazone) (Sigma, Steinheim, Germany) by weight for three or seven days *ad libitum*. Age and gender matched littermates receiving powdered rodent chow served as the control group.

Acquisition of thymus samples

The weight of the mice was measured at the beginning and at the end of the treatment period. Then, animals were euthanised with an overdose of ketamine hydrochloride intraperitoneally, and their chest was opened. The thymi were photographed, carefully dissected and their wet weight was measured. They were freshly processed for RNA isolation, fixed for electron microscopy, frozen for histochemistry and immunohistochemistry, or homogenised in phosphate buffered saline (PBS) with a glass/glass homogeniser. Alternatively, thymic cell suspension was prepared by gentle mechanic agitation followed by filtering through a nylon mesh. The suspension was washed once and the cells were resuspended in PBS. An aliquot of cells was diluted 1:100, the cells were counted using the Trypan blue method with a hemocytometer, and the cell number was set to $5x10^5$ or 10^6 per sample.

Thymic epithelial cell (TEC) enrichment

TECs were enriched as previously described [20]. Briefly, the thymic lobes were digested using a collagenase-based solution. Then TECs were labelled with anti-epithelial cell adhesion molecule- (EpCAM1) antibody followed by their direct enrichment using magnetic beads (Dynabeads). TEC purity was repeatedly found to be approx. 90% based on qRT-PCR measurements as published previously.

Apoptosis detection

For apoptosis detection, double staining with Annexin V-fluorescein isothyocyanate (FITC; BD Pharmingen, CA) and propidium-iodide (Sigma-Aldrich) was performed according to Vermes et al. [21]. Briefly, $5x10^5$ thymocytes were resuspended in 100 μl Annexin binding buffer (10mM HEPES/NaOH, pH 7.4, 140mM NaCl and 2.5mM $CaCl_2$) and incubated for 20 minutes at room temperature with Annexin V-FITC in the dark, before then being diluted with 400 μl Annexin binding puffer. Propidium-iodide was given to the cells immediately before the flow-cytometric analysis. Two-parameter dot-plots showing Annexin V/propidium-iodide staining (FL1/FL3 channels) were created to determine the ratio of apoptotic cells in the thymus glands.

Flow-cytometry

For the simultaneous detection of cell surface expressed CD4, CD8 and CD3, a triple labelling technique was used. Thymocyte samples were incubated with monoclonal antibody cocktails for 30 min in 100 ml binding buffer on ice (PBS containing 0.1% NaN_3 and 0.1% BSA), then washed twice in PBS, and finally resuspended in 500 ml 0.1% buffered PFA (paraformaldehyde) in PBS. For staining the following monoclonal antibodies were used: phycoerythrin (PE) conjugated rat anti-mouse CD4, CyChrome (CyC) conjugated rat anti-mouse CD8 and FITC conjugated rat anti-mouse CD3, all purchased from BD Pharmingen, CA. Samples were measured and analysed in a FACSCalibur flow-cytometer (Becton Dickinson, San Jose, CA), using the CellQuest software. Generally 10.000 events were recorded. Thymocytes were gated according to their size and granularity on forward and side scatter dot plots. The gate set on untreated control living thymocytes was used for the analysis of all samples. We used fluorescent dot plots for both comparing the different samples and for calculating the ratio of positively stained cells.

Immunofluorescence

Frozen thymic sections (7–10 μm thick) were fixed in cold acetone, then air-dried and blocked using 5% bovine serum albumin (BSA) in PBS for 20 min before staining with a-Ly51-PE (clone

6C3, BD Biosciences) and a-EpCAM1-FITC (clone G8.8, hybridoma from the Dept. Immunology and Biotechnology, University of Pecs) antibodies for at least 30 minutes to visualise the thymic epithelial network (EpCAM-1 is a marker for all TECs, but stains the medullar area stronger than the cortical area, while Ly51 stains only cortical TECs). The remaining sections were stained under the same conditions with a-CD4-FITC (YTS191.1, hybridoma from the Dept. Immunology and Biotechnology, University of Pecs) and a-CD8-Alexa fluor 647 (clone 53–6.7, BD Biosciences) to analyse the staining pattern of the thymocytes. The sections were analysed using an Olympus BX61 microscope equipped with CCD-camera and AnalySIS software.

Electron microscopy

In order to investigate ultra-structural changes of the thymic lobes, mice were sacrificed after three days of treatment and their thymi were fixed in buffered 2.5% formaldehyde—2.5% glutaraldehyde solution for 24 hours at 4°C. After washing in phosphate buffer, the samples were fixed in 1% osmium tetroxide in 0.1 M PBS for 35 minutes. After that, the samples were washed in buffer several times for 10 minutes and dehydrated in an ascending ethanol series, including a step of uranyl acetate (1%) solution in 70% ethanol to increase contrast. Dehydrated blocks were transferred to propylene oxide before being placed into aluminium-foil boats containing Durcupan resin (Sigma) and then embedded in gelatine capsules containing Durcupan. The blocks were placed in thermostate for 48 hours at 56°C. From the embedded blocks 1 μm semithin and serial ultrathin sections (70 nanometer) were cut with Leica ultramicrotome, and mounted either on mesh, or on Collodion-coated (Parlodion, Electron Microscopy Sciences, Fort Washington, PA) single-slot copper grids. Additional contrast was provided to these sections with uranyl acetate and lead citrate solutions, and they were examined with JEOL 1200EX-II electron microscope.

Immunoblot analysis

Tissue samples were taken from animals sacrificed after three or seven days of treatment. The thymi of the mice were carefully dissected and 25 mg tissues were homogenised in ice-cold 10 mM Tris buffer, pH 7.4 (containing 0.5 mM sodium metavanadate, 1mM EDTA and protease inhibitor cocktail (1:200); all purchased from Sigma-Aldrich, Steinheim, Germany). Homogenates (10 μg each) were boiled and subjected to 10% sodium dodecyl sulphate polyacrylamide gel electrophoresis then were transferred to nitrocellulose membranes. The membranes were blocked in 5% low fat milk for 1.5 h at room temperature before then being exposed to primary antibodies at 4°C overnight in a blocking solution. The following antibodies were used: Polyclonal caspase 3 (1:500, clone H-277), monoclonal Histone H1(1:200), polyclonal Cytochrome c, polyclonal AIF, monoclonal phospho-p38 MAPK (Thr180/Tyr182), polyclonal phospho-extracellular signal-regulated kinase (ERK)1/2 (Thr202/Tyr204), polyclonal phospho-specific c-Jun N-terminal kinase (JNK) Thr183-Tyr185, polyclonal Bad (D24A9), polyclonal phospho-Bad (Ser112), polyclonal BIM and polyclonal Bax antibodies (each 1:500 dilution), monoclonal Glyceraldehyde-3-phosphate dehydrogenase (1:2000, clone 6C5). Antibodies were purchased from Cell Signaling Technology (Beverly, MA, USA) except from caspase 3, Histone H1 that were bought from Santa Cruz Biotechnology (Wembley, UK), Glyceraldehyde-3-phosphate dehydrogenase antibody was obtained from Merck Millipore. Appropriate horseradish peroxidase-conjugated secondary antibodies were used at a 1:5.000 dilution (anti-mouse and anti-rabbit IgGs; Sigma-Aldrich, Steinheim, Germany) and visualised by enhanced chemiluminescence (Amersham Biosciences, Piscataway, New Jersey, USA). The films were scanned, and the pixel volumes of the bands were determined using NIH Image J software (Bethesda, Maryland, USA). For membrane stripping and re-probing, the membranes were washed in a stripping

buffer (0.1 M glycine, 5 M $MgCl_2$, pH 2.8) for an hour at room temperature. After washing and blocking, the membranes were incubated with primary antibodies for non-phosphorylated or loading control proteins.

RNA isolation and quantitative polymerase chain reaction (qPCR) analysis

To investigate the relative expression of thymic epithelial cell markers major histocompatibility complex (MHC)II and autoimmune regulator (AIRE), we used a real-time qPCR approach after seven days of treatment. From carefully dissected thymi, the total RNA was extracted and DNase digestion was performed using the NucleoSpin RNA isolation kit (Macherey-Nagel, Düren, Germany) as described in the manufacturer's manual. For quality control, RNA purity was verified using the optical density $(OD)_{260/280}$ ratio and was found to be between 1.8 and 2.0. The total RNA (1.0μg) was reverse-transcribed to cDNA using the High-Capacity cDNA reverse transcription kit (Applied Biosystems). Subsequent qPCR reactions for MHCII and AIRE were performed in duplicate on the Applied Biosystems HT7500 system using the Absolute QPCR SYBR Green low ROX Mix (Abgene, Epsom, UK) with specific primers (MHC II forward primer: 5′ -CTA GCC AAG TCC CTC CTA AGG-3′ , reverse primer: 5′ - ATC TCA GAC TGA TCC TGG CAT -3′ ; AIRE forward primer: 5′ -ACC TAA ACC AGT CCC GGA AAG-3 ', reverse primer: 5′ -CGA GGC TCC AGT GCT T-3′). The three step qPCR was performed using 58°C annealing temperature and 30sec elongation period. Analysing melting curves validated the specificity of products from each primer set. All experimental samples were analysed and normalised with the internal control gene, 18 S rRNA (forward primer: 5′ -GGG TCG GGA GTG GGT AAT TT-3′ , reverse primer: 5′ -AGA AAC GGC TAC CAC ATC CAA-3′). Relative quantification of the fold-change was performed comparing *Ct* values from individual mice, applying the $2^{-\Delta\Delta Ct}$ method [22,23].

Statistical analysis

All experiments were repeated at least three times, including at least three animals in each group, for each experiment. Accordingly, the mean + the standard error of the mean (SEM) values of the individual animals ($n \geq 9$) were presented in the figures and throughout the text. On the other hand, for comparing groups, we utilised data of the experiments repeated at least three times, including at least three animals in each groups. We used one-way or two-way analysis of variance, followed by Tukey's post-hoc test. When the F-test indicated unequal variances, the Kruskal-Wallis test was performed. Differences were considered significant at values of $p<0.05$ or lower.

Results

Cuprizone induced acute thymic atrophy

In order to investigate the effect of cuprizone on the thymus, four-week-old male C57BL/6 mice were fed with pulverised chow containing 0.2% of the drug. As early as after one week of cuprizone administration, severe thymic atrophy was observed (Fig 1) that was accompanied by significant thymic tissue mass loss when compared to the control (Fig 1B). Since cuprizone treatment resulted in a significant weight loss for the animals as well (Fig 1C), we normalised their thymic mass to their body mass, and found this relative thymus mass still reduced in the cuprizone-treated mice (Fig 1D), indicating a disproportional thymus involution in these animals. The absolute thymocyte number was also found to be lowered from $1.7\pm0.2 \times 10^8$ to $7.8 \pm 2.3 \times 10^6$ upon cuprizone treatment.

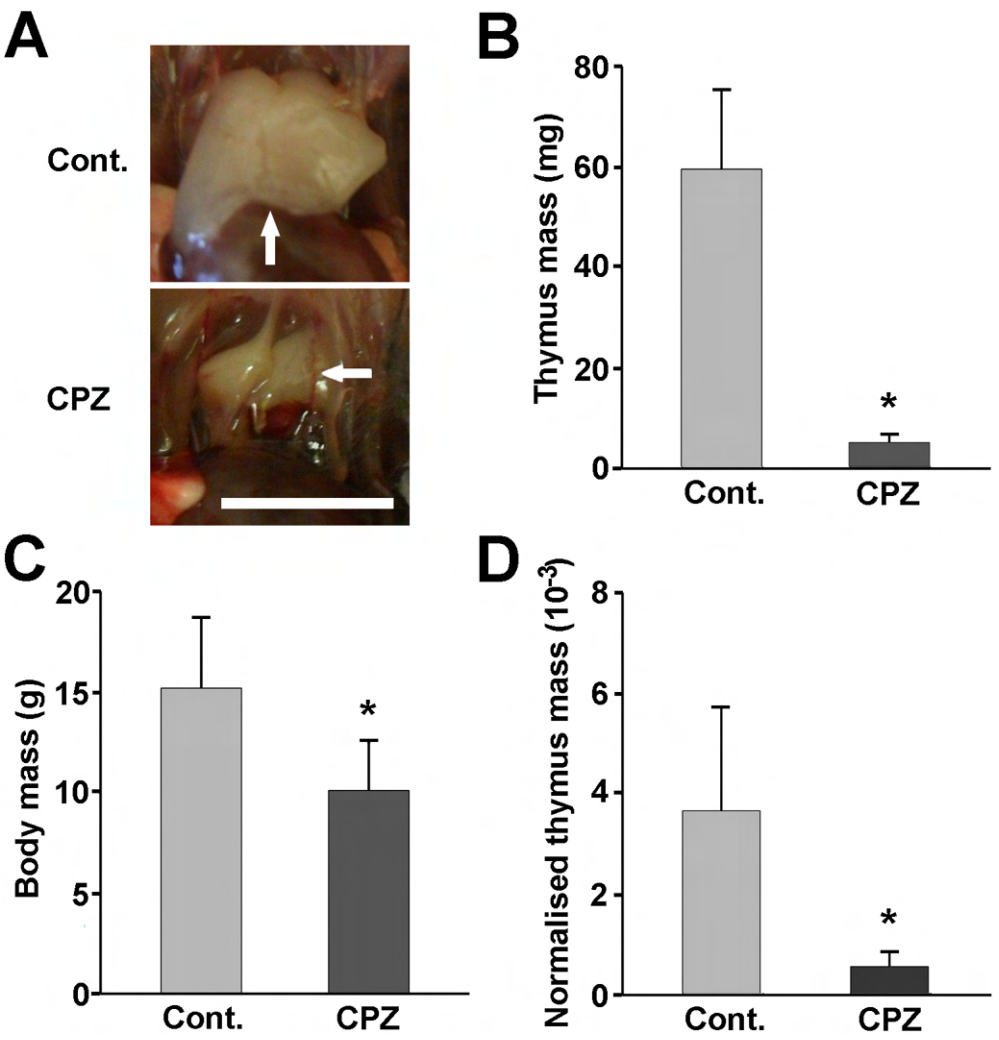

Fig 1. Macroscopic changes of the thymi upon cuprizone treatment. Four week-old male mice were treated with cuprizone for one week. Representative photographs (A) of the open chest of a control (Cont.) and a cuprizone-treated (CPZ) animal are demonstrated. Arrows point to the thymi of the mice. The scale bar indicates 5 mm. Thymus mass (B), body mass (C) and relative thymus mass (thymus tissue mass/ body mass) (E) of control (grey bars) and cuprizone-treated (black bars) animals are presented as bar diagrams, mean + SEM ($n \geq 9$). * denotes a significant difference from control $p<0.05$.

doi:10.1371/journal.pone.0129217.g001

Cuprizone-induced cell death was predominantly apoptotic

We investigated the type of cell death responsible for the substantial cuprizone-induced thymic involution by performing flow-cytometry on the thymic cell suspension following double staining the cells with FITC-conjugated Annexin V and propidium iodide. Propidium iodide is excluded by viable cells. On the other hand, it can penetrate cell membranes of dying or dead cells, and intercalate into double-stranded nucleic acids, thereby increasing the intensity of its fluorescence manyfold. Annexin V binds to phosphatidylserine exposed on the surface of apoptotic cells only, and therefore, this staining technique can differentiate between living (double negative), early apoptotic (Annexin V single positive), and late apoptotic/necrotic (AnnexinV and propidium iodide double positive) cells. As we found, in the untreated control mice, most of the cells were double negative (83.9 ± 4.1%), which was substantially decreased in cuprizone treated animals (22.8 ± 13.2%, $p<0.001$, Fig 2). In these mice, the decrease in the living cells

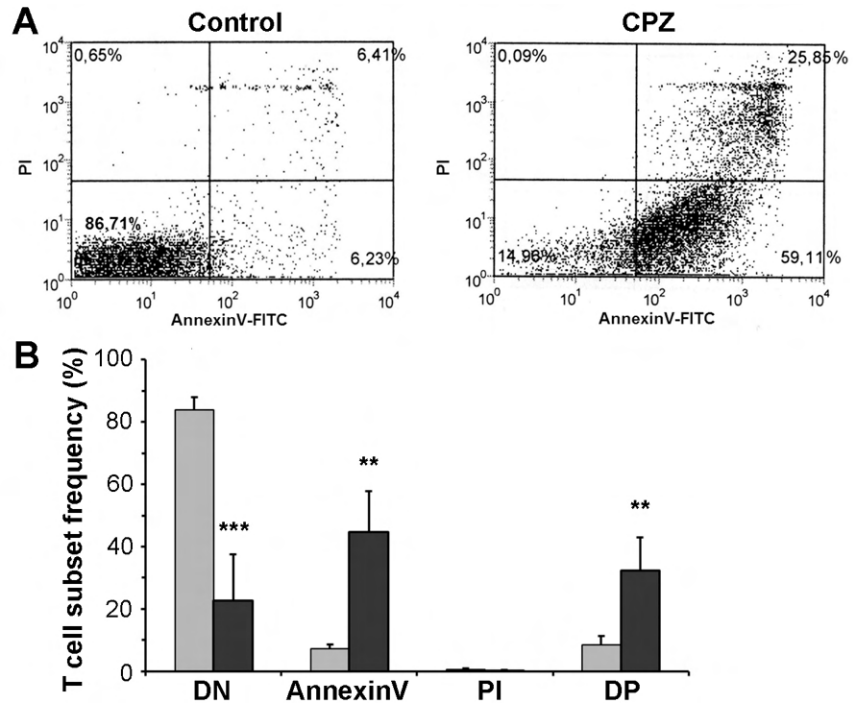

Fig 2. Characterisation of cuprizone-induced cell death. Four week-old male mice were treated with cuprizone for one week. Type of cell death was determined using flow cytometry following double staining with FITC-labelled AnnexinV and propidium iodide thymus suspensions of untreated (Control, grey bars) and cuprizone-treated (CPZ, black bars) mice. Results are presented as representative dot-plots (A) and bar diagrams (B), mean + SEM ($n \geq 9$). Significant difference from control; **p<0.01, *** p<0.001. DN: live cells (lower left quadrant); AnnexinV: early apoptotic cells (lower right quadrant); PI: necrotic cells (upper left quadrant); DP: late apoptotic cells (upper right quadrant).

doi:10.1371/journal.pone.0129217.g002

was accompanied by a significant increase of the early apoptotic (44.6 ± 13.2%, $p<0.001$) and late apoptotic/necrotic cells (32.4 ± 10.5%, $p<0.01$, respectively Fig 2). We could not observe propidium iodide single positivity among the animals regardless of the treatment. All these data indicate that the cuprizone-induced death was preponderantly apoptotic.

Cuprizone-induced cell loss in the cortex was more severe than in the medulla

We determined macroscopic morphological characteristics of the cuprizone-induced thymus involution by fluorescent microscopy after double staining thymus sections with FITC-labelled anti-EpCAM1 and PE-labelled anti-Ly-51 antibodies. The former antibody stains mostly the medulla while the latter stains the cortex of the thymus. We observed more substantial cell loss in the cortex than in the medulla (Fig 3A). To support these findings, we determined the MHCII and AIRE mRNA levels in the thymi of the control and cuprizone treated mice. We found a significant abundance of both of these medulla-associated markers in the cuprizone treated animals (Fig 3B), indicating that cuprizone preferentially affected cortical cells.

Cuprizone eliminated mostly the CD4-CD8 double positive immature thymocytes

To further analyse cuprizone's effect on the thymus, we performed anti-CD4 (green) and anti-CD8 (red) immunofluorescence microscopies. On merged images of the control thymi, the

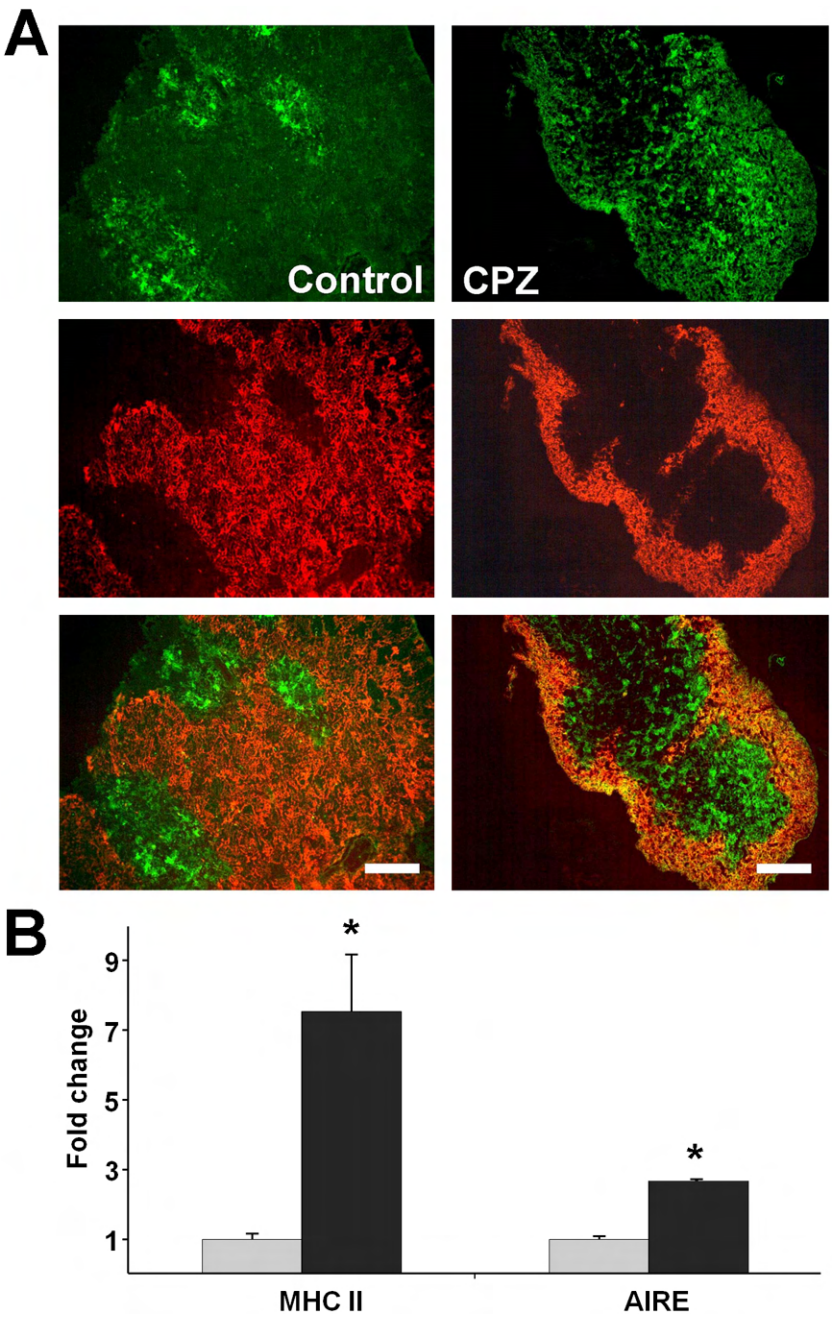

Fig 3. Effect of cuprizone on thymic epithelial cells. Four week-old male mice were treated with cuprizone for one week, then immune-staining (A) with FITC-labelled anti-EpCAM1 (green) and PE-labelled anti-Ly-51 (red) antibodies was performed on thymic sections of untreated (Control) and cuprizone-treated (CPZ) mice. Representative images (A) are presented of the green channel (top panels), the red channel (middle panels) and the merged channels (bottom panels) of three independent experiments, including at least three animals in each group for each experiment. Fluorescent photographs were taken using a 10x objective. The scale bar indicates 200 μm. In a parallel experiment, thymic MHC II and AIRE mRNA expression (B) was determined by using qPCR analysis in untreated (grey bars) and cuprizone-treated (black bars) mice. Results are presented as fold change, mean + SEM ($n \geq 9$). Significant difference from control; *$p<0.05$.

doi:10.1371/journal.pone.0129217.g003

cortex appeared yellow as it is mainly occupied by $CD4^+CD8^+$ thymocytes while the medulla appeared green because of the predominance of $CD4^+$ cells (Fig 4A). Cuprizone-treatment resulted in an almost complete disappearance of the double positive and a relative increase of the $CD4^+$ areas, as well as an overall less dense staining of the shrunken thymi (Fig 4A). To ensure that the double positivity of the control cortices indeed resulted mainly from the presence of the $CD4^+CD8^+$ thymocytes, we performed anti-CD4 and anti-CD8 flow-cytometry on the thymic suspensions. To exclude dead or apoptotic cells, the gate was set on untreated control thymocytes and was fixed for the whole analysis. In the case of the four week-old male C57BL/6 control mice, we found that the most considerable population was that of $CD4^+CD8^+$ thymocytes (73.4 ± 2.6%, Fig 4B and 4C). The most immature $CD4^-CD8^-$ thymocytes made up 9.8 ± 5.3%, while the most mature $CD4^+$ and $CD8^+$ thymocytes represented 11.6 ± 2.2 and 5.3 ± 1.7% of the total population, respectively (Fig 4B and 4C). One week of cuprizone treatment completely eradicated $CD4^+CD8^+$ thymocytes (1.0 ± 0.1%, $p<0.001$, Fig 4B and 4C). If we consider the total cell numbers of the thymi, this decrease was from $1.3 \pm 0.2 \times 10^8$ to $8.1 \pm 3.5 \times 10^4$ double positive thymocytes suggesting a complete disappearance of this cell population. This finding is reflected by a decrease of the double positive/double negative thymocyte ratio from 7.5 ± 4.5 to 0.04 ± 0.02 ($p<0.001$) upon cuprizone treatment, while all other ratios ($CD4^+/CD8^+$ and $CD4^+$/double negative) remained practically unchanged (Fig 4C).

CD3 expression increases along thymocyte maturation. Accordingly, we stained thymus suspensions for CD3, performed flow-cytometry, and assessed the ratio of immature ($CD3^{low}$) and mature ($CD3^{high}$) thymocytes in the untreated and cuprizone-treated groups. In four week-old male C57BL/6 control mice, we found that the $CD3^{low}$ and $CD3^{high}$ thymocytes comprised about 76 and 19%, respectively, of the whole thymocyte population. One week of cuprizone treatment resulted in a significantly lower proportion of immature thymocytes (28.2 ± 8.8, $p<0.001$) and a corresponding increase in the ratios of mature (67.5 ± 8.5, $p<0.001$) thymocytes (Fig 5A and 5B). Thereby, cuprizone treatment increased the $CD3^{high}/CD3^{low}$ ratio from about 0.25 to 2.4 ($p<0.001$, Fig 5B) indicating that cuprizone eliminated immature thymocytes preferentially. Additionally, we triple stained thymocytes of control and cuprizone-treated animals for CD3, CD4 and CD8, and performed flow cytometry on them. When we filtered the results for the $CD3^{low}$ (Fig 5C and 5D) and $CD3^{high}$ (Fig 5E and 5F) subpopulations, we found changes in the T-cell subset frequencies upon cuprizone treatment that were completely consistent with those we found on the unfiltered population, as well as being consistent with our present knowledge of CD3, CD4 and CD8 expression during thymocyte maturation. Namely, almost all CD4-CD8 double positive cells were $CD3^{low}$ and were almost completely depleted by cuprizone (Fig 5C and 5D). Additionally, there was CD8 and CD4 dominance in the $CD3^{low}$ and $CD3^{high}$ subset, respectively that was augmented by the cuprizone treatment (Fig 5C–5F).

Cuprizone induces subcellular structural alterations in thymic cells

Cuprizone was reported to induce giant mitochondria formation and mitochondrial malfunctioning in mouse liver [24]. Since mitochondria are major regulators of the cell death process [25], we assessed cuprizone's effect on thymic mitochondria by using electron microscopy. As demonstrated in Fig 6, cuprizone-treated thymic cells contained both enlarged and medium-sized mitochondria (Fig 6B); the latter are similar to those observed in untreated animals (Fig 6A). The diameter of the enlarged mitochondria did not reach 1 μm, the conventional threshold to be categorised as mega-mitochondria [26]. In addition to enlarged mitochondria, cuprozine treatment resulted in the degradation of cellular organelles, such as mitochondria (Fig 6C). Myelin-bodies (Fig 6C), large lipid droplets (Fig 6D) and large lysosomes packed with dark-staining material (Fig 6E) were also frequently observed.

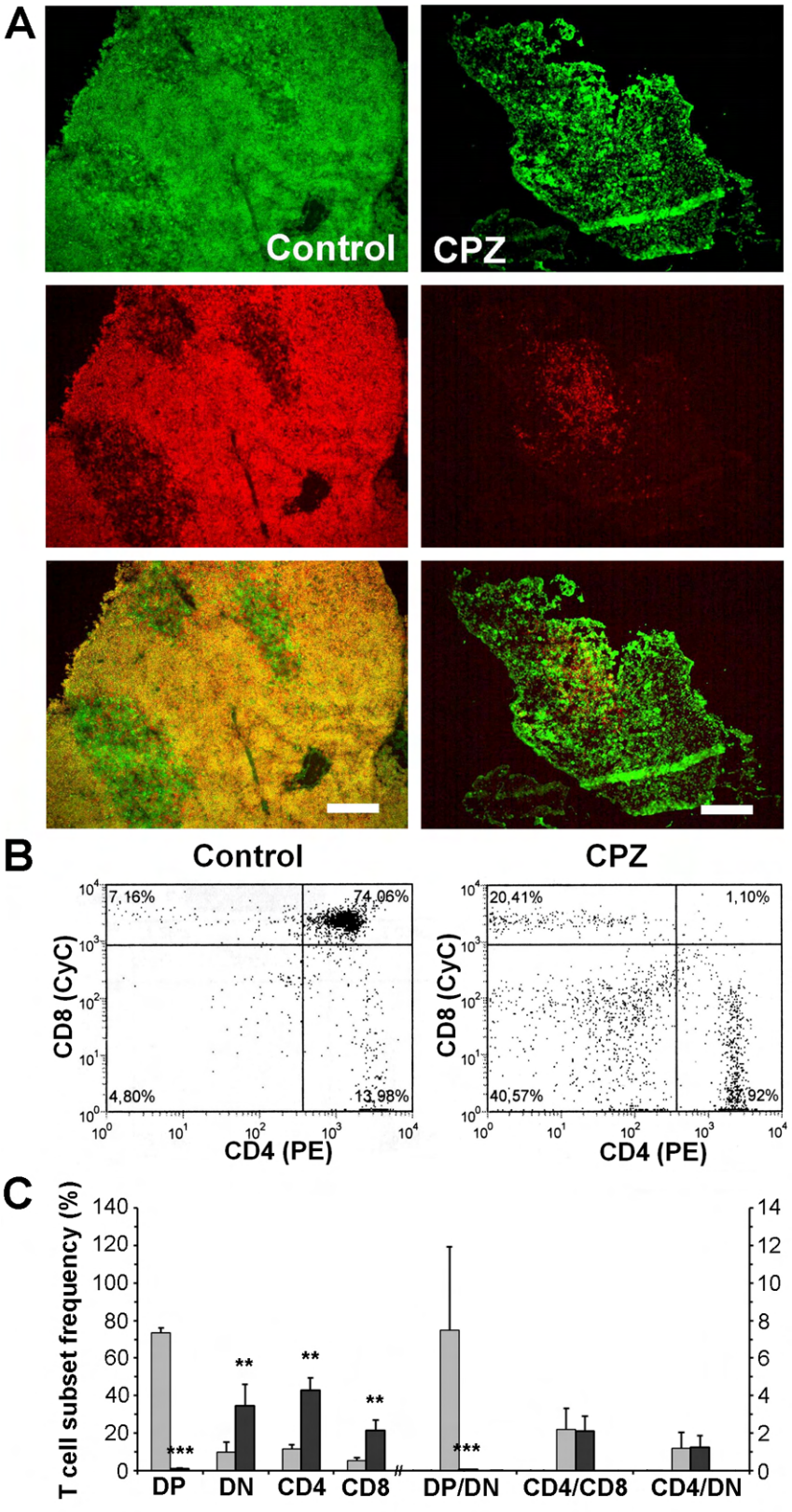

Fig 4. Effect of cuprizone treatment on thymocytes. Four week-old male mice were treated with cuprizone for one week, then immune-staining (A) with FITC-labelled anti-CD4 (green) and Alexa647-labelled anti-CD8

(red) antibodies was performed on thymic sections of untreated (Control) and cuprizone-treated (CPZ) mice. Representative images (A) are presented of the green channel (top panels), the red channel (middle panels) and the merged channels (bottom panels) of three independent experiments including at least three animals in each group for each experiment. Fluorescent photographs were taken using a 10x objective. The scale bar indicates 200 μm. In a parallel experiment, flow cytometry was performed on thymus suspensions of untreated (Control, grey bars) and cuprizone-treated (CPZ. black bars) mice following double staining with PE-labelled CD4 and CyChrome (CyC)-labelled CD8 antibodies. Results are presented as representative dot-plots (B) and bar diagrams (C), mean + SEM ($n \geq 9$). Significant difference from control; **$p<0.01$, *** $p<0.001$. DN: $CD4^-/CD8^-$ cells (lower left quadrant); CD4: $CD4^+$ cells (lower right quadrant); CD8: $CD8^+$ cells (upper left quadrant); DP: $CD4^+/CD8^+$ cells (upper right quadrant); DP/DN: ratio of DP and DN cells; CD4/CD8: ratio of $CD4^+$ and $CD8^+$ cells; CD4/DN: ratio of $CD4^+$ and DN cells. Please note that the x-axis is broken, and the ratios are measured on the right y-axis.

doi:10.1371/journal.pone.0129217.g004

Cuprizone-treatment activated mitochondrial death pathways

To investigate which death pathways were involved in cuprizone-induced thymic atrophy, we examined caspase activation, pro-apoptotic mitochondrial inter-membrane protein release, and major pro- and anti-apoptotic B cell lymphoma (BCL) proteins by using immunoblot analysis of thymus homogenates of untreated and cuprizone-treated animals. We used thymi after only three days of cuprizone-feeding since we were interested in the processes leading to the massive thymocyte loss.

We detected a substantial release to the cytoplasm of cytochrome C, in addition to a resulting increased cleavage i.e. activation of caspase 3 (Fig 7A), but not of caspase 8 (data not shown). We also observed nuclear translocation of AIF (Fig 7A), indicating that the cuprizone-induced apoptosis was of mainly mitochondrial origin. We found that the pro-apoptotic Bcl-2 family members Bim, Bax and Bad had overlapping functions in cuprizone-induced killing of CD4-CD8 double-positive thymocytes. The expression level of all three proteins was increased significantly after three days of cuprizone-treatment, although, Bax expression was augmented at least 10 times over the other two (Fig 7B). Additionally, increased Bad expression was accompanied by decreased phosphorylation of the protein (Fig 7B) that emphasises its pro-apoptotic role in cuprizone-induced thymocyte loss.

Cuprizone-treatment activated all three MAP kinases

A number of reports implicate MAPK activation as a causative factor of mitochondrial damage and apoptotic cell death [27,28]. Therefore, we assessed phosphorylation i.e. activation of JNK, ERK and p38 in thymus homogenates by using phosphorylation-specific primary antibodies and immunoblotting. After three days of cuprizone-feeding we found increased activation of all three MAP kinases. JNK and p38 phosphorylation were increased upon cuprizone treatment by over 600% while ERK phosphorylation increased by only about 30% (Fig 7C).

Discussion

To enhance our knowledge of the degenerative animal model of MS, we investigated the effect of cuprizone on the thymus, the site of T-cell maturation and selection. Although, thymus involution in the cuprizone model is extremely apparent (Fig 1A), we could not find any previous report mentioning it. Cuprizone-treatment results in reduced thriving of the animals [29]; however, thymus retardation upon cuprizone-treatment was more pronounced than that of the rest of the body (Fig 1D), resulting mainly from apoptotic death (Fig 2).

By using immunostaining and fluorescent microscopy, we demonstrated that cuprizone-treatment affected the cortex over the medulla (Fig 3A), supported by the relatively higher expression level (Fig 3B) of AIRE, a gene expressed by the thymic medullary epithelial cells [30],

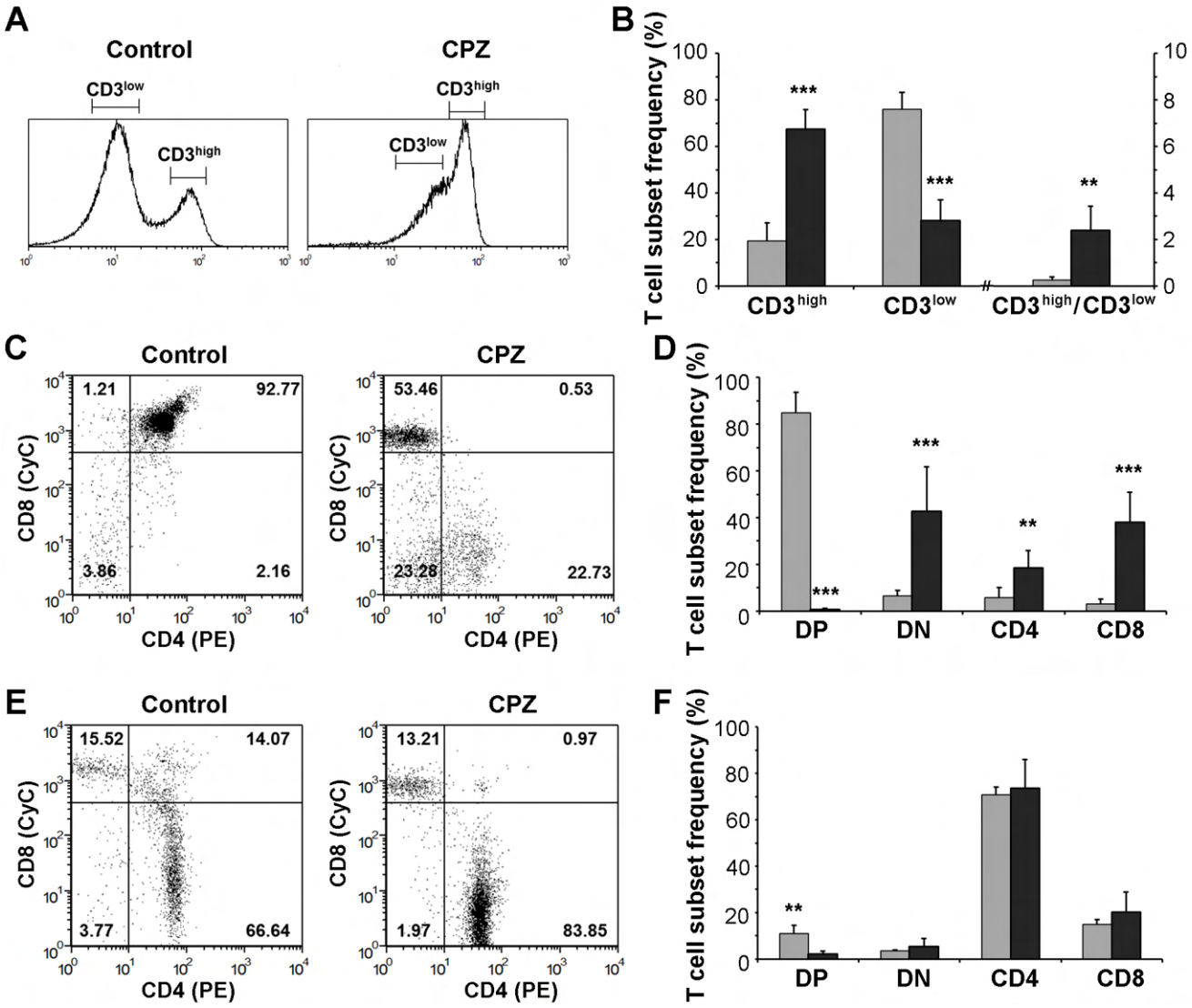

Fig 5. Effect of cuprizone treatment on thymocyte subpopulations. Four week-old male mice were treated with cuprizone for one week, then flow cytometry was performed on thymus suspensions on thymus suspensions of untreated (Control, grey bars) and cuprizone-treated (CPZ, black bars) mice following triple staining with FITC-labelled CD3, PE-labelled CD4 and CyChrome (CyC)-labelled CD8 antibodies. Based on CD3 positivity (A, B) the data on CD4 and CD8 were allocated to low ($CD3^{low}$; C, D) and high ($CD3^{high}$; E, F) CD3 positivity subgroups (the ranges are indicated in A). Results are presented as representative line charts (A), dot-plots (C, E) and bar diagrams (B, D, F), mean + SEM ($n \geq 9$). Significant difference from control; **p<0.01, *** p<0.001. DN: $CD4^-/CD8^-$ cells (lower left quadrant); CD4: $CD4^+$ cells (lower right quadrant); CD8: $CD8^+$ cells (upper left quadrant); DP: $CD4^+/CD8^+$ cells (upper right quadrant); $CD3^{high}/CD3^{low}$: ratio of $CD3^{high}$ and $CD3^{low}$ cells. Please note that the x-axis in B is broken, and the ratio is measured on the right y-axis.

doi:10.1371/journal.pone.0129217.g005

in the thymi of cuprizone-treated mice. Since the cortex is associated mostly with the positive selection of T-cells while the medulla is the location of the negative selection of auto-reactive T-cells from the mature repertoire, this result indicated that cuprizone affected immature T-cells more severely than it affected the mature ones. Accordingly, the observed relatively higher expression level of MHCII (Fig 3B) in the thymi of cuprizone-treated mice resulted mainly from the preservation of mature T-cells residing dominantly in the medulla.

We intended to identify the T-cell subpopulation that was most sensitive to cuprizone. Immunofluorescence and flow-cytometry analysis revealed that cuprizone eradicated $CD4^+CD8^+$ T-cells while practically did not affect ratios of other T cell subpopulations (Fig 4).

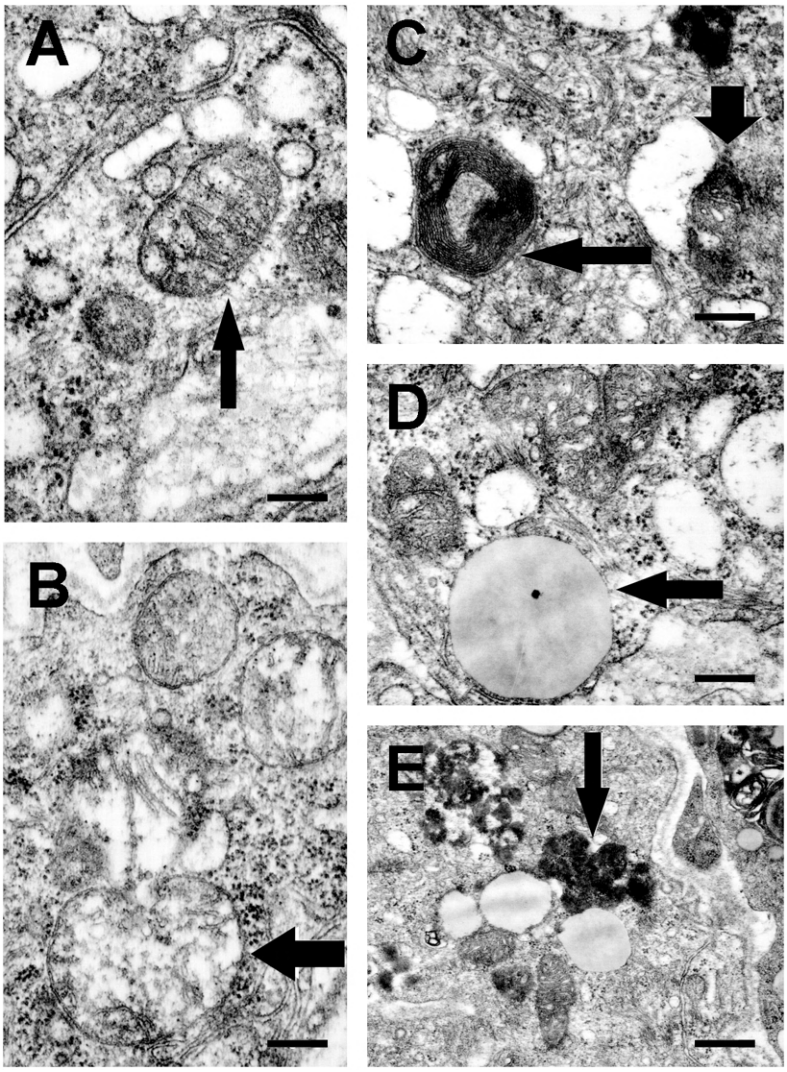

Fig 6. Effect of cuprizone treatment on subcellular morphology. Four week-old male mice were treated with cuprizone for one week. Subcellular morphology was assessed in ultrathin thymic sections of control (A) and cuprizone-treated (B-E) mice. Representative images are presented of three independent experiments including at least three animals in each group for each experiment. Arrows indicate normal (A) and enlarged (B) mitochondria, a large lipid droplet (D), and large lysosomes packed with darkly stained material (E). Horizontal thin and vertical thick arrows in (C) point to myelin body and a degraded mitochondrion, respectively. Scale bars indicate 200 nm.

doi:10.1371/journal.pone.0129217.g006

These results were confirmed when we filtered the results of CD4 and CD8 positivity of the cells according to their CD3 status. The double positive subset of T-cells of low CD3 status was abolished by cuprizone while there was $CD8^+$ dominance among the surviving cells, and a corresponding $CD4^+$ dominance was observed among the cuprizone-resistant T-cells of high CD3 status (Fig 5). These data are in accord with our aforementioned findings and the present view of T-cell maturation. Namely, immature double negative T-cells first express CD8 before becoming double positive, which cells undergo positive and negative selection to reach their mature $CD4^+$ or $CD8^+$ phenotype, while CD3 positivity increases along the maturation process.

By chelating copper, cuprizone may interfere with cellular energy metabolism. Supporting this notion, megamitochondrion formation was observed as early as after three days of

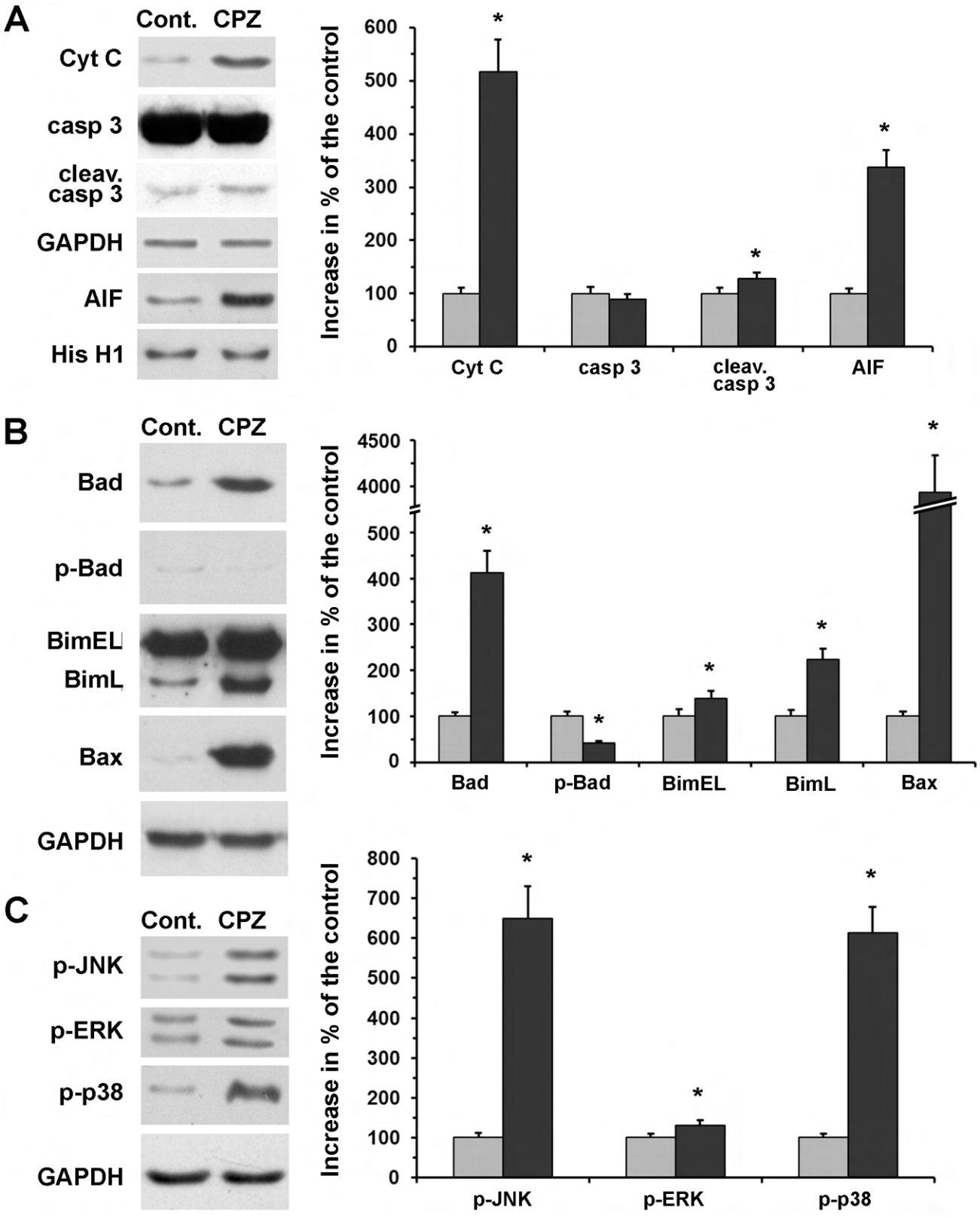

Fig 7. Effect of cuprizone treatment on death pathway and signalling proteins in the thymus. Four week-old male mice were treated with cuprizone for three days. Steady-state cytoplasmic levels of cytochrome C (Cyt C) (A), caspase 3 (casp 3) (A), cleaved caspase 3 (cleav. casp 3) (A) and nuclear

apoptosis inducing factor (AIF) content (A), as well as cellular levels of Bad (B), BimEL (B), BimL (B) and Bax (B) were assessed in the thymi of untreated (Cont., grey bars) and cuprizone-treated (CPZ, black bars) mice by using specific primary antibodies and immunoblotting. The activation state of Bad (p-Bad) (B), JNK (p-JNK) (C), ERK (p-ERK) (C) and p38 MAPK (p-p38) (C) was also determined by using phosphorylation-specific primary antibodies and immunoblotting. GAPDH (A-C) and histone H1 (His H1) (A) were used as loading controls for cytoplasmic/cellular and nuclear fractions, respectively. Results are presented as representative immunoblots and bar diagrams, mean + SEM ($n \geq 9$). Significant difference from control; *$p<0.05$. Please note that the y-axis in B is broken to accommodate the very high Bax value.

doi:10.1371/journal.pone.0129217.g007

cuprizone-feeding in mouse liver [24,29], and the oligodendrocytes of the corpus callosum [31]. Furthermore, increased ROS production, and decreased activities of the various complexes of the respiratory chain were found in the mitochondria of cuprizone-treated oligodendroglia cells [32,33]. We found degraded, as well as enlarged, although not giant, mitochondria in the thymi of cuprizone-treated mice (Fig 6). Additionally, myelin-bodies, large lipid droplets, and large lysosomes were also frequently present in these cells (Fig 6). The observed large lysosomes could result from lysosome membrane permeabilisation, which contributes to thymocyte apoptosis by releasing lysosomal proteases, thereby causing the degradation of vital cytosolic proteins and the activation of additional hydrolases, including caspases [34]. This scenario is consistent with the finding that, unlike in the case of oligodendrocytes [6], both AIF- and caspase-mediated apoptosis was observed in the thymi of cuprizone-treated mice (Fig 7A). On the other hand, cytoplasmic translocation of mitochondrial cytochrome C (Fig 7A) may entirely account for the observed caspase-3 activation.

Both nuclear translocation of AIF and cytoplasmic translocation of cytochrome C could result from mitochondrial outer membrane permeability, which is regulated by pro-apoptotic members of the BCL-2 family [35]. Bad forms heterodimers with other family members or BH3-only proteins such as Bax and Bim, attach to the outer mitochondrial membrane, and destabilize it [35]. Bim, an essential mediator of apoptosis in thymocytes, has three isoforms (BimS, BimL and BimEL), which promote intrinsic apoptosis to different extents [36]. Accordingly, we detected enhanced expression of Bad, Bax and Bim upon cuprizone treatment (Fig 7B). Activation of ERK1/2 was reported to promote phosphorylation of BimEL targeting it to proteosomal degradation [37]. ERK1/2 was also indicated in Bad phosphorylation, preventing its association with other pro-apoptotic BCL-2 proteins [38]. In contrast, JNK and p38 MAPK activation was found to trigger Bad and Bim expression, labilise mitochondrial integrity, induce ROS production and promote apoptosis [39]. Accordingly, we found that all three MAPK families become activated upon cuprizone treatment; however, JNK and p38 activation was overwhelmingly more pronounced than was that of ERK1/2 (Fig 7C).

During development, thymocytes undergo positive and negative selection, eliminating roughly 98% of $CD4^+CD8^+$ cells before they maturate along the $CD4^+$ or $CD8^+$ phenotype. Additionally, when the thymus undergoes physiologic or pathologic involution during aging, infectious diseases, sepsis, malnutrition, physical or emotional stress, chemotherapeutics, glucocorticoids or radiation injury, cortical double positive cells, primarily, suffer apoptosis, while $CD4^+$ or $CD8^+$ cells are less affected [40–43], indicating that cortical double positive cells represent the most vulnerable cell population in the thymus. In this respect, cuprizone-induced thymus involution is similar to all aforementioned conditions. In other respects, the cuprizone model shows both similarities and differences compared to physiological or steroid-induced thymic aging.

The thymus undergoes adiposeous involution during aging. We observed large lipid droplets (Fig 6D) similar to those found in physiological and steroid-induced accelerated aging [41]. However, the thymic epithelium is affected differently by these conditions. The medullary region suffers less damage compared to the cortical region in the cuprizone model, which is in marked contrast to physiological or steroid-induced aging [44,45]. The observed enlarged lysosomes (Fig 6E) could be involved not only in apoptosis but also in other types of cell death.

There is increasing evidence that the lysosome is also involved in the pathogenesis of a variety of neurodegenerative diseases, including Alzheimer's disease, Parkinson's disease, Huntington's disease, and amyotrophic lateral sclerosis [34].

The thymus can have dual functions in MS. It can be the organ, where potentially self-reactive T-cells mature and differentiate inducing or exacerbating the disease. However, it is also the cradle of regulatory T-cells that can potentially suppress self-reactive immune responses, locally [46,47] Our results do not indicate a functional relationship between cuprizone-induced thymus involution and the absence of inflammatory responses or the selective demyelination observed in the cuprizone model. Rather, cuprizone-induced thymocyte and oligodendrocyte apoptosis seems to occur parallel to each other, and in both cases the toxin affects the most vulnerable cells in the given organ. It raises the possibility that similar selective elimination of the most vulnerable cell type in other organs is responsible for the absence of thriving that is characteristic of the cuprizone model. An important feature of the cuprizone model is that after termination of the toxin feeding, an accelerated thriving and regeneration occurs. Therefore, the cuprizone model could be valuable in studying thymus regeneration as well as the remyelination processes.

Author Contributions

Conceived and designed the experiments: IS KK ZB FG. Performed the experiments: IS KK GT SV PA KF PZ. Analyzed the data: IS KK AS ZB. Contributed reagents/materials/analysis tools: IS KK SV PA KF PZ ZB. Wrote the paper: FG ZI AS ZB FG.

References

1. Matsushima GK, Morell P. The neurotoxicant, cuprizone, as a model to study demyelination and remyelination in the central nervous system. Brain Pathol. 2001; 11(1):107–16. PMID: 11145196
2. Remington LT, Babcock AA, Zehntner SP, Owens T. Microglial recruitment, activation, and proliferation in response to primary demyelination. Am J Pathol. 2007; 170(5): 1713–24. PMID: 17456776
3. Torkildsen O, Brunborg LA, Myhr KM, Bø L. The cuprizone model for demyelination. Acta Neurol Scand Suppl. 2008; 188: 72–6. doi: 10.1111/j.1600-0404.2008.01036.x PMID: 18439226
4. Lucchinetti C, Brück W, Parisi J, Scheithauer B, Rodriguez M, Lassmann H. Heterogeneity of multiple sclerosis lesions: implications for the pathogenesis of demyelination. Ann Neurol. 2000; 47(6): 707–17. PMID: 10852536
5. van der Star BJ, Vogel DY, Kipp M, Puentes F, Baker D, Amor S. In vitro and in vivo models of multiple sclerosis. CNS Neurol Disord Drug Targets. 2012; 11(5): 570–88. PMID: 22583443
6. Veto S, Acs P, Bauer J, Lassmann H, Berente Z, Setalo G Jr, et al. Inhibiting poly(ADP-ribose) polymerase: a potential therapy against oligodendrocyte death. Brain. 2010; 133(Pt 3): 822–34 doi: 10.1093/brain/awp337 PMID: 20157013
7. Tandler B, Hoppel CL. Division of giant mitochondria during recovery from cuprizone intoxication. J Cell Biol. 1973; 56(1): 266–72. PMID: 4118453
8. Komoly S. Experimental demyelination caused by primary oligodendrocyte dystrophy. Regional distribution of the lesions in the nervous system of mice [corrected]. Ideggyogy Sz. 2005; 58(1–2): 40–3. PMID: 16252890
9. Venturini G. Enzymic activities and sodium, potassium and copper concentrations in mouse brain and liver after cuprizone treatment in vivo. J Neurochem. 1973; 21(5): 1147–51. PMID: 4357499
10. Russanov EM, Ljutakova SG. Effect of cuprizone on copper exchange and superoxide dismutase activity in rat liver. Gen Pharmacol. 1980; 11(6): 535–8. PMID: 7461431
11. Baxter AG. The origin and application of experimental autoimmune encephalomyelitis. Nat Rev Immunol. 2007; 7(11): 904–12. PMID: 17917672
12. Lassmann H. Experimental models of multiple sclerosis. Rev Neurol (Paris). 2007; 163(6–7): 651–5.
13. Utz U, McFarland HF. The role of T cells in multiple sclerosis: implications for therapies targeting the T cell receptor. J Neuropathol Exp Neurol. 1994; 53(4): 351–8. PMID: 8021708

14. Benveniste EN. Role of macrophages/microglia in multiple sclerosis and experimental allergic encephalomyelitis. J Mol Med (Berl). 1997; 75(3): 165–73. PMID: 9106073

15. Smith ME. Phagocytic properties of microglia in vitro: implications for a role in multiple sclerosis and EAE. Microsc Res Tech. 2001; 54(2):81–94 PMID: 11455615

16. Hiremath MM, Chen VS, Suzuki K, Ting JP, Matsushima GK. MHC class II exacerbates demyelination in vivo independently of T cells. J Neuroimmunol. 2008; 203(1): 23–32. doi: 10.1016/j.jneuroim.2008.06.034 PMID: 18805594

17. Emerson MR, Biswas S, LeVine SM. Cuprizone and piperonyl butoxide, proposed inhibitors of T-cell function, attenuate experimental allergic encephalomyelitis in SJL mice. J Neuroimmunol. 2001; 119 (2): 205–13. PMID: 11585623

18. Maña P, Fordham SA, Staykova MA, Correcha M, Silva D, Willenborg DO, et al. Demyelination caused by the copper chelator cuprizone halts T cell mediated autoimmune neuroinflammation. J Neuroimmunol. 2009; 210(1–2): 13–21 doi: 10.1016/j.jneuroim.2009.03.008 PMID: 19345424

19. Herder V, Hansmann F, Stangel M, Schaudien D, Rohn K, Baumgärtner W, et al. Cuprizone inhibits demyelinating leukomyelitis by reducing immune responses without virus exacerbation in an infectious model of multiple sclerosis. J Neuroimmunol. 2012 Mar; 244(1–2): 84–93. doi: 10.1016/j.jneuroim.2012.01.004 PMID: 22306300

20. Kutlesa S, Wessels JT, Speiser A, Steiert I, Müller CA, Klein G. E-cadherin-mediated interactions of thymic epithelial cells with CD103+ thymocytes lead to enhanced thymocyte cell proliferation. J Cell Sci. 2002; 115(Pt 23): 4505–15. PMID: 12414996

21. Vermes I, Haanen C, Steffens-Nakken H, Reutelingsperger C. A novel assay for apoptosis. Flow cytometric detection of phosphatidylserine expression on early apoptotic cells using fluorescein labelled Annexin V. J Immunol Methods. 1995; 184(1): 39–51. PMID: 7622868

22. Winer J, Jung CK, Shackel I, Williams PM. Development and validation of real-time quantitative reverse transcriptase-polymerase chain reaction for monitoring gene expression in cardiac myocytes in vitro. Anal Biochem. 1999; 270(1): 41–9. PMID: 10328763

23. Schmittgen TD, Zakrajsek BA, Mills AG, Gorn V, Singer MJ, Reed MW. Quantitative reverse transcription-polymerase chain reaction to study mRNA decay: comparison of endpoint and real-time methods. Anal Biochem. 2000; 285(2): 194–204. PMID: 11017702

24. Suzuki K. Giant hepatic mitochondria: production in mice fed with cuprizone. Science. 1969; 163 (3862): 81–2. PMID: 5763494

25. Green DR, Galluzzi L, Kroemer G. Metabolic control of cell death. Science. 2014; 345(6203): 1250256. doi: 10.1126/science.1250256 PMID: 25237106

26. Ghadially FN. Case for the panel. Mitochondrial inclusions in prostate adenocarcinoma. Ultrastruct Pathol. 1997; 21(5): 475–7. PMID: 9273979

27. Racz B, Hanto K, Tapodi A, Solti I, Kalman N, Jakus P,et al. Regulation of MKP-1 expression and MAPK activation by PARP-1 in oxidative stress: a new mechanism for the cytoplasmic effect of PARP-1 activation. Free Radic Biol Med. 2010; 49(12): 1978–88. doi: 10.1016/j.freeradbiomed.2010.09.026 PMID: 20920579

28. Procaccio V, Bris C, Chao de la Barca JM, Oca F, Chevrollier A, Amati-Bonneau P, et al. Perspectives of drug-based neuroprotection targeting mitochondria. Rev Neurol (Paris). 2014; 170(5): 390–400. doi: 10.1016/j.neurol.2014.03.005 PMID: 24792485

29. Suzuki K, Kikkawa Y. Status spongiosus of CNS and hepatic changes induced by cuprizone (biscyclohexanone oxalyldihydrazone). Am J Pathol. 1969; 54(2): 307–25. PMID: 5765567

30. Peterson P, Org T, Rebane A. Transcriptional regulation by AIRE: molecular mechanisms of central tolerance. Nat Rev Immunol. 2008; 8(12): 948–57. doi: 10.1038/nri2450 PMID: 19008896

31. Acs P, Komoly S. Selective ultrastructural vulnerability in the cuprizone-induced experimental demyelination. Ideggyogy Sz. 2012; 65(7–8): 266–70. PMID: 23126218

32. Pasquini LA, Calatayud CA, Bertone Uña AL, Millet V, Pasquini JM, Soto EF. The neurotoxic effect of cuprizone on oligodendrocytes depends on the presence of pro-inflammatory cytokines secreted by microglia. Neurochem Res. 2007; 32(2): 279–92. PMID: 17063394

33. Acs P, Selak MA, Komoly S, Kalman B. Distribution of oligodendrocyte loss and mitochondrial toxicity in the cuprizone-induced experimental demyelination model. J Neuroimmunol. 2013; 262(1–2): 128–31. doi: 10.1016/j.jneuroim.2013.06.014 PMID: 23890808

34. Zhang L, Sheng R, Qin Z. The lysosome and neurodegenerative diseases. Acta Biochim Biophys Sin (Shanghai). 2009; 41(6): 437–45. PMID: 19499146

35. Ryan JA, Brunelle JK, Letai A. Heightened mitochondrial priming is the basis for apoptotic hypersensitivity of CD4(+) CD8(+) thymocytes. Proceedings of the Proc Natl Acad Sci U S A. 2010; 107(29): 12895–900. doi: 10.1073/pnas.0914878107 PMID: 20615979

36. Ruppert SM, Li W, Zhang G, Carlson AL, Limaye A, Durum SK, Khaled AR. The major isoforms of Bim contribute to distinct biological activities that govern the processes of autophagy and apoptosis in interleukin-7 dependent lymphocytes. Biochim Biophys Acta. 2012; 1823(10): 1877–93. doi: 10.1016/j.bbamcr.2012.06.017 PMID: 22728771

37. Ley R, Balmanno K, Hadfield K, Weston C, Cook SJ. Activation of the ERK1/2 signaling pathway promotes phosphorylation and proteasome-dependent degradation of the BH3-only protein, Bim. J Biol Chem. 2003; 278(21): 18811–6. PMID: 12646560

38. Park HJ, Park KH, Shin KS, Lee MK. The roles of cyclic AMP-ERK-Bad signaling pathways on 6-hydroxydopamine-induced cell survival and death in PC12 cells. Toxicol In Vitro. 2013; 27(8): 2233–41. doi: 10.1016/j.tiv.2013.09.014 PMID: 24055892

39. Miloso M, Scuteri A, Foudah D, Tredici G. MAPKs as mediators of cell fate determination: an approach to neurodegenerative diseases. Curr Med Chem. 2008; 15(6): 538–48. PMID: 18336268

40. Grillot DA, Merino R, Núñez G. Bcl-XL displays restricted distribution during T cell development and inhibits multiple forms of apoptosis but not clonal deletion in transgenic mice. J Exp Med. 1995; 182(6): 1973–83. PMID: 7500043

41. Pearse G. Normal structure, function and histology of the thymus. Toxicol Pathol. 2006; 34(5): 504–14. PMID: 17067941

42. Savino W, Dardenne M, Velloso LA, Dayse Silva-Barbosa S. The thymus is a common target in malnutrition and infection. Br J Nutr. 2007; 98 Suppl 1:S11–6. PMID: 17922946

43. Strasser A, Harris AW, Cory S. Bcl-2 transgene inhibits T cell death and perturbs thymic self-censorship. Cell. 1991; 67(5): 889–99. PMID: 1959134

44. Kvell K, Varecza Z, Bartis D, Hesse S, Parnell S, Anderson G, et al. Wnt4 and LAP2alpha as pacemakers of thymic epithelial senescence. PLoS One. 2010; 5(5): e10701. doi: 10.1371/journal.pone.0010701 PMID: 20502698

45. Talaber G, Kvell K, Varecza Z, Boldizsar F, Parnell SM, Jenkinson EJ, et al. Wnt-4 protects thymic epithelial cells against dexamethasone-induced senescence. Rejuvenation Res. 2011; 14(3): 241–8. doi: 10.1089/rej.2010.1110 PMID: 21453014

46. Costantino CM, Baecher-Allan C, Hafler DA. Multiple sclerosis and regulatory T cells. J Clin Immunol. 2008; 28(6): 697–706. doi: 10.1007/s10875-008-9236-x PMID: 18763026

47. Venken K, Hellings N, Liblau R, Stinissen P. Disturbed regulatory T cell homeostasis in multiple sclerosis. Trends Mol Med. 2010; 16(2): 58–68. doi: 10.1016/j.molmed.2009.12.003 PMID: 20159585

frontiers in Immunology

ORIGINAL RESEARCH
published: 24 April 2019
doi: 10.3389/fimmu.2019.00862

Transgenic Exosomes for Thymus Regeneration

Krisztina Banfai[1,2], *Kitti Garai*[1,2], *David Ernszt*[2,3], *Judit E. Pongracz*[1,2] *and Krisztian Kvell*[1,2]*

[1] Department of Pharmaceutical Biotechnology, Faculty of Pharmacy, University of Pécs, Pécs, Hungary, [2] Szentagothai Research Center, University of Pécs, Pécs, Hungary, [3] Faculty of Medicine, Institute of Physiology, University of Pécs, Pécs, Hungary

During senescence, Wnt4 expression is down-regulated (unlike their Frizzled receptors), while PPARgamma expression increases in the thymus. Together, these changes allow for thymic degeneration to occur, observed as adipose involution. However, when restored, Wnt4 can efficiently counteract PPARgamma and prevent thymic senescence from developing. The Wnt-pathway activator miR27b has also been reported to inhibit PPARgamma. Our goal was to evaluate the Wnt4 and miR27b levels of Wnt4-transgenic thymic epithelial cell (TEC)-derived exosomes, show their regenerative potential against age-related thymic degeneration, and visualize their binding and distribution both *in vitro* and *in vivo*. First, transgenic exosomes were harvested from Wnt4 over-expressing TECs and analyzed by transmission electron microscopy. This unveiled exosomes ranging from 50 to 100 nm in size. Exosomal Wnt4 protein content was assayed by ELISA, while miR27b levels were measured by TaqMan qPCR, both showing elevated levels in transgenic exosomes relative to controls. Of note, kit-purified TEI (total exosome isolate) outperformed UC (ultracentrifugation)-purified exosomes in these parameters. In addition, a significant portion of exosomal Wnt4 proved to be displayed on exosomal surfaces. For functional studies, steroid (Dexamethasone or DX)-induced TECs were used as cellular aging models in which DX-triggered cellular aging was efficiently prevented by transgenic exosomes. Finally, DiI lipid-stained exosomes were applied on the mouse thymus sections and also iv-injected into mice, for *in vitro* binding and *in vivo* tracking, respectively. We have observed distinct staining patterns using DiI lipid-stained transgenic exosomes on sections of young and aging murine thymus samples. Moreover, *in vivo* injected DiI lipid-stained transgenic exosomes showed detectable homing to the thymus. Of note, Wnt4-transgenic exosome homing outperformed control (Wnt5a-transgenic) exosome homing. In summary, our findings indicate that exosomal Wnt4 and miR27b can efficiently counteract thymic adipose involution. Although extrapolation of mouse results to the human setting needs caution, our results appoint transgenic TEC exosomes as promising tools of immune rejuvenation and contribute to the characterization of the immune-modulatory effects of extracellular vesicles in the context of regenerative medicine.

Keywords: aging, thymus, exosome, Wnt4, miR27b

OPEN ACCESS

Edited by:
Denise Doolan,
James Cook University, Australia

Reviewed by:
Axel T. Lehrer,
University of Hawaii at Manoa, United States
Csaba Vizler,
Hungarian Academy of Sciences, Hungary

***Correspondence:**
Krisztian Kvell
kvell.krisztian@pte.hu

Specialty section:
This article was submitted to Vaccines and Molecular Therapeutics, a section of the journal Frontiers in Immunology

Received: *06 July 2018*
Accepted: *04 April 2019*
Published: *24 April 2019*

Citation:
Banfai K, Garai K, Ernszt D, Pongracz JE and Kvell K (2019) Transgenic Exosomes for Thymus Regeneration. Front. Immunol. 10:862. doi: 10.3389/fimmu.2019.00862

INTRODUCTION

Transcription factor FoxN1 is the mastermind of thymus organogenesis and identity (1), and is also an acknowledged direct molecular target of the glycolipoprotein Wnt4 (2). As a consequence, Wnt4 plays a key role during embryonic thymus development (3, 4) and the maintenance of its identity in adulthood (5–7). Thymic epithelial cells secrete less Wnt4, while their Frizzled receptors (Fz4 and Fz6) become up-regulated indicating a potential compensatory mechanism and possibly enhanced Wnt4-binding (8). This loss of Wnt4 expression weakens thymic epithelial identity and allows for thymic adipose involution to occur (9). This latter process leads to the expansion of thymic adipose tissue orchestrated by transcription factor PPARgamma (10). The Wnt/b-catenin pathway and PPARgamma have been reported to act as mutual inhibitors of one another in several tissue contexts, including the thymus (11–13). We have previously shown that the addition of exogenous Wnt4 reinforces thymic epithelial identity and confers resistance in a steroid-induced model of senescence through suppressing PPARgamma (2, 14).

Previous records reported that Wnt4 loses its activity when purified as a sole compound, but retains activity as supernatant fraction (15). In harmony, recent publications of various tissue contexts have suggested that Wnt molecules (including Wnt4) travel in conjunction with extracellular vesicles (EVs), more specifically exosomes (12, 16). It has also been reported that a significant portion of the Wnts—including Wnt4—may actually be displayed on exosomal surfaces. Along with Wnt4, the Wnt-pathway activator miR27b has also been shown to specifically inhibit PPARgamma activity via binding to its promoter region (17, 18). Similar to the Wnts above, miRNA species have also been suggested to preferentially reside and travel in EVs, especially in exosomes (19, 20).

EVs are released by most cell types of all phyla and mediate various biological effects. EVs are classified by their size where exosomes represent the smallest vesicles with a diameter of between 30 and 200 nm. Exosomes are produced by a multi-step process where multi-vesicular bodies (MVBs) are formed first by cell-membrane invaginations, followed by the extracellular release of exosomes (21). Biological functions attributed with exosomes encompass several physiological and pathological conditions, including cell and tissue regeneration (22, 23). The thymus epithelium has also been reported to be a rich source of exosomes with key immunological relevance (24–26) e.g., in thymocyte selection (25, 27), Yet to date, TEC (thymic epithelial cell) exosomes have not been linked with thymus tissue regeneration. Thymus tissue regeneration is not only relevant for aging studies, but also in conditions that accelerate thymus degeneration due to environmental stimuli including specific toxins, viruses, or heavy metals (28).Due to the reasons above, we have set out to characterize transgenic exosomes produced by Wnt4 over-expressing TECs for their Wnt4 and miR27b content, to test their biological activity in the context of tissue regeneration, and distribution properties both *in vitro* and *in vivo*.

MATERIALS AND METHODS

Cell Cultures

In vitro experiments were performed using the TEP1 primary-derived (BALB/c) thymic epithelial cell lines or the A549 human lung epithelial cell line (A549 served as control producer cell compared to TEP1). The Wnt4 over-expressing version of TEP1 and the Wnt5a over-expressing version of A549 were generated via lentiviral transfection linked to the green fluorescent protein (GFP) as published previously (Wnt5a served as control compared to Wnt4) (29, 30). Cells were maintained in DMEM (Dulbecco's Modified Eagle's medium, Lonza) supplemented with 10% FBS (EuroClone), Penicillin-Streptomycin, L-glutamine, Hepes buffer, non-essential amino acids (Lonza), and β-mercapto-ethanol (Sigma). In order to differentiate thymic epithelial cells (TECs) toward adipose, lineage steroid treatment was used. Dexamethasone (DX) was diluted from a stock solution of 4 mg/mL to a final concentration of 1 μM as formerly described (10). To counteract the aging effect of steroid treatment, isolated Wnt4 exosomes were added to the cell cultures.

Flow-Cytometry

Cell suspensions were prepared from both TEP1 and Wnt4 over-expressing TEP1 cell lines in order to check the presence of Wnt4 over-expression via analyzing the GFP-positive cells. A total of 150,000 cells were collected and washed with 1x PBS (Fisher BioReagents) then fixed using paraformaldehyde containing PBS solution. BD FACSCanto™ II flow-cytometer (Becton Dickinson) was used for data acquisition at a medium flow rate and stopped at 10,000 events. Measurements were performed and analyzed with BD FACSDiva Software version 6.1.3.

Exosome Staining, Collection and Isolation

Control mouse TECs(thymic epithelial cells), Wnt4 over-expressing mouse TECs and Wnt5a over-expressing human A549 cells were cultured in Stemline® T Cell Expansion Medium (Merck) and serum-free DMEM (Lonza) until they reached 80–90% confluence. Serum-free media were used to eliminate the effect of serum-derived exosomes. Equal volume of FBS-free cell culture media were collected from T75 tissue culture flasks (TPP) and centrifuged at 2,000 g for 30 min to completely remove cell debris and apoptotic bodies. Supernatants were filtered through a 0.45 μm filter (Merck Millipore) and incubated overnight at 4°C having added Total Exosome Isolation Reagent (Invitrogen). Following a 1 h centrifugation at 10,000 g, pellets were collected and re-suspended in sterile PBS (GE Healthcare Life Sciences) for further use. Exosomes were fluorescently-stained using DiI lipid stain (Invitrogen). DiI lipid-stain was added to the cell culture medium the day before collecting cell supernatant. DiI lipid-stain stock solution (50 mg/mL dissolved in DMSO) was diluted 10,000-fold (31).

Transmission Electron Microscopy

Pelleted exosomes were added in 50 μl of PBS onto mesh grids and dried overnight without the use of any fixative (32). Contrast staining was performed using uranyl-acetate and lead-citrate. Exosomes were examined using a Morgagni

268D transmission electron microscope. Images were acquired using an integrated MegaView III digital camera (Olympus Soft Imaging Solutions GmbH).

Immune-Fluorescent Staining

Immune-fluorescent staining was performed on 2-month-old and 21-month-old mouse thymus cryosections. Seven micrometer thick tissue sections were mounted onto glass slides and dried overnight. Tissue samples were fixed with cold acetone then unspecific protein-protein interactions were blocked with 5% BSA in PBS solution before applying fluorochrome-conjugated primary antibodies. FITC-conjugated a-mouse CD326 (EpCAM) (Clone G8.8, BioLegend) was used at 1:100 dilution and DAPI (1:1,000, Life Technologies) was added as a nuclear counterstain. Slides were also incubated overnight with previously DiI-stained Wnt4 exosomes. Following washing steps with 1x PBS, samples were imaged using Nikon Eclipse Ti-U microscope equipped with a CCD camera (Andor 4Zyla 5.5) and

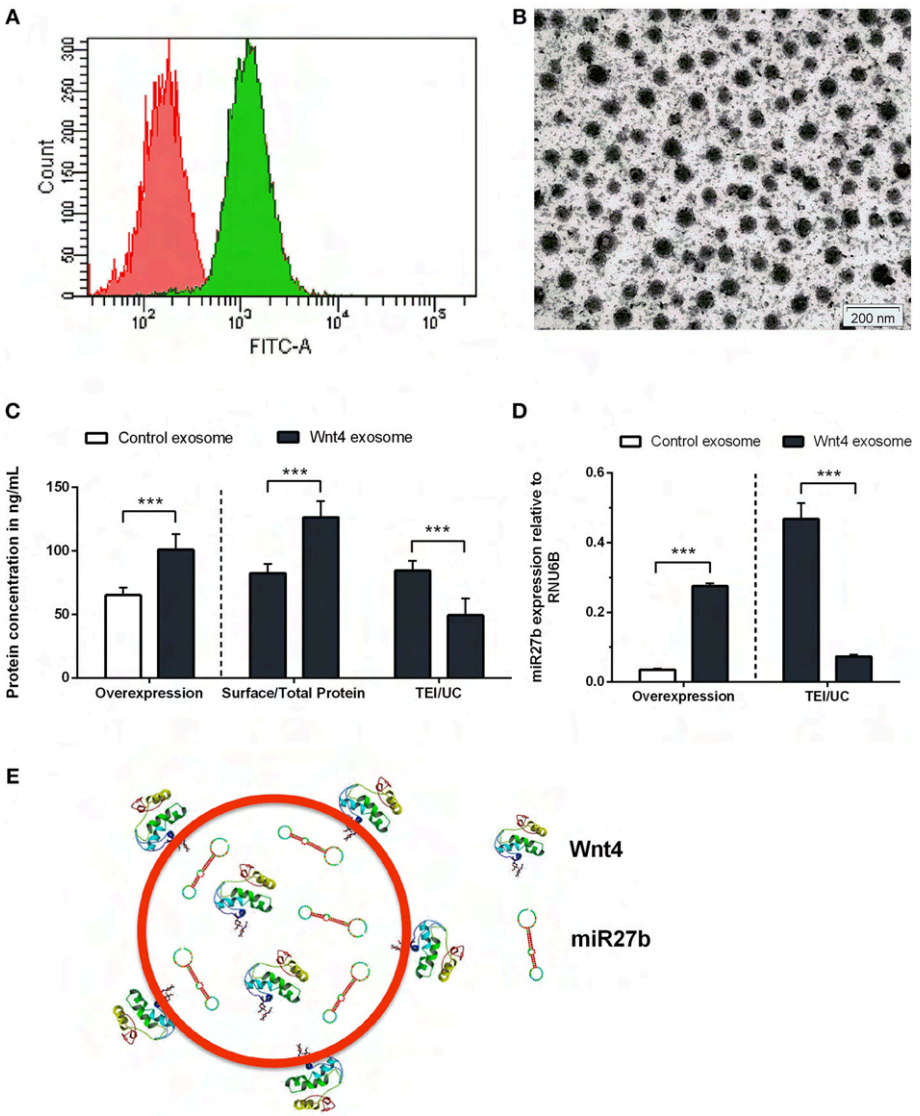

FIGURE 1 | Characterization of transgenic exosomes. Flow-cytometric analysis of control (shown in red) and GFP+ Wnt4 over-expressing TECs (thymic epithelial cells) (shown in green) is presented **(A)**. FITC-A corresponds to FL1 channel where GFP-emitted fluorescence is detected. Please note that FITC-A scale is logarithmic. Transmission electron micrograph shows TEI exosomes of approx. 50–100 nm in size **(B)**. Wnt4 protein **(C)** and miR27b RNA **(D)** levels of TEI (total exosome isolate) and UC (ultracentrifuged) exosomes are shown as obtained by ELISA and TaqMan qPCR, respectively. From left to right column pairs show level of over-expression, surface/total content, and TEI/UC content, as applicable. Absolute concentration is shown in ng/ml for Wnt4 **(C)** and absolute copy number is shown for miR27b relative to rnu6b **(D)**. Eight **(C)** and three **(D)** replicates were used for statistical analysis. Significant differences are shown by asterisks (n/a for not applicable, ns for not significant, $^{*}p \leq 0.05$, $^{**}p \leq 0.01$, $^{***}p \leq 0.001$) and were calculated using independent samples *t*-test. For exact numerical values and statistical analysis please refer to **Supplementary Material**. Representative drawing of a DiI lipid-stained (red) Wnt4-transgenic exosome showing Wnt4 (surface and internal) content and miR27b (internal) cargo **(E)**.

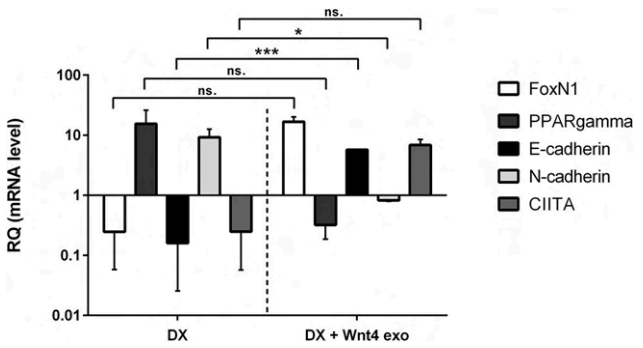

FIGURE 2 | *In vitro* biological effect of transgenic exosomes. Gene expression changes of FoxN1, PPARgamma, E-cadherin, N-cadherin, and CIITA are shown as measured by SYBR-green qPCR following steroid (DX)-treatment alone (DX, left half of figure), or in combination with transgenic exosomes (DX + Wnt4 exo, right half of figure). Three samples of each were used for statistical analysis. Fold change (relative quantity or RQ) expression is shown, where RQ = 1 represents baseline control. RQ is relative to control level (left half of figure), or relative to DX-treatment (right half of figure). Please note that Y-axis is logarithmic. Significant differences are shown by asterisks (n/a for not applicable, ns for not significant, $^{*}p \leq 0.05$, $^{**}p \leq 0.01$, $^{***}p \leq 0.001$) and were calculated using independent samples *t*-test. For exact numerical values and statistical analysis please refer to **Supplementary Material**.

images were captured using NIS-Elements Software. Images were analyzed using ImageJ Software. Thymus lobes of iv-injected mice were sectioned to 5 μm thickness and the same staining procedure was used as described above. Staining procedures were optimized using previous literature data (33–36).

RNA Isolation, cDNA Preparation, qRT-PCR, TaqMan Array

Total RNA was isolated using NucleoSpin RNA II Kit (Macherey-Nagel). High Capacity cDNA Reverse Transcription Kit (Applied Biosystems) was used for preparation of cDNA to a final concentration of 1 μg/μL. For qPCR analysis, PikoReal™ Real-Time PCR System (Thermo Fisher Scientific) was used adding Luminaris Color HiGreen qPCR Master Mix (Thermo Fisher Scientific) to the samples. Gene expression was normalized to mouse β-actin and HPRT housekeeping genes (See **Figures 1**, **2** for detailed primer list). To detect miR27b levels in exosomes, Total Exosome RNA & Protein Isolation Kit (Invitrogen) was used for miRNA isolation. cDNA synthesis was carried out using High Capacity cDNA Reverse Transcription Kit (Applied Biosystems) and specific primers for U6B as endogenous control and miR27b as target gene. Quantification of miR27b was performed using specific gene targeted TaqMan™ MicroRNA Assay adding TaqMan Universal PCR Master Mix (Applied Biosystems). Measurements were run on a PikoReal™ Real-Time PCR System as well using FAM as a fluorophore. Data evaluation was accomplished using Microsoft Excel.

ELISA

Human Wnt4 ELISA Kit (Merck) was used to measure the Wnt4 protein levels of isolated exosomes. Exosomes isolated from TEP1 cell culture media were used as controls. We aimed to quantify surface and total exosome protein levels separately. To detect surface proteins, pelleted exosomes were dissolved in PBS (for intact exosomes), while to determine total protein concentration, exosomes were diluted in Exosome Resuspension Buffer (for disintegrated exosomes) as suggested by Total Exosome RNA & Protein Isolation Kit Manual (Invitrogen). Plates were measured immediately at 450 nm using EnSpire® Multimode Plate Reader (PerkinElmer) with its integrated data analysis software. Using OD values mean absorbance of standards and samples were calculated and results were analyzed with the help of Microsoft Excel. Standard curve was plotted and protein concentrations were calculated in ng/ml. The obtained R^2 values showed >0.91 alignment to the standard curve in all cases.

Ultracentrifugation

In order to compare TEI efficiency (37) with standard ultracentrifugation methods confirming previous literature data (38, 39), 1 ml serum-free medium containing exosomes was centrifuged at 100,000 g for 3 h at 4°C (40) using Sorvall™ MTX 150 Micro-Ultracentrifuge (Thermo Scientific™). Pelleted exosomes were re-suspended in PBS and used for further experiments. Protein concentration of ultracentrifuged exosomes were determined with ELISA and following miRNA isolation, miR27b levels were assessed by TaqMan™ MicroRNA Assay.

In vivo Exosome Homing

Eight week-old BALB/c mice were used for intravenous introduction of DiI lipid-stained exosomes in a pilot study (41, 42). For control purpose a mouse received 2 doses of DiI lipid-stained Wnt5a exosomes diluted in 200 μL of sterile PBS. Another mouse was injected with the same dosage of DiI lipid-stained Wnt4 exosomes diluted in 200 μL of sterile PBS. After 24 h, mice were sacrificed and organs were analyzed for fluorescent intensity with the help of IVIS Lumina III *in vivo* Imaging System. Imaging of the thymus, lungs, liver, and spleen was performed at 520 nm using Living Image Software. Thymus lobes were embedded into cryomold and sectioned to confirm tissue homing. Mice were housed under minimal disease (MD) conditions and kept in the Laboratory Animal Core Facility of the University. Experimental procedures were carried out according to the "1988/XXVIII act of the Hungarian Parliament on Animal Protection (243/1988)" which complies with recommendations of the Helsinki Declaration. All animal experiments were performed with the consent of the Ethics Committee on Animal Research of the University (ref. no.: #BA02/2000-46/2016).

Statistical Analysis

Statistical analyses were conducted using SPSS version 22. Descriptive statistics (mean ± SD) were calculated for all data. Normality was assessed using the Shapiro-Wilk test ($n < 50$). Comparisons were performed using one sample *t*-test and independent samples *t*-test. The level of significance was set at $P \leq 0.05$.

RESULTS

Characterization of Transgenic Exosomes

Stable Wnt over-expressing BALB/c TEC (thymic epithelial cell) lines have been generated using lentiviral vectors as described previously (30). In the current setting, we focused on the characterization of exosomes secreted by the transgenic cell lines. Purity and transgenic status of cell lines was confirmed by GFP expression provided by the same bicistronic construct that also drives Wnt secretion. Flow-cytometric analysis verified that the transgenic cells express GFP and hence secrete Wnt4 at a uniform level (see **Figure 1A**). TECs have been reported to be rich EV and exosome sources. Using a commercially available PEG-based kit (40) we then enriched transgenic exosomes (TEI: total exosome isolate) from TEC line supernatant. The enriched supernatant fraction was confirmed by transmission electron microscopy to contain of uniform-sized exosomes of approx. 50–100 nm in diameter (see **Figure 1B**). Along with Wnt4, the Wnt-pathway activator miR27b has also been reported to suppress PPARgamma (17, 18, 43, 44). For this reason, we have measured both Wnt4 protein and miR27b RNA quantities in transgenic exosomes relative to their control counterparts, using ELISA and TaqMan qPCR methods, respectively. As expected, both Wnt4 and miR27b showed elevated and statistically significant levels in exosomes of transgenic TECs compared to their control counterparts (see **Figures 1C,D**). Furthermore, we have measured total Wnt4 concentration (via lysis of exosomes) and surface Wnt4 concentration (using intact exosomes) showing that a significant portion of Wnt4 is surface-displayed, in harmony with literature (8, 19) (**Figure 1C**). Of note, UC (ultracentrifugation) has repeatedly provided poor exosomal protein and miRNA yield as compared to TEI (see **Figures 1C,D**). **Figure 1E** shows schematic drawing of DiI lipid-stained transgenic exosome with Wnt4 content and miR27b cargo.

Biological Effect of Transgenic Exosomes

We have previously reported that the supernatant of the Wnt4 over-expressing BALB/c TEC (thymic epithelial cell) line confers resistance to steroid (Dexamethasone or DX)-induced accelerated aging in our cellular model system (2). In short, DX-treatment triggers adipose transformation of TECs via epithelial-to-mesenchymal transition (EMT) (10). We have used the same experimental setting using enriched transgenic exosomes instead of transgenic supernatant. As expected and shown by SYBR-green qPCR (see **Figure 2**), the applied DX-treatment triggers loss of TEC identity (decreased FoxN1 and MHCII or CIITA expression), promotes EMT (cadherin switch or decreased E-cadherin and increased N-cadherin expression), and initiates adipose transformation (increased PPARgamma expression). In perfect conformity with our previous reports using transgenic supernatant (2, 4), the transgenic exosomes

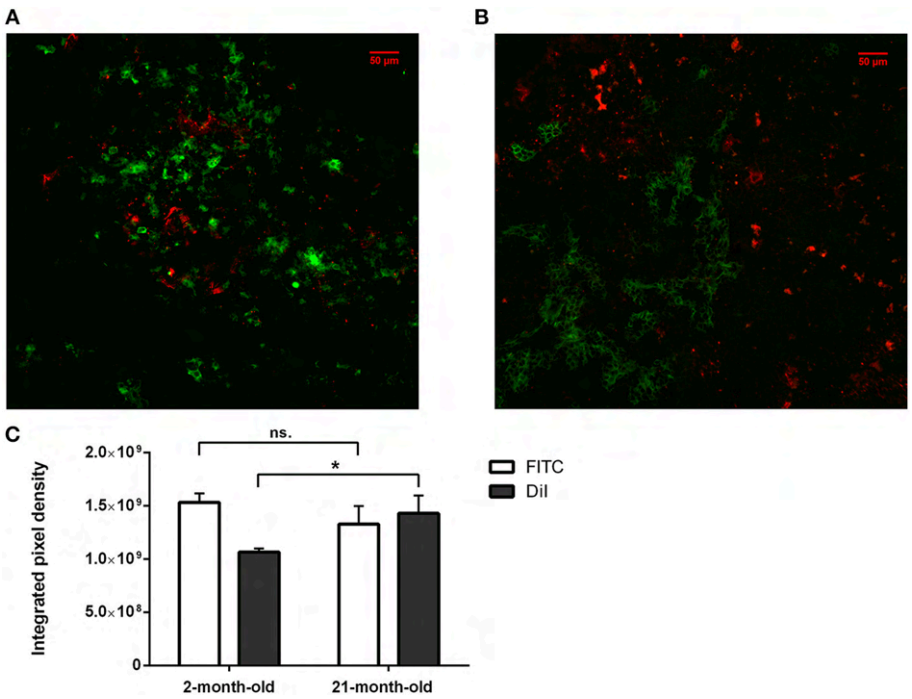

FIGURE 3 | *In vitro* binding and distribution of transgenic exosomes. Frozen mouse thymic sections from young adult (2 months, **A**) and senior adult (21 months, **B**) are shown. Sections were labeled using EpCAM1-FITC (shown in green). Transgenic exosomes were pre-stained using DiI lipid stain (shown in red). Representative slide is presented. Data were calculated using five slides each. Integrated pixel density values are shown for EpCAM1 (shown in green) and DiI lipid stain (shown in red) **(C)**. Significant differences are shown by asterisks (n/a for not applicable, ns for not significant, $*p \leq 0.05$, $**p \leq 0.01$, $***p \leq 0.001$) as obtained using independent sample *t*-test. Data were calculated using five slides each. For exact numerical values and standard deviation please refer to **Supplementary Material**.

also efficiently counteract all of the above gene expressional changes, preserving TEC identity, blocking EMT, and adipose transformation from developing.

In vitro Binding and Distribution of Transgenic Exosomes

We have shown above that our transgenic exosomes harbor elevated amounts of Wnt4 of which a significant portion is surface-displayed. Previously we have reported that Wnt4-binding Frizzled receptors (Fz4 and Fz6) are up-regulated in aged TECs (thymic epithelial cells) as compared to young TECs (8). Next, we have tested whether thymic histological sections can bind transgenic exosomes using standard immune-fluorescent staining protocol. We were also interested to see if histological *in vitro* binding shows a particular pattern and furthermore, if this pattern changes with the age of the epithelium as suggested by Frizzled up-regulation (2, 8). For this reason, DiI lipid-stained transgenic exosomes have been applied on thymic sections of mice of 2-month-old (young) and 21-month-old (aged) for histological staining. As anticipated, both young and old mouse thymic sections efficiently bind transgenic exosomes (see **Figures 3A,B**, respectively). Relative to the histological presentation of the EpCAM-1^{++} medullary epithelium, the transgenic exosomes showed preferential binding to medullary regions at a young age (see **Figure 3A**), while a more profound cortical binding pattern was observed at an old age (see **Figure 3B**). Not only does the binding pattern change with age (shifting from medullary at a young age to cortical at an old age), but binding efficiency also increases with age (observed as increased, statistically significant DiI/fluorescent integrated pixel density at old age compared to young age, see **Figure 3C**). Please also note that the medullary area shrinks with age relative to other areas, in harmony with our previous records (4) observed here as mild indicative decrease of FITC integrated pixel density at old age compared to young age (see **Figure 3C**).

In vivo Binding and Distribution of Transgenic Exosomes

The thymic epithelium has been reported to be highly active in exosome trafficking (24, 25, 45). We have shown above that our Wnt4-transgenic exosomes readily bind to the thymic epithelium *in vitro* on histological sections. However, we were interested to see if *in vivo* binding of transgenic exosomes also occurs in the thymic epithelium. For this reason, DiI lipid-stained Wnt5a-transgenic (serving as control) human (A549), and Wn4-transgenic (serving as sample) BALB/c (TEP1) exosomes have been injected into tail veins of young adult BALB/c mice to check their *in vivo* topological distribution after 24 h. It has been reported that certain organs (e.g., liver, lungs, and spleen) capture a significant portion of exosomes rapidly and non-specifically following systemic administration (46). Using IVIS Lumina III imaging and performing topological reconstruction of murine organs over standard mouse contour, we were able to record detectable homing of transgenic exosomes to the thymus despite significant non-specific capture by other organs (e.g., liver, lungs, and spleen) (see **Figure 4A**). Fluorescent signals of DiI lipid-stained sample Wnt4-transgenic TEC (thymic epithelial cell) exosomes exceeded control values of Wnt5a-transgenic exosomes (see **Figure 4B**). It is worthy of note that thymic signals exceed pulmonary and splenic signals, despite significant size differences. Furthermore, immune-fluorescently labeled sections of the *in vivo* Wnt4-transgenic exosome-infiltrated thymus revealed the histological level homing pattern observed after 24 h (see **Figures 5A,B**) that allows for the quantitative evaluation of transgenic exosome homing (see **Figure 5C**).

DISCUSSION

In harmony with literature data, our results confirm that the thymic epithelium is a particularly rich source of EVs and exosomes (24, 25, 45). The Wnt4 over-expressing transgenic TEC (thymic epithelial cell) line proves to be a reliable source of transgenic exosomes that are easy to visualize, enrich to high purity, characterize, and apply in experiments. As anticipated, the transgenic exosomes contain elevated levels of Wnt4 protein, as well as the Wnt-pathway activator miR27b, which potentially synergizes with Wnt4 to counteract PPARgamma.

Based on our current results obtained with our thymus aging cellular model system the transgenic exosomes transmit the biological activity that was previously attributed to supernatant transfer (2, 4). The applied transgenic exosomes efficiently prevent steroid-triggered adipose transformation as supported by reinforced epithelial identity (increased FoxN1 and CIITA expression), lack of EMT (sustained E-cadherin and low N-cadherin expression) and resistance to adipose differentiation (low PPARgamma expression) in line with our previous reports using transgenic supernatants.

Histological level analysis of *in vitro* transgenic exosome binding provides information in more depth. At a young age (2-month-), transgenic exosomes readily bind to the thymic epithelium with slight medullary preference. In contrast, at an old age (21-month-), transgenic exosomes show a moderate cortical preference. Furthermore, transgenic exosomes show significantly higher overall binding frequency at an old age, suggesting that the senescent thymic epithelium readily adsorbs Wnt4-transgenic exosomes. This is supported by literature data and our own results showing that a significant portion of exosomal Wnt4 is surface-displayed and that Wnt4-binding Frizzled receptors (Fz4 and Fz6) are up-regulated in senescent TECs (8). Combined, our previous and current results suggest that as Wnt4 secretion decreases with age and since cortical areas show preferential binding of the remaining Wnt4 (a key factor of TEC identity) at an old age, age-related medullary involution may precede cortical involution due to the medullary lack of Wnt4-effect (10, 14, 47). To our knowledge, this is a novel molecular level explanation of accelerated medullary involution. Highlighting the relevance of our *in vitro* binding assay, our *in vivo* transgenic exosome homing assay shows detectable homing to the thymus when using mouse TEC-derived Wnt4-transgenic exosomes as opposed to control exosomes (human A549-derived Wnt5a-transgenic exosomes). Histological

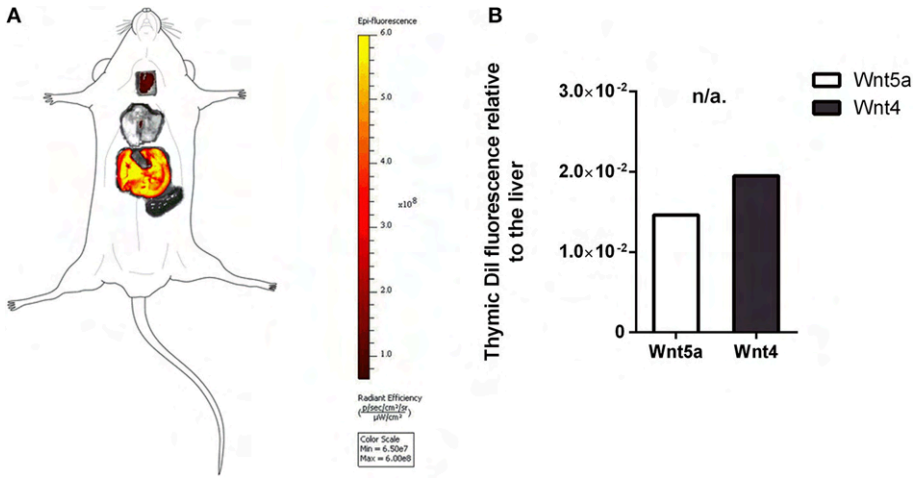

FIGURE 4 | *In vivo* binding and distribution of transgenic exosomes. DiI lipid-stained and iv-injected exosomes show differential topological distribution patterns (radiant efficiency) after 24 h. Organotopic distribution was reconstructed using standard mouse contour. The thymus, lungs, spleen, and liver were analyzed using IVIS Lumina imaging **(A)**. Radiant efficiency of thymus relative to liver (RQ) is shown for of DiI lipid-stained and iv-injected transgenic exosomes after 24 h for Wnt5a (control) and Wnt4 (sample) **(B)**. Significant differences are shown by asterisks (n/a for not applicable, ns for not significant, $^{*}p \leq 0.05$, $^{**}p \leq 0.01$, $^{***}p \leq 0.001$) as obtained using independent samples *t*-test. Pilot study is shown. For exact numerical values please refer to **Supplementary Material**.

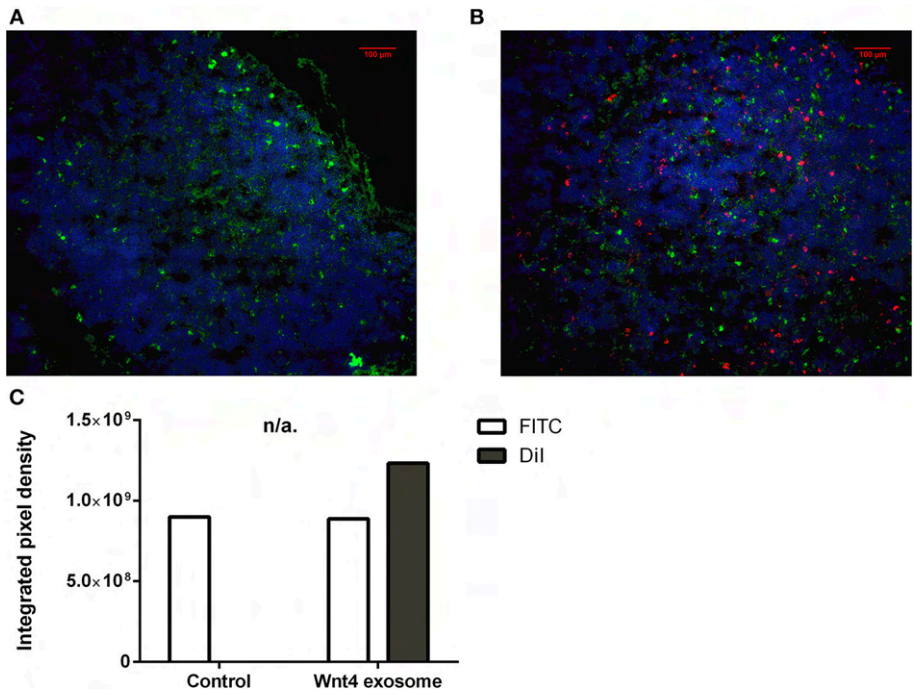

FIGURE 5 | *Ex vivo* binding and distribution of transgenic exosomes. Frozen mouse thymic sections from control **(A)** and DiI lipid-stained Wnt4-transgenic exosome iv-injected mouse **(B)** are shown 24 h after administration. Sections were stained for EpCAM1-FITC (shown in green). Transgenic exosomes were pre-stained using DiI lipid stain (shown in red). DAPI was used as nuclear counter-stain (shown in blue). Integrated pixel density values are shown for EpCAM1 (shown in green) and DiI lipid stain (shown in red) **(C)**. Significant differences are shown by asterisks (n/a for not applicable, ns for not significant, $^{*}p \leq 0.05$, $^{**}p \leq 0.01$, $^{***}p \leq 0.001$) as obtained using independent samples *t*-test. Pilot study is shown. For exact numerical values please refer to **Supplementary Material**.

analysis of Wnt4-transgenic exosome-infiltrated thymus sections confirms their presence also showing distribution pattern and binding frequency.

In summary, based on our cellular aging model system, along with *in vitro* and *in vivo* binding and homing studies, respectively; our results confirm that transgenic exosomes

readily and efficiently provide a permissive niche for immune regeneration in the mouse setting and hold promise for human application as well.

ETHICS STATEMENT

Experimental procedures were carried out according to the 1988/XXVIII act of the Hungarian Parliament on Animal Protection (243/1988) which complies with recommendations of the Helsinki Declaration. All animal experiments were performed with the consent of the Ethics Committee on Animal Research of the University (ref. no.: #BA02/2000-46/2016).

AUTHOR CONTRIBUTIONS

KB performed histological, cellular- and molecular biology work in the project and was involved in manuscript preparation. KG prepared exosome fractions and performed statistical analysis. DE executed *in vivo* tracking. JP was involved in planning experiments, manuscript preparation and also supervised the host department. KK planned experiments, prepared the manuscript and supervised the project.

FUNDING

Scientific research support was provided by the Hungarian National Science Foundation (No. 78310) and PTE AOK KA-2016-16 to KK. The project was also supported by the University of Pecs in the frame of Pharmaceutical Talent Center program and the Viral Pathogenesis Talent Center program via KK. The Janos Bolyai Scholarship of the Hungarian Academy of Sciences and ÚNKP-18-4 (Bolyai+) also supported KK. JP was supported by the European Union and he State of Hungary, co-financed by the European Social Fund in the framework of GINOP 2.3.2–15–2016-00022 TAMOP-4.2.2. A-11/1/KON-2012-0024, TAMOP-4.2.4.A/2-11/1-2012-0001 National Excellence Program, PTE AOK-KA-2013/22 and EFOP-3.6.1-16-2016-00004.

ACKNOWLEDGMENTS

We are grateful to Prof. Graham Anderson (Institute of Immunology and Immunotherapy, University of Birmingham, UK) for providing us the TEP1 mouse thymic epithelial cell line. The authors wish to thank Prof. Hajnalka Abraham MD, Ph.D. (Central Electron Microscope Laboratory, University of Pecs, Hungary) for the technical aid in taking transmission electron microscope images, Prof. Peter Balogh MD Ph.D. (Department of Immunology and Biotechnology, University of Pecs, Hungary) for providing professional help during *in vivo* administration of exosomes, and also Tamas Kiss diagnostic assistant (*in vivo* Imaging Core Facility, Szentagothai Research Center, University of Pecs, Hungary). The authors wish to thank Ricky Odedra (Humeltis Ltd) and prof. Mary Keen (University of Birmingham, UK) for improving the manuscript using their native speaker skills.

SUPPLEMENTARY MATERIAL

The Supplementary Material for this article can be found online at: https://www.frontiersin.org/articles/10.3389/fimmu.2019.00862/full#supplementary-material

REFERENCES

1. Romano R, Palamaro L, Fusco A, Giardino G, Gallo V, Del Vecchio L, et al. FOXN1: a master regulator gene of thymic epithelial development program. *Front Immunol.* (2013) 4:187. doi: 10.3389/fimmu.2013.00187
2. Kvell K, Varecza Z, Bartis D, Hesse S, Parnell S, Anderson G, et al. Wnt4 and LAP2alpha as pacemakers of thymic epithelial senescence. *PLoS ONE.* (2010) 5:e10701. doi: 10.1371/journal.pone.0010701
3. Pongracz JE, Parnell SM, Jones T, Anderson G, Jenkinson EJ. Overexpression of ICAT highlights a role for catenin-mediated canonical Wnt signalling in early T cell development. *Eur J Immunol.* (2006) 36:2376–83. doi: 10.1002/eji.200535721
4. Kvell K, Fejes A V, Parnell SM, Pongracz JE. Active Wnt/beta-catenin signaling is required for embryonic thymic epithelial development and functionality *ex vivo*. *Immunobiology.* (2014) 219:644–52. doi: 10.1016/j.imbio.2014.03.017
5. Heinonen KM, Vanegas JR, Brochu S, Shan J, Vainio SJ, Perreault C. Wnt4 regulates thymic cellularity through the expansion of thymic epithelial cells and early thymic progenitors. *Blood.* (2011) 118:5163–73. doi: 10.1182/blood-2011-04-350553
6. Taub DD, Longo DL. Insights into thymic aging and regeneration. *Immunol Rev.* (2005) 205:72–93. doi: 10.1111/j.0105-2896.2005.00275.x
7. Pongracz J, Hare K, Harman B, Anderson G, Jenkinson EJ. Thymic epithelial cells provide Wnt signals to developing thymocytes. *Eur J Immunol.* (2003) 33:1949–56. doi: 10.1002/eji.200323564
8. Varecza Z, Kvell K, Talabér G, Miskei G, Csongei V, Bartis D, et al. Multiple suppression pathways of canonical Wnt signalling control thymic epithelial senescence. *Mech Ageing Dev.* (2011) 132:249–56. doi: 10.1016/j.mad.2011.04.007
9. Marinova TT. Epithelial framework reorganization during human thymus involution. *Gerontology.* (2005) 51:14–18. doi: 10.1159/000081429
10. Talaber G, Kvell K, Varecza Z, Boldizsar F, Parnell SM, Jenkinson EJ, et al. Wnt-4 protects thymic epithelial cells against dexamethasone-induced senescence. *Rejuvenation Res.* (2011) 14:241–8. doi: 10.1089/rej.2010.1110
11. Gustafson B, Smith U. The WNT inhibitor Dickkopf 1 and bone morphogenetic protein 4 rescue adipogenesis in hypertrophic obesity in humans. *Diabetes.* (2012) 61:1217–24. doi: 10.2337/db11-1419
12. Lecarpentier Y, Claes V, Vallée A, Hébert J-L. Thermodynamics in cancers: opposing interactions between PPAR gamma and the canonical WNT/beta-catenin pathway. *Clin Transl Med.* (2017) 6:14. doi: 10.1186/s40169-017-0144-7
13. Lecarpentier Y, Vallée A. Opposite Interplay between PPAR gamma and canonical Wnt/Beta-catenin pathway in amyotrophic lateral sclerosis. *Front Neurol.* (2016) 7:100. doi: 10.3389/fneur.2016.00100
14. Kvell K, Pongracz JE. *Central Immune Senescence, Reversal Potentials*. InTech (2012). Available online at: http://www.ncbi.nlm.nih.gov/pubmed/28045481 (accessed July 4, 2018).
15. Willert K, Brown JD, Danenberg E, Duncan AW, Weissman IL, Reya T, et al. Wnt proteins are lipid-modified and can act as stem cell growth factors. *Nature.* (2003) 423:448–52. doi: 10.1038/nature01611
16. Zhang L, Wrana JL. The emerging role of exosomes in Wnt secretion and transport. *Curr Opin Genet Dev.* (2014) 27:14–9. doi: 10.1016/j.gde.2014.03.006

17. Wang T, Xu Z. miR-27 promotes osteoblast differentiation by modulating Wnt signaling. *Biochem Biophys Res Commun.* (2010) 402:186–9. doi: 10.1016/j.bbrc.2010.08.031
18. Jennewein C, von Knethen A, Schmid T, Brüne B. MicroRNA-27b contributes to lipopolysaccharide-mediated peroxisome proliferator-activated receptor gamma (PPARgamma) mRNA destabilization. *J Biol Chem.* (2010) 285:11846–53. doi: 10.1074/jbc.M109.066399
19. Gross JC, Chaudhary V, Bartscherer K, Boutros M. Active Wnt proteins are secreted on exosomes. *Nat Cell Biol.* (2012) 14:1036–45. doi: 10.1038/ncb2574
20. Xu D, Tahara H. The role of exosomes and microRNAs in senescence and aging. *Adv Drug Deliv Rev.* (2013) 65:368–75. doi: 10.1016/j.addr.2012.07.010
21. Théry C, Zitvogel L, Amigorena S. Exosomes: composition, biogenesis and function. *Nat Rev Immunol.* (2002) 2:569–79. doi: 10.1038/nri855
22. Wu Y, Deng W, Klinke DJ. II. Exosomes: improved methods to characterize their morphology, RNA content, and surface protein biomarkers. *Analyst.* (2015) 140:6631–42. doi: 10.1039/c5an00688k
23. Prattichizzo F, Micolucci L, Cricca M, De Carolis S, Mensà E, Ceriello A, et al. Exosome-based immunomodulation during aging: a nano-perspective on inflamm-aging. *Mech Ageing Dev.* (2017) 168:44–53. doi: 10.1016/j.mad.2017.02.008
24. Skogberg G, Telemo E, Ekwall O. Exosomes in the thymus: antigen transfer and vesicles. *Front Immunol.* (2015) 6:366. doi: 10.3389/fimmu.2015.00366
25. Turiák L, Misják P, Szabó TG, Aradi B, Pálóczi K, Ozohanics O, et al. Proteomic characterization of thymocyte-derived microvesicles and apoptotic bodies in BALB/c mice. *J Proteomics.* (2011) 74:2025–33. doi: 10.1016/j.jprot.2011.05.023
26. Skogberg G, Gudmundsdottir J, van der Post S, Sandström K, Bruhn S, Benson M, et al. Characterization of human thymic exosomes. *PLoS ONE.* (2013) 8:e67554. doi: 10.1371/journal.pone.0067554
27. Lundberg V, Berglund M, Skogberg G, Lindgren S, Lundqvist C, Gudmundsdottir J, et al. Thymic exosomes promote the final maturation of thymocytes. *Sci Rep.* (2016) 6:36479. doi: 10.1038/srep36479
28. Solti I, Kvell K, Talaber G, Veto S, Acs P, Gallyas F, et al. Thymic atrophy and apoptosis of CD4+CD8+ thymocytes in the cuprizone model of multiple sclerosis. *PLoS ONE.* (2015) 10:e0129217. doi: 10.1371/journal.pone.0129217
29. Feller D, Kun J, Ruzsics I, Rapp J, Sarosi V, Kvell K, et al. Cigarette smoke-induced pulmonary inflammation becomes systemic by circulating extracellular vesicles containing Wnt5a and inflammatory cytokines. *Front Immunol.* (2018) 9:1724. doi: 10.3389/fimmu.2018.01724
30. Kvell K, Nguyen TH, Salmon P, Glauser F, Werner-Favre C, Barnet M, et al. Transduction of CpG DNA-stimulated primary human B cells with bicistronic lentivectors. *Mol Ther.* (2005) 12:892–9. doi: 10.1016/j.ymthe.2005.05.010
31. Ragnarson B, Bengtsson L, Haegerstrand A. Labeling with fluorescent carbocyanine dyes of cultured endothelial and smooth muscle cells by growth in dye-containing medium. *Histochemistry.* (1992) 97:329–33.
32. Wei M, Yang T, Chen X, Wu Y, Deng X, He W, et al. Malignant ascites-derived exosomes promote proliferation and induce carcinoma-associated fibroblasts transition in peritoneal mesothelial cells. *Oncotarget.* (2017) 8:42262–71. doi: 10.18632/oncotarget.15040
33. Ter-Ovanesyan D, Kowal EJK, Regev A, Church GM, Cocucci E. Imaging of isolated extracellular vesicles using fluorescence microscopy. *Methods Mol Biol.* (2017) 1660:233–41. doi: 10.1007/978-1-4939-7253-1_19
34. Rana S, Yue S, Stadel D, Zöller M. Toward tailored exosomes: the exosomal tetraspanin web contributes to target cell selection. *Int J Biochem Cell Biol.* (2012) 44:1574–84. doi: 10.1016/J.BIOCEL.2012.06.018
35. Lankford KL, Arroyo EJ, Nazimek K, Bryniarski K, Askenase PW, Kocsis JD. Intravenously delivered mesenchymal stem cell-derived exosomes target M2-type macrophages in the injured spinal cord. *PLoS ONE.* (2018) 13:e0190358. doi: 10.1371/journal.pone.0190358
36. Mineo M, Garfield SH, Taverna S, Flugy A, De Leo G, Alessandro R, et al. Exosomes released by K562 chronic myeloid leukemia cells promote angiogenesis in a src-dependent fashion. *Angiogenesis.* (2012) 15:33–45. doi: 10.1007/s10456-011-9241-1
37. Ludwig A-K, De Miroschedji K, Doeppner TR, Börger V, Ruesing J, Rebmann V, et al. Precipitation with polyethylene glycol followed by washing and pelleting by ultracentrifugation enriches extracellular vesicles from tissue culture supernatants in small and large scales. *J Extracell Vesicles.* (2018) 7:1528109. doi: 10.1080/20013078.2018.1528109
38. Phan J, Kumar P, Hao D, Gao K, Farmer D, Wang A. Engineering mesenchymal stem cells to improve their exosome efficacy and yield for cell-free therapy. *J Extracell Vesicles.* (2018) 7:1522236. doi: 10.1080/20013078.2018.1522236
39. Ramirez MI, Amorim MG, Gadelha C, Milic I, Welsh JA, Freitas VM, et al. Technical challenges of working with extracellular vesicles. *Nanoscale.* (2018) 10:881–906. doi: 10.1039/C7NR08360B
40. Van Deun J, Mestdagh P, Sormunen R, Cocquyt V, Vermaelen K, Vandesompele J, et al. The impact of disparate isolation methods for extracellular vesicles on downstream RNA profiling. *J Extracell Vesicles.* (2014) 3:24858. doi: 10.3402/jev.v3.24858
41. Takahashi Y, Nishikawa M, Shinotsuka H, Matsui Y, Ohara S, Imai T, et al. Visualization and *in vivo* tracking of the exosomes of murine melanoma B16-BL6 cells in mice after intravenous injection. *J Biotechnol.* (2013) 165:77–84. doi: 10.1016/j.jbiotec.2013.03.013
42. Wei G, Jie Y, Haibo L, Chaoneng W, Dong H, Jianbing Z, et al. Dendritic cells derived exosomes migration to spleen and induction of inflammation are regulated by CCR7. *Sci Rep.* (2017) 7:42996. doi: 10.1038/srep42996
43. Karbiener M, Fischer C, Nowitsch S, Opriessnig P, Papak C, Ailhaud G, et al. microRNA miR-27b impairs human adipocyte differentiation and targets PPARgamma. *Biochem Biophys Res Commun.* (2009) 390:247–51. doi: 10.1016/j.bbrc.2009.09.098
44. Lin Q, Gao Z, Alarcon RM, Ye J, Yun Z. A role of miR-27 in the regulation of adipogenesis. *FEBS J.* (2009) 276:2348–58. doi: 10.1111/j.1742-4658.2009.06967.x
45. Skogberg G, Lundberg V, Berglund M, Gudmundsdottir J, Telemo E, Lindgren S, et al. Human thymic epithelial primary cells produce exosomes carrying tissue-restricted antigens. *Immunol Cell Biol.* (2015) 93:727–34. doi: 10.1038/icb.2015.33
46. Wen SW, Sceneay J, Lima LG, Wong CSF, Becker M, Krumeich S, et al. The biodistribution and immune suppressive effects of breast cancer-derived exosomes. *Cancer Res.* (2016) 76:6816–27. doi: 10.1158/0008-5472.CAN-16-0868
47. Ernszt D, Banfai K, Kellermayer Z, Pap A, Lord JM, Pongracz JE, et al. PPARgamma deficiency counteracts thymic senescence. *Front Immunol.* (2017) 8:1515. doi: 10.3389/fimmu.2017.01515

Conflict of Interest Statement: The authors declare that the research was conducted in the absence of any commercial or financial relationships that could be construed as a potential conflict of interest.

Copyright © 2019 Banfai, Garai, Ernszt, Pongracz and Kvell. This is an open-access article distributed under the terms of the Creative Commons Attribution License (CC BY). The use, distribution or reproduction in other forums is permitted, provided the original author(s) and the copyright owner(s) are credited and that the original publication in this journal is cited, in accordance with accepted academic practice. No use, distribution or reproduction is permitted which does not comply with these terms.

Available online at www.sciencedirect.com
SCIENCE DIRECT
Immunology Letters 104 (2006) 18–28
Immunology Letters
www.elsevier.com/locate/

Review

Still waiting for the toll?☆

E.L. Cooper[a], K. Kvell[b,*], P. Engelmann[b], P. Nemeth[b]

[a] *Laboratory of Comparative Neuroimmunology, Department of Neurobiology, David Geffen School of Medicine at UCLA, University of California, Los Angeles, LA 90095-1763, USA*
[b] *Department of Immunology and Biotechnology, Faculty of Medicine, University of Pécs, Pécs 7643, Hungary*

Received 1 November 2005; received in revised form 9 November 2005; accepted 9 November 2005
Available online 5 December 2005

Abstract

Multicellular organisms including invertebrates and vertebrates live in various habitats that may be aquatic or terrestrial where they are constantly exposed to deleterious pathogens. These include viruses, bacteria, fungi, and parasites. They have evolved various immunodefense mechanisms that may protect them from infection by these microorganisms. These include cellular and humoral responses and the level of differentiation of the response parallels the evolutionary development of the species. The first line of innate immunity in earthworms is the body wall that prevents the entrance of microbes into the coelomic cavity that contains fluid in which there are numerous leukocyte effectors of immune responses. When this first barrier is broken, a series of host responses is set into motion activating the leukocytes and the coelomic fluid. The responses are classified as innate, natural, non-specific, non-anticipatory, non-clonal (germ line) in contrast to the vertebrate capacity that is considered adaptive, induced, specific, anticipatory and clonal (somatic). Specific memory is associated with the vertebrate response and there is information that the innate response of invertebrates may under certain conditions possess specific memory. The invertebrate system when challenged affects phagocytosis, encapsulation, agglutination, opsonization, clotting and lysis. At least two major leukocytes, small and large mediate lytic reactions against several tumor cell targets. Destruction of tumor cells in vitro shows that phagocytosis and natural killer cell responses are distinct properties of these leukocytes. This has prompted newer searches for immune function and regulation in other systems. The innate immune system of the earthworm has been analyzed for more than 40 years with every aspect examined. However, there are no known entire sequences of the earthworm as exists in these other invertebrates. Because the earthworm lives in soil and has been utilized as a successful monitor for pollution, there are studies that reveal up and down regulation of responses in the immune system after exposure to a variety of environmental pollutants. Moreover, there are partial sequences that appear in earthworms after exposure to environmental pollutants such as cadmium and copper. There are now attempts to define the AHR receptor crucial for intracellular signaling after exposure to pollutants, but without linking the signals to changes in the immune system. There are several pathways for signal transduction, including JAK/STAT, TOLL, TRAF PIP3, known in invertebrates and vertebrates. For resistance to pathogens, conserved signal transduction components are required and these include a Toll/IL-1 receptor domain adaptor protein that functions upstream of a conserved p38 MAP kinase pathway. This pathway may be an ancestral innate immune signaling pathway found in a putative common ancestor of nematodes, arthropods and even vertebrates. It could also help us to link pollution, innate immunity and transduction in earthworms.
© 2005 Elsevier B.V. All rights reserved.

Keywords: Toll; Signal transduction; Pollution; Innate immunity

1. Introduction

1.1. Anticipating innate immunity in earthworms without a TOLL

Invertebrate animals express various immune mechanisms against their environmental pathogens and these are accomplished through cellular and humoral responses, similar to some of those of the vertebrate immune system. In earthworms innate immunity is maintained by cellular components, different coelomocytes (leukocytes), housed in the coelomic cavity whose fluid also contains many immunologically active (antimicrobial) molecules (lysenin, fetidin, eiseniapore, coelomic cytolytic factor, CCF-1, Lumbricin I) [1]. Earthworm coelomocytes (leukocyte subpopulations) have been characterized by different immunological techniques using mammalian antigen-specific monoclonal antibodies. For characterizing the role of leukocytes in humoral immune mechanisms, different functional assays (cytotoxicity and antibacterial assays) have been employed.

☆ EFIS2005—13th Signal Transduction Meeting, Balatonöszöd, Hungary.
* Corresponding author. Tel.: +36 725 362 88; fax: +36 725 362 89.
E-mail address: krisztian.kvell@aok.pte.hu (K. Kvell).

0165-2478/$ – see front matter © 2005 Elsevier B.V. All rights reserved.
doi:10.1016/j.imlet.2005.11.012

These molecules may combine with conserved antimicrobial agents to solve the problems of multi-antibiotic resistant strains of pathogens. In addition to antimicrobial molecules, coelomocytes contain several lysosomal enzymes that participate in the digestion of phagocytosed microorganisms. Despite this wealth of information the signaling mechanisms are not defined.

In multicellular organisms, the phagocytic response plays a major role in immune mechanisms against environmental pathogens and in clearance of apoptotic cells. The innate immune system is capable of recognizing conserved microbial structures or products of microbial metabolism (pathogen associated molecular patterns [PAMPs]) through a set of germ line encoded receptors called pattern recognition receptors (PRRs). The PRRs of the innate immune system, particularly the family of Toll-like receptors (TLRs) are responsible for initiating inflammatory responses against invading pathogens. Toll and Toll-like receptor signaling is essential for phagocytosis and antimicrobial peptide production in insects and vertebrates [2–6]. Toll-like receptor is also present in the nematode worm *Caenorhabditis elegans*, however, antimicrobial peptide expression is independent from the Toll pathway [7]. The point of this review therefore is to present some of the recent characteristics of the innate cellular response in earthworms (annelid worms) a complement to humoral immune functions [1]. Earthworms possess a pattern recognition molecule (CCF), which may trigger the prophenoloxidase cascade, a crucial innate response and an impressive array of other innate responses [8–9] (Fig. 1). However, Toll-like proteins have not yet been discovered (Tables 1 and 2). Again there is a need to define the signaling pathways.

1.2. Toll/IL-1 in innate immunity of a nematode worm

During the latter part of the 20th century, the discovery of mammalian Toll-like receptors (TLRs), homologues of insect Toll receptors, linked innate and adaptive immunity. This was the first instance that an immune pathway discovered outside of mammals could be superimposed onto the human immune system, thus unifying aspects of evolution of immune competence. There are entire sequences of genomes from several invertebrates (e.g. the fruitfly *Drosophila*, the nematode *C. elegans*, the tunicate *Ciona*, the mosquito *Anopheles*). In addition, there are established roles of JAK/STAT signaling in *Drosophila* immune responses [10–11]. Genetic and functional genomic approaches have begun to define the molecular determinants of pathogen resistance in *C. elegans* [12]. For resistance to pathogens, conserved signal transduction components are required and these include a Toll/IL-1 receptor domain adaptor protein that functions upstream of a conserved p38 MAP kinase pathway. This pathway may be an ancestral innate immune signaling pathway found in a putative common ancestor of nematodes, arthropods and even vertebrates. Furthermore, it probably predated the involvement of the well-known Toll signaling pathways in innate immunity. Pathogen resistance in *C. elegans* offers fertile opportunities for continuous probing into evolutionary and mechanistic insights of signal transduction and function in innate immunity.

2. Earthworms and nk cells: dissociation of phagocytosis and nk cell activity

2.1. Characterizing earthworm leukocyte mitochondria

Clearly phagocytosis is fundamental but in the case of earthworms there has been substantial effort toward characterizing earthworm leukocytes even past the level of phagocytosis. To characterize NK-like cells we have found that earthworm coelomocytes (leukocytes) exist in two forms, i.e., small (SC) and large (LC) cells, as demonstrated by velocity sedimentation, electron microscopy, and FCM [13]. However, we know

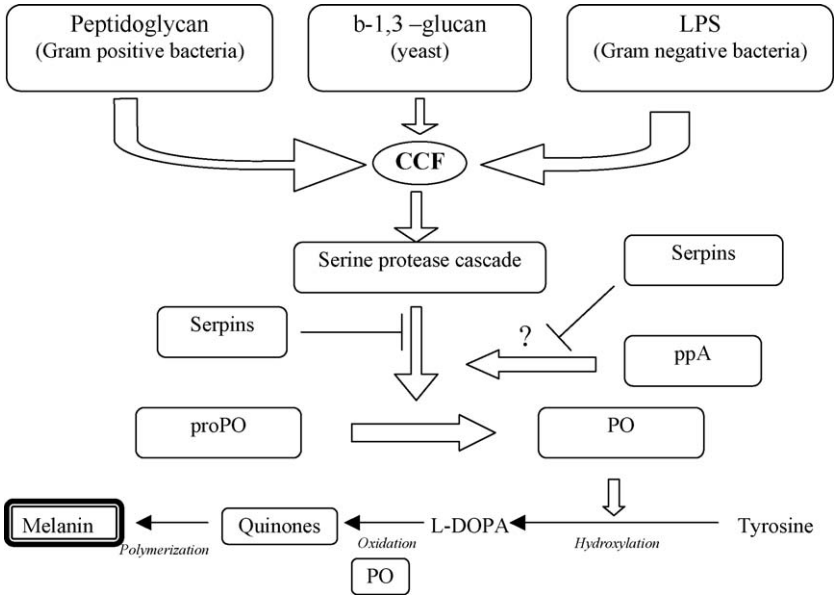

Fig. 1. A supposed activation cascade of the earthworm immune response triggered by a pattern recognition molecule, CCF, bound to pathogen-associated molecular patterns (β-1,3 glucans, LPS, peptidoglycans). The cascade involves serine proteases, phenoloxidase (PO) and a putative prophenoloxidase-activating enzyme (ppA).

Table 1
Characterization of earthworm innate immunity with respect to leukocytes and humoral mediators: signaling mechanisms?

Characteristics	Evidence
1. Leukocytes are positive for different mammalian antigen-specific monoclonal antibodies	Discrimination of self and foreign by using molecules similar to CD90, β_2-microglobulin, J-chain of immunoglobulins (Ig superfamily)
1.1. Early detection of leukocyte surface markers by classical microscopy and serology	Three subpopulations of coelomocytes by phenotype:
1.2. What is the evidence from FACS analyses? Putative CD markers revealed by using mammalian monoclonal antibodies	Small: CD11a, CD45,CDw49b, CD54, β2-m, CD90
	Large: marker negative phagocytic cells
	Third: Thy-1, CD24, TNF-α
2. Monoclonal antibodies identify four distinct invertebrate leukocyte markers	Production and characterization of EFCC mAbs
2.1. Earthworm coelomocyte differentiation clusters	EFCC1: common antigen
2.2. Recognition of common antigen	EFCC2: chloragocytes
2.3. Specificity: sharing of epitopes by tissues and cells	EFCC3: hyaline coelomocytes
2.4. Are clusters equivalent to cells revealed by other assays?	EFCC4: few cells of coelomic fluid
2.5. Coelomocyte functional heterogeneity	Phagocytosis and encapsulation of bacteria
	EFCC3 cluster: highly phagocytic cells
	EFCC4 cluster: only surface binding of bacteria
3. Relation of coelomocytes to humoral immunity: emerging cytokines and an emerging pattern recognition molecule	Anti-microbial and immune-regulatory molecules includes lysozyme, lysenin, fetidin, lumbricin, CCF-1, TNF-α, TGF-α, superoxide dismutase (SOD)
4. Is there evidence for neuroendocrine-immune linkage?	Hormone-like activities resembling TSH, insulin

Table 2
Defining the cytotoxic response in earthworm innate immunity: signaling mechanisms?

Characteristics	Evidence
1. Expanding the repertoire of vulnerable targets to test cytotoxicity	Cytolytic and hemaglutinating activity of coelomic fluid and cell lysates on adherent mammalian cell lines (HEp-2, HeLa) due to perforin-like molecules
1.1. In vitro cytotoxicity of coelomocyte lysates and cell-free coelomic fluid against HeLa, HEp-2, PC-12 and PA317 cell in vitro	Heat-inactivation and proteinase K but not trypsin digestion dramatically decreases cytotoxic activity
1.2. Denaturing coelomocyte lysates inhibits toxicity	Supernatant of short-term (24 hours) coelomocyte cultures kills 100% of target cells in 10 hours
1.3. Supernatant of short-term cultured coelomocytes slowly kill tumor cell lines and suggest a pathway independent of sphyngomyelin	Nematodes are killed through a pathway other than sphyngomyelin
1.4. Apoptosis versus necrosis in target cells after treatment with coelomocyte lysates	Cell damage resembles necrosis as supported by lack of DNA ladder formation
2. Leukocytes contain lysosomal enzymes that respond to bacterial challenge	Certain cells contain hydrolytic enzymes: acid phosphatase, peroxidase, non-specific esterase, alkaline phosphatase, aryl sulphatase
2.1. Role of hydrolytic enzymes	Granular and hyaline amoebocytes release hydrolytic enzymes from preformed discrete granules
2.2. Cytochemistry: lysosomal enzymes	Chloragosomes may be encapsulated in “brown bodies” (granulomas) containing lipofuscin and melanin
2.3. Digestive enzymes and melanization	
3. Origins of coelomocytes	EFCC staining pattern confirms mesodermal origin
4. Perspectives of invertebrate immunity revealed by the earthworm	Comparative analyses of insect and earthworm immunity in regard of leukocytes, agglutinating and lysing functions with special attention on Toll-mediated pathways

little concerning the functional activities of various, important organelles, such as mitochondria known to play an important role in apoptosis. In comparison with SC, LC from *Eisenia foetida* have a higher number of mitochondria, and, accordingly, showed a greater fluorescence intensity when mitochondrial mass was measured by nonyl-acridine orange and FCM. To measure MMP we used both the lipophylic cationic probe JC-1 and Rh123. The intracellular localization of JC-1 in SC and LC was observed by fluorescence microscopy. In coelomocytes there may be several energy-independent Rh123-binding sites whose role must still be elucidated. It is possible to analyze mitochondrial parameters by FCM in intact invertebrate leukocytes and that the type of cell and the probe used have a critical importance.

2.2. Speci city of cytotoxicity by autogeneic and allogeneic effectors

Moving to functional assays earthworm coelomocytes have been used as effector cells against the human tumor target, K562. To first assess the viability of effectors, incorporation of [3H]-

thymidine was tested and was higher in autogeneic (A ⇐ A, self) than in allogeneic (A ⇔ B, nonself) coelomocytes. A ⇔ A showed significantly greater numbers in S, G2, or M phases than A ⇔ B coelomocytes. When A ⇔ A or A ⇔ B were cultured, no significant cell killing occurred in either, as measured in a 4-h 51Cr release assay. A ⇔ A but not A ⇔ B killed K562 target cells. Cytotoxicity was dependent upon membrane binding between small, electron-dense coelomocytes and targets; it was enhanced by adding PHA. The heat labile supernatant from A ⇔ A but not from A ⇔ B killed K562 targets after cultivation for 10 min at 22 °C, but not immediately after washing. Recognition of, binding to, and killing of foreign cells in a natural killer cell-like reaction may reflect aspects of natural immunity in earthworms [14].

2.3. Coelomocyte lysates exert cytotoxic properties

There have been efforts to extend the previous investigation. The earthworm coelomic fluid contains biologically active molecules and leukocytes that participate in phagocytosis and granuloma formation. Presumably they synthesize and secrete several effector modulators of innate immune responses such as antibacterial molecules, cytotoxic proteins and cytokines [15]. Several lytic molecules have been detected in the coelomic fluid but it is not yet clear which are actually released from the coelomocytes. The cytotoxic effects of coelomocytes on mammalian target cells were analyzed and provided evidence that the lytic factors originate from coelomocytes. Cell-free coelomic fluid, supernatants of short-term cultured coelomocytes and lysates from coelomocytes – derived by mechanical and detergent extraction – were used in cytotoxicity assays performed on different mammalian standard tumor cell lines and mouse fibroblasts. Native and denaturized (using proteinase K, trypsin digestions or heat-inactivation) coelomocyte lysates (CCL) were used. The viability controls of targeted cells were made by photometric measures and analyzed by inverted microscopy. Our results revealed that the coelomic fluid, the supernatant of cultured coelomocytes and the CCL significantly decreased ratios of living cells compared to controls in a dose-dependent manner. Experiments performed with CCLs suggest that coelomocytes are responsible for the production of cytotoxic components presumably proteins [16].

2.4. Dissociation of phagocytosis from cell killing

Clearly the presence of NK cells throughout the phylogenetic series of multicellular animals must be dissociated from the earliest of ubiquitous functions, i.e., phagocytosis. Although natural killer (NK) cells are known to preferentially kill cells that lack major histocompatibility complex class I antigens, it is not clear what the signals are that cause attack of these targets [17]. Several membrane receptors have recently been implicated in the signaling process and include molecules with immunoreceptor tyrosine-based activation motifs (ITAM) and motifs that bind phosphoinositide-3 kinase (PI3K). Evidence is emerging that NK cells may use a combination of several receptors and signaling pathways to protect the host against infection and possibly against malignancies. Perhaps NK cells are regulated by the balance of activating and inhibitory signals transmitted by membrane receptors that recognize ligands on cell surfaces of potential target cells. Because many of these receptors are constitutively expressed on NK cells, this suggests that immune responses could be controlled by the presence or absence of ligands for these receptors on potential target cells.

Now the evidence for NK-like cell killing by earthworm leukocytes is pertinent and compelling. Co-culturing earthworm leukocytes with tumor cell targets answers several questions concerning cell killing and characterizes the cells for the first time with respect to putative surface markers. Earthworm coelomocytes (leukocytes) affect cytotoxicity at significantly high levels against NK-sensitive, human tumor cell line, K562 and NK-resistant targets (U937, BSM, CEM) [18]. By cytofluorimetric analyses using mouse anti-human monoclonal antibodies and by morphological evaluations, two leukocyte types were identified: (1) small (8–11 μm) electron-dense cells (SC): CD11a+, CD45RA+, CD45RO+, CDw49b+, CD54+, beta 2-m+ and Thy-1+ (CD90); (2) large (12–15 μm) electron-lucent cells (LC) that are negative for these markers. Both cell types were negative for other CD and MHC class I and class II markers. SC were active during recognition, rapidly binding to targets; LC were phagocytic. Release of 51Cr revealed rapid, significant, and equal levels of killing at 4, 20 and 37 °C. We propose that primitive NK-like activity appeared early in evolution and that it appeared later than the universal phagocytic event. Of course may question specificity of the response but it seems inherent in the two classes of cells that bear markers.

2.5. After cytotoxicity, granulomas can form in vitro (encapsulation)

Structural changes occur when effector coelomocytes and target K562 erythromyeloid human tumor cells interact during cytotoxic activity [19]. In in vitro cultures: (1) the two earthworm cell types (i.e., small and large coelomocytes) retained their morphological features; (2) their DNA content was significantly less than that of human lymphocytes and the erythromyeloid human tumor cell line K562; (3) significant percentages of coelomocytes were found to be in S or G2/M phases of the cell cycle. When cultivated alone for up to 3 h, coelomocytes formed no aggregates. However, when mixed with K562, coelomocytes spontaneously killed tumor cells, and cytotoxic reactivity was accompanied by the formation of multiple aggregates similar to granulomas. These results are the first to describe this type of earthworm non-specific "inflammatory" response in vitro against tumor cells and it mirrors this routine response in vivo.

3. Cell signaling in invertebrates in relation to innate immunity in nematode worms and fruit ies (Table 3)

3.1. PCB alters tyrosine kinase-mediated cell signaling in mussels

Polychlorinated biphenyls (PCBs) are industrial chemicals that have been released into the environment resulting in

Table 3
Clues in earthworms and evidence concerning signaling in other invertebrates in relation to pollution

Organism	Effect	Investigator
Earthworm annetocin (member of vasopressin/oxytocin superfamily)	Effects of zinc and lead on gene expression	Ricketts et al. [4]
Earthworms	Copper and cadmium changes 2 metallothionein isoforms	Galay-Burgos et al. [24]
Mussel hemocytes	PCB increases tyrosine phosphorylation of transcription factor STAT5	Canesi et al. [20]
Mussel hemocytes	Modulation by heterologous cytokines via tyrosine kinase-mediated signal transduction	Canesi et al. [21]
Oyster hemocytes	Oyster IκB kinase is conserved	Escoubas and Roch [23]

widespread and persistent contamination [20]. PCBs exist as 209 different congeners depending on the chlorine substitution on the biphenyl rings; the physical properties and the toxic effects of a PCB congener are structure-dependent. Individual ortho-substituted non-coplanar PCB congeners were tested for their effects on functions of mussel (*Mytilus galloprovincialis* Lam.) hemocytes. The results demonstrate that Mitogen Activated Protein Kinases MAPKs, and in particular the stress-activated p38 and JNK MAPKs, that represent a key step in the response of mussel hemocytes to bacterial infection, are a target for different non-coplanar and coplanar PCB congeners. The results also show functional differences between different PCB congeners with respect to the hemocyte functions. However, chlorine substitution at the ortho positions is not necessarily related to immunotoxicity: the hexachlorinated P128 (2,2′,3,3′,4,4′-hexachlorobiphenyl) had no significant effect on mussel hemocytes, whereas its isomer P153, that represents a major component of environmental PCBs, and that is accumulated in mussel tissues, significantly affected both aspects of the immune response and relevant signal transduction pathways. These are the first data on the effects and possible mechanisms of immunotoxicity of non-coplanar PCBs in mussel hemocytes. The results support the hypothesis that the innate immune system is a sensitive target for these contaminants in both vertebrates and invertebrates. Moreover, when considering that non-coplanar congeners are present both in commercial mixtures and, in higher proportions, in environmental samples, the results suggest that bivalve hemocytes represent a useful model for evaluating the potential immunotoxicity of PCB contamination.

3.2. Tyrosine kinase-mediated signaling activates mussel hemocytes

In bivalve molluscs, innate cell immunity is mediated by circulating hemocytes that resemble the vertebrate monocyte/macrophage lineage that destroys microbes by phagocytosis and cytotoxic reactions [21]. According to earlier results, activation of Mitogen Activated protein Kinases (MAPKs) is involved in mussel hemocyte responses to bacterial challenge. Cell pretreatment with the macrophage activator IFN-γ significantly increased bactericidal activity of mussel hemocyte towards *E. coli*. Human recombinant IFN-γ stimulated tyrosine phosphorylation of different members of STAT-like proteins (Signal Transducers and Activators of Transcription), as evaluated by Western blotting of hemocyte protein extracts with specific anti-phospho-STAT antibodies. A similar increase in phosphorylation of immunoreactive STATs was observed in hemocytes incubated with *E. coli*. This indicates that tyrosine phosphorylation of STAT-like members represents a physiological step in hemocyte activation. IFN-γ causes persistent phosphorylation of immunoreactive STAT1, a transcription factor that plays a critical role in innate immunity towards Gram negative bacteria in mammalian systems; moreover, hemocyte pretreatment with IFN-γ significantly increased bacteria-induced STAT1 phosphorylation, whereas IFN-α did not. IFN-γ also transiently affected the phosphorylation state of different MAPKs. The extent and time course of MAPK phosphorylation induced by IFN-γ were distinct from those elicited by either IFN-α or bacterial challenge. Thus, hemocyte function can be modulated by heterologous cytokines and bacterial signals that act together through tyrosine kinase-mediated transduction pathways converging on STAT- and MAP-like members.

3.3. Genomics, biomarkers and pollution in earthworms

The emergence of new technologies from the genomics revolution will transform the potential application of biomarkers to assess how pollutants impact people, animals and ecosystems [22]. Genetic databases provide an enormous resource from which candidate molecular biomarkers can be identified and later utilized for further analyses. However, a major challenge is to link these novel molecular indices to ecologically relevant whole-organism life-cycle traits (such as reproduction and growth). Such a functional link is provided by annetocin, previously characterized as a member of the vasopressin/oxytocin superfamily of neuropeptides. It is expressed in annelid worms within the neurons of the central nervous system and has been shown to be involved in the induction of egg-laying behavior. Here annetocin has been validated as a novel biomarker of reproductive fitness in the earthworm *Eisenia fetida*. The design of primer pairs targeted toward oligochaete annetocin has facilitated the isolation of a full-length annetocin cDNA from this species. Optimization of a real-time quantitative PCR procedure exploiting the fluorescent DNA-binding molecule, Sybr Green, has allowed the measurement of annetocin transcript levels over a range covering six orders of magnitude. Using this approach, gene expression was measured in earthworms exposed to soils polluted with high concentrations of zinc and lead. Traditional

growth and reproductive indices, including cocoon production, were also recorded and related to the molecular parameter. The future use of annetocin as a molecular genetic biomarker in terrestrial ecotoxicology is discussed.

3.4. Epitope mapping in earthworms and the target of EFCC1 mAb

Here we present new relevant information. A library of random nine amino acid long peptide sequences has been displayed on filamentous phage surfaces incorporated in coat-protein VIII. Following several rounds of enrichment using the EFCC1 mAb 60 of the best growing bacterial clones containing phages were selected and further tested by ELISA. Of those 11 clones were sequenced to determine their peptide content originating from the library. The sequences retained partially overlapped outlining the following consensus sequence being the epitope recognized by EFCC1 mAb: SLSDSC. The specificity of the method has been verified by ELISA. When the SLSDSC peptide sequence was blasted to determine possible homology in the nucleotide databases, several interesting molecules were discovered (including rat membrane cofactor protein, rat olphactory receptor, human arginine aminopeptidase). Recently performed re-blast has added even newer molecules to the list of homologous peptide sequences: Na/H ion exchanger isoform of *C. elegans* a transcription factor of *Str. purpureatus* and a protein kinase of *Leishmania major* (unpublished observations). This is extremely pertinent to the current effort toward finding earthworm signaling mechanisms.

3.5. An Oyster IkappB kinase (oIKK) involved in signaling

Searched for genes involved in oyster immunity and successfully isolated a cDNA encoding a polypeptide closely related to the mammalian IkappaB kinase (IKK) family [23]. IKK proteins play a central role in cell signaling by regulating nuclear factor-kappaB (NF-kappaB) activation. They cloned an oyster IKK-like protein (oIKK) that is organized similarly to mammalian IKK proteins. The molecule possesses an amino-terminal kinase domain followed by a leucine zipper region and a carboxyl-terminal helix-loop-helix motif. When transfected into human cell lines, oIKK activated the expression of NF-kappaB-controlled reporter gene, whereas transfections with mutants of oIKK deleted within the kinase domain or within the helix-loop-helix motif abolished and greatly reduced reporter gene activation. Thus, oIKK can replace hIKK-alpha in catalyzing NF-kappaB nuclear translocation and trigger gene expression. They propose evolutionarily conserved signaling machinery in which IKK plays a major role.

4. Earthworm natural immunity in relation to pollution

4.1. Gene expression in earthworms as an index of pollution exposure

Physiological responses to environmental stressors may induce changes in gene expression as a component of an organism's homeostatic mechanisms [24]. Thus, molecular genetic biomarkers can monitor sublethal chemical exposure in ecosystems. The TaqMan real-time quantitative polymerase chain reaction has been used to measure gene transcription in earthworms (*Lumbricus rubellus*) maintained on control or cadmium- or copper-spiked soil. Changes in expression of two target genes, that encode metallothionein isoform 2 (MT-2) and the mitochondrial large ribosomal subunit (MLRS), were quantified against the internal control gene beta-actin. Transcript levels displayed qualitative and quantitative differences in responses to the two metal ions. MLRS gene levels were unaffected by exposure to cadmium but displayed a response to high levels of copper. Cadmium by contrast greatly induced MT-2 gene expression, but copper only altered transcription of this gene at high exposure concentrations. Thus, gene expression in earthworms can be used as an index of pollution exposure since they are environmentally appropriate animal models.

4.2. Protein kinases in earthworms after exposure to copper and cadmium

When earthworms are exposed to extreme conditions (cadmium, copper, heat) they express proteins similar to known vertebrate kinases as revealed by evidence of sequence homologies [25–28] (Fig. 2). Although there has been no specific study performed, one particular sequence suggests that *L. rubellus* expresses a protein similar to tyrosine protein kinase found in B lymphocytes when exposed to cadmium. By contrast those earthworms exposed to copper express a protein similar to a testis specific phosphoglycerate kinase (Fig. 3). The most likely pathway for us to investigate in earthworms (which explains why we were anticipating innate immunity without a TOLL and now still waiting for TOLL!) with what we know already seems to be that associated with the AHR (aryl hydrocarbon receptor) receptor and ARNT (aryl hydrocarbon receptor nuclear translocator). These are receptors of pollutants which when combined and activated by the receptors can change gene expression profiles, turning on or off certain genes. This could explain the up and down regulation of known innate immune responses after exposure to various pollutants (Figs. 4 and 5).

4.3. Aryl hydrocarbon receptor (AHR)-like molecule in earthworms?

Strong pathogenic effects, including immunotoxicity and carcinogenesis of xenobiotics like TCDD and PCBs, in mammals are mainly mediated by the aryl hydrocarbon receptor (AHR) [29]. AHR-homologs have recently been shown for *C. elegans* (Nematoda), *Drosophila melanogaster* (Diptera) and *Mya arenaria* (Bivalvia). Since immune modulating effects have been described in earthworms after exposure to xenobiotics such as PCBs investigations focused on the existence of an AHR-like molecule in *E. fetida*. Results revealed two proteins in tissue extracts and one protein in coelomocyte lysates that cross-reacted with an affinity purified AHR-antibody by Western blot analysis. Reverse transcription of poly $(A)^+$RNA from *E. fetida* and amplification of cDNA with the degenerate primers,

AUTHORS:Chaseley,J., Hedley,B.A., Morgan,J.C., Sturzenbaum,S., Blaxter,M. and Kille,P.; Contact: Jennifer Chaseley BIOSI 1 Cardiff University, Cardiff, Wales

PREDICTED: similar to Tyrosine-protein kinase BLK (B lymphocyte)

SEQUENCE:

```
  1 gctactccat atgctggaag aaagtgcgga agtcgaagcc ttattgaaaa ctggacacag
 61 aatgccacgt cccgatgaat gtccaccaga actgtttgat ggtgttgtca ctccttgctg
121 gaacgtcgct gccaagaaga gacctgattt caagactctg tgcaagtcga tcagaagctt
181 ccgccagggt ggtagtgatc agcaggaggg ttactacacc gctgacctaa cacgcaaaac
241 ttacgacaac cctaaagaac gtacaaatga ctacactgca ggacgtgctg gaaaatcagc
301 ggccaaaccg gattcaatct atgacgatac tcgaaaatag aaatactcgt ttctcttcgg
361 ttagatatga ctgcataaga ctgatcagac tccgagtgta accgtgcgta taatgtgtat
421 agtagaacat acacgcttat acttgtgcct atcccgaact ttgaacttta tatgcatgta
481 atgtatactg cattgtattg taggcctacc tacaaattta taaagcttct ttcacagtgc
541 acaccaatca gtgtgaatga cacgagaaaa gagagtagtt ttaacacggc gtanagatgt
601 gatttagggt actgtaggta atagacaaga acgtgtcgct ggagatttca aagtgcaaga
661 ccaatgaagg cataagctgg agttttggcc aaagcagtag tatacattca tgcataattg
721 catatagact acacatacaa ccataggcct tatcttctac ataa
```

LOCUS DR077578, 764 bp mRNA linear (EST 08-JUN-2005); cDNA clone Lr Cd2CF 65C04 similar to UniRef100 UPI00004A69F4; ACCESSION: DR077578

Fig. 2. The *Lumbricus rubellus* EST program—sequences from a Cadmium exposure library.

AUTHORS: Calafato,S., Chaseley,J., Hedley,B.A., Morgan,A.J., Spurgeon,D.J., Sturzenbaum,S., Kille,P. and Blaxter,M.; Contact: Jennifer Chaseley BIOSI 1 Cardiff University, Cardiff, Wales

PREDICTED: similar to testis-specific phosphoglycerate kinase

SEQUENCE:

```
  1 gacgagggga accttcgctt cacattgaag aggaaggaaa ggtcacggct gaaaacggtg
 61 aaaagctaaa ggctgaacct gaagacgttg acaagtttcg agccagtctc agcaaacttg
121 gagatatata cgttaacgac gcctttggca ctgcgcacag accacacagt tcaatggttg
181 gatgtaatct gccaatcaaa gcttccggtc ttctgctgaa gaaagaacta tcgtactttg
241 caaaggtcat ggaaaagcca gaaaagccat accttgccat tttaggagga gccaaggtgg
301 ctgacaagat tcagttgatt gagaatcttc tggacaaagt gaccgatatg atcattggtg
361 gtggcatggc cttcacgttc ctcaaagtca acaacaacat ggagattgga aagtctctgt
421 tcgatgagga aggctcgaag atcgtgggaa agctgatgga gaaggcgaaa gccaagaagg
481 tcaacataac gctgccggtt gactttgtca ccggtgacaa gttcgacgcg aaagcgaccg
541 tcggtgcagc caccgtgaaa gagggcatca aaggcgaatg gatgggacta gacattgggc
601 cacagtcgat caagttgttc actgatgcca tcatgaaagc caagacgatc gtgtggaatg
661 gacctcctgg tgtgtttgag atggacaact ttgcgaaggg tactaaggga gttatggacg
721 ctgttgtaaa tgccacgaag aaaggagcta ttaccatcat
```

LOCUS DR009215, 760 bp linear mRNA (EST 18-MAY-2005); cDNA clone Lr Cu2CF 30H04 similar to UniRef100 UPI00004EE20E; ACCESSION: DR009215

Fig. 3. The *Lumbricus rubellus* EST program—sequences from a Copper exposure library.

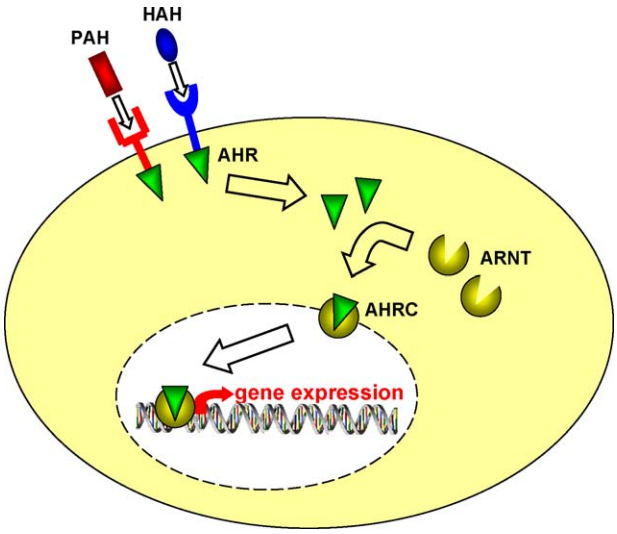

Fig. 4. The AHR signal transduction pathway: binding of polycyclic or halogenated aromatic hydrocarbon (PAH and HAH) ligand causes release of AHR, which then associates with the AHR nuclear translocator protein (ARNT) to generate the heterodimeric "transformed" AHRC. The transformed AHRC binds xenobiotic responsive elements in responsive genes and turns on their transcription [40].

designed for AHR detection in invertebrates and aquatic vertebrates, produced two independent bands of approximately 550 and 250 bp. Efforts to identify an AHR cDNA homolog in *E. fetida* with RT-PCR analysis using poly $(A)^+$RNA were not successful. More analyses that use different primers and/or specific tissues and developmental stages are required to substantiate whether or not an AHR-like molecule exists in *E. fetida*.

4.4. Innate immunity, xenobiotics and signaling

During the 1960s, work on the immune system of earthworms was concerned with inflammatory and cellular responses after tissue transplantation [30]. Later, interest in the humoral immune system emphasized those molecules that cause death of the targets or regulate immune-related activities. Specific interest focused on cytolysins, agglutinins, proteases, protease inhibitors and phenoloxidase. Responses of the immune system were used as markers to evaluate the effects of xenobiotics on the environment. Earthworms were confronted with three contaminants (Arochlor 1254, 2,4 D and carbaryl) and the T2 toxin. Lysozyme was enhanced by Arochlor, but inhibited by carbaryl and T2 toxin, whereas 2,4 D had no effect. Only Arochlor and carbaryl significantly increased intracellular serine protease activity. Plasma serine protease inhibitory activity was completely suppressed by carbaryl and also reduced by T2 toxin. Phagocytosis was dramatically depressed and the effect could be observed on macrophage morphology. All xenobiotics increased plasma cytolytic activity. Detoxification metabolism was stimulated by carbaryl but not by T2 toxin. Since T2 toxin did not increase cytochrome P450 detoxification pathway, this may explain its inhibitory effect on phagocytosis, serine protease inhibitors and lysozyme. Long-term effects of environmental contamination by toxic substances may interfere with earthworm populations through their immune capacities. The signaling pathways can then be analyzed in relation to pollution.

AHR homologues have been identified in vertebrates including mammals, birds, amphibians, bony fish, cartilaginous fish and jawless fish [31–38]. Various analytic efforts including ligand-binding assays, antibody cross-reactivity and photoaffinity labeling have been used in attempts to identify an invertebrate AHR homologue [39–40]. A wide range of invertebrate species (molluscs, arthropods, annelids, echinoderms) has been examined but these efforts failed to identify an AHR homologue with certainty [39–43]. Nevertheless immune modulating and other effects have been observed after exposure of some invertebrates to xenobiotics such as PCBs or TCDD [44–48]. There is a precedent for the use of *C. elegans* in rapid toxicity assessment of

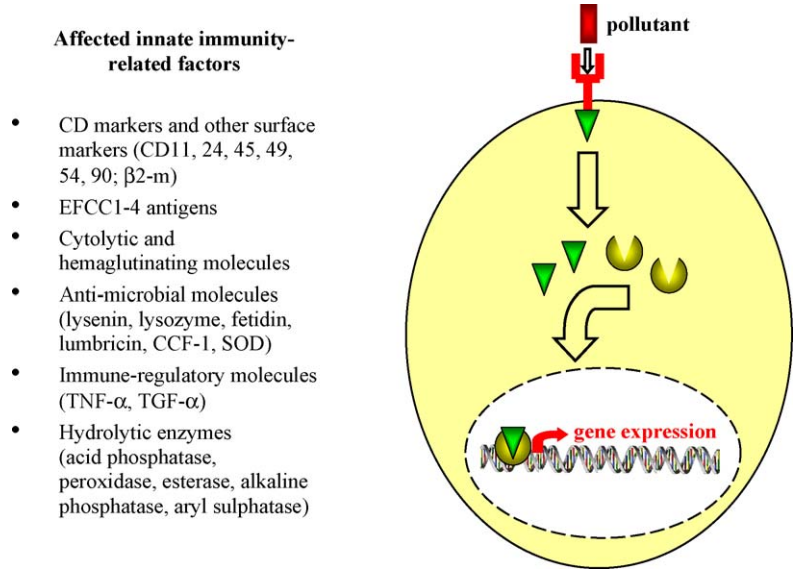

Fig. 5. Pollutant signal transduction pathway: hypothetical pathway of pollutant changing gene expression profile affecting innate immunity.

pharmaceutical compounds [49], gene expression of P450 genes [50], genotoxicity and reproductive success [51] and analysis of cadmium stress [52].

4.5. Non-speci c cellular immunity may be regulated by PAH

Exposure to ubiquitous environmental chemicals, such as polycyclic aromatic hydrocarbons (PAH), may affect the earthworm cellular immune-defense system [47]. They examined cellular functions of coelomocytes such as phagocytosis and H_2O_2 activity by flow cytometry after exposure to soil contaminated with 7,12-dimethylbenzanthracene (DMBA). In addition, increased synthesis of cytochrome P450 was employed by immunohistochemistry and Western blots. Coelomocytes were harvested from earthworms and processed for in vitro phagocytosis and H_2O_2 activity. Phagocytosis was assessed by ingestion of fluorescence beads and H_2O_2 activity examined using 2′,7′-dichloro-fluorescin diacetate that was measured by flow cytometery 2 h after incubation. Results indicated that cell functions were down regulated in a dose-dependent manner after exposure to sublethal doses of DMBA. Cytochrome P450 expression increased as revealed by immunohistochemistry and Western blots. These expressions of innate immunity permit us to evaluate biological activity of earthworms and the effect of soil contamination for future ecotoxicological studies and a search for the role of signaling.

4.6. PCBs, carbaryl and 2,4 dichlorophenoxy acetic acid (2,4 D) modulate earthworm molecular-related natural immunity

Both humoral and cellular immunodefense responses of the earthworms, *E. fetida andrei, Eisenia hortensis*, and *Lumbricus terrestris* have been compared after exposure to the PCB Aroclor 1254 [44–45]. Responses mediated by free factors, detected by in vitro assays for lysozyme, hemolysis and proteases, were increased in both *Eisenia*. Antibacterial activity directed against pathogenic bacteria was increased in *E.f. andrei*. The resistance of *L. terrestris* against non-pathogenic bacteria was decreased, confirming that the bacteria were treated by different systems according to their pathogenicity. Nonspecific cellular functions, including phagocytosis and those related to wound healing, decreased dramatically in all earthworms. As determined by contact test assay, carbaryl activity is characterized by a low LC50 value. Incubating earthworms with low doses of carbaryl inhibited lysozyme and phagocytic activity detected in the cytosol (CL). On the other hand, low doses of carbaryl significantly stimulated cytolysis serine protease activity in the coelomic fluid (CF) and serine protease activity in the CL. Concerning 2,4 D, both cytolysis in the CF and serine protease activity in the CL were stimulated. Phagocytosis was inhibited only with 18 $\mu g/cm^2$ and lysozyme and serine protease inhibitor activities were not affected. The immunotoxicological assays we developed in earthworms, allow distinguishing between chemicals with different immuno-modulatory properties.

5. Perspectives and future directions

5.1. Where do we go from here with existing expertise that includes evolution?

In these laboratories there is a wealth of expertise on aspects of signaling (e.g. the role of kinases and steroid hormones) in lymphocytes. Such availability can rapidly lead to an enhanced activity directed toward understanding the origins and evolution of early mechanisms of signaling. Thus to continue these analyses using the earthworm model, similar techniques, assays and interpretations would be easily obtained or applied in the field that emphasizes signaling pathways as related to the immune system in general and innate immunity in particular. In addition, there is also proficiency in using lentiviral gene delivery techniques that permanently mark and change cells both genetically and phenotypically. This has the capacity to allow gene function testing and establish cells that over-express putative kinases or immune related markers whose behavior can then be followed.

5.2. Signal transduction in relation to tyrosine kinases and steroid hormones

Recent structural studies of several vertebrate receptor tyrosine kinases (RTKs) revealed that their juxta membrane regions negatively regulate their catalytic activities [53]. This autoinhibition depends upon interaction between the kinase domain and tyrosine residues within the juxta membrane region. Autoinhibition is released when these tyrosines become phosphorylated following receptor stimulation. Sequence homology suggested analogous regulation for ZAP-70 and similar regulation was also noted for the related Syk kinase. ZAP-70, a Syk family cytoplasmic protein tyrosine kinase (PTK) is required to couple the activated T-cell antigen receptor (TCR) to downstream signaling pathways. These findings suggest that a general autoinhibitory mechanism employed by RTKs is also used by some cytoplasmic tyrosine kinases [54]. Steroid hormones are known to mediate rapid non-genomic effects occurring within minutes besides the classical genomic actions mediated by the nuclear translocation of the cytoplasmic glucocorticoid receptor (GR) [55]. The glucocorticoid hormone (GC) has a significant role in T lymphocyte regulation. These results suggest that GC rapidly influences the proximal tyrosine phosphorylation events in T-cells. The phenomena observed involving kinases and steroid receptors might apply for their counterparts involved in adaptive immunity as well. Future studies could help elucidating the problem.

5.3. Employment of lentiviral vectors in functional assays of putative genes

Lentiviral vectors derived from HIV-1 are promising tools for gene function assays as they can mediate in vivo delivery and long-term expression of transgenes [56]. Pseudotyped vectors that have undergone multiple attenuations devoid of all virulence genes conserve the ability of transducing numerous target cells. Using HIV-1-derived lentivectors, efficient transduction of human primary B-lymphocytes co-cultured with thy-

Table 4
Comparative analyses of attribution in laboratory species

	Earthworms (*Lumbricus terrestris* and *Eisenia foetida*)	*Caenorhabditis elegans*	*Drosophila melanogaster*
Signaling	++	+++++	+++++
Ecotoxicology	+++++	+++++	+
Fishing	+++++	–	–
Food	+++++	–	–
Complementary and alternative medicine (CAM)	++++	–	–

moma cells has been achieved [57]. It has been recently found that transduction of B cells in a system using CpG DNA was comparable to results of co-cultures [58]. A bicistronic vector, encoding either secreted or intracellular molecules, efficiently introduced the transgene into target cells. The expressed transgenic proteins were fully intact as supported by evidence of functional assays. This system has already been valuable for gene function research in vertebrates. Upcoming experiments shall prove the usefulness of the method when applied to functional research of putative genes in invertebrate immunity coupled with other previously defined procedures [59–63] (Table 4).

References

[1] Cooper EL, Kauschke E, Cossarizza A. Digging for innate immunity since Darwin and Metchnikoff. BioEssays 2002;24:319–33.
[2] Xu Y, Tao X, Shen B, Horng T, Medzhitov R, Manley JL, et al. Structural basis for signal transduction by the Toll/interleukin-1 receptor domains. Nature 2000;408:111–5.
[3] Horng T, Medzhitov R. Drosophila MyD88 is an adapter in the Toll signaling pathway. Proc Natl Acad Sci USA 2001;98:12654–8.
[4] Kocsis B, Emody L. Pathogen-associated molecular pattern of bacteria and its recognition by the host. Hun Immunol 2003;2:10–9.
[5] Blander JM, Medzhitov R. Regulation of phagosome maturation by signals from toll-like receptors. Science 2004;304:1014–8.
[6] Pasare C, Medzhitov R. Toll-like receptors and acquired immunity. Semin Immunol 2004;16:23–6.
[7] Couillault C, Pujol N, Reboul J, Sabatier L, Guichou JF, Kohara Y, et al. TLR-independent control of innate immunity in *Caenorhabditis elegans* by the TIR domain adaptor protein TIR-1, an ortholog of human SARM. Nat Immunol 2004;5:488–94.
[8] Beschin A, Bilej M, Hanssens F, Raymakers J, Van Dyck E, Revets H, et al. Identification and cloning of a glucan- and lipopolysaccharide-binding protein from *Eisenia foetida* earthworm involved in the activation of prophenoloxidase cascade. J Biol Chem 1998;273:24948–54.
[9] Engelmann P, Cooper EL, Nemeth P. Anticipating innate immunity without a Toll. Mol Immunol 2005;42(8):931–42.
[10] Flajnik MF, DuPasquier L. Evolution of innate and adaptive immunity: can we draw a line? Trends Immunol 2004;25:640–4.
[11] Agaisse H, Perrimon N. The roles of JAK/STAT signalling in Drosophila immune responses. Immunol Rev 2004;198:72–82.
[12] Kim DH, Ausubel FM. Evolutionary perspectives on innate immunity from the study of *Caenorhabditis elegans*. Curr Opin Immunol 2005;17:4–10.
[13] Cossarizza A, Cooper EL, Quaglino D, Salvioli S, Kalachnikova G, Franceschi C. Mitochondrial mass and membrane potential in coelomocytes from the earthworm *Eisenia foetida*: studies with fluorescent probes in single intact cells. Biochem Biophys Res Commun 1995;214:503–10.
[14] Cooper EL, Cossarizza A, Suzuki MM, Salvioli S, Capri M, Quaglino D, et al. Autogeneic but not allogeneicearthworm effector coelomocytes kill the mammalian tumor cell target K562. Cell Immunol 1995;166:113–22.
[15] Engelmann P, Kiss J, Csongei V, Cooper EL, Nemeth P. Earthworm leukocytes kill HeLa, HEp-2, PC-12 and PA317 cells in vitro. J Biochem Biophys Methods 2004;61:215–27.
[16] Koenig S, Wagner F, Kauschke E, Peter-Katalinic J, Cooper EL, Eue I. Mass spectrometric analyses of CL_{39}, CL_{41} and H_1, H_2, H_3 confrim identity with fetidin and lyseni produced by earthworm leukocytes. Dev Comp Immunol 2003;27:513–20.
[17] Lanier LL. On guard-activating NK cell receptors. Nat Immunol 2001;2:23–7.
[18] Cossarizza A, Cooper EL, Suzuki MM, Salvioli S, Capri M, Gri G, et al. Earthworm leukocytes that are not phagocytic and cross-react with several human epitopes can kill human tumor cell lines. Exp Cell Res 1996;224:174–82.
[19] Quaglino D, Cooper EL, Salvioli S, Capri M, Suzuki MM, Ronchetti IP, et al. Earthworm coelomocytes in vitro: cellular features and "granuloma" formation during cytotoxic activity against the mammalian tumor cell target K562. Eur J Cell Biol 1996;70:278–88.
[20] Canesi L, Ciacci C, Betti M, Scarpato A, Citterio B, Pruzzo C, et al. Effects of PCB congeners on the immune function of *Mytilus* hemocytes: alterations of tyrosine kinase-mediated cell signaling. Aquat Toxicol 2003;63:293–306.
[21] Canesi L, Betti M, Ciacci C, Citterio B, Pruzzo C, Gallo G. Tyrosine kinase-mediated cell signaling in the activation of *Mytilus* hemocytes: possible role of STAT-like proteins. Biol Cell 2003;95:603–13.
[22] Ricketts HJ, Morgan AJ, Spurgeon DJ, Kille P. Measurement of annetocin gene expression: a new reproductive biomarker in earthworm ecotoxicology. Ecotoxicol Environ Saf 2004;57:4–10.
[23] Escoubas JM, Briant L, Montagnani C, Hez S, Devaux C, Roch P. Oyster IKK-like protein shares structural and functional properties with its mammalian homologues. FEBS Lett 1999;453:293–8.
[24] Galay-Burgos M, Spurgeon DJ, Weeks JM, Sturzenbaum SR, Morgan AJ, Kille P. Developing a new method for soil pollution monitoring using molecular genetic biomarkers. Biomarkers 2003;8:229–39.
[25] Sturzenbaum SR, Georgiev O, Morgan AJ, Kille P. Cadmium detoxification in earthworms: from genes to cells. Environ Sci Technol 2004;38:6283–9.
[26] Spurgeon DJ, Sturzenbaum SR, Svendsen C, Hankard PK, Morgan AJ, Weeks JM, et al. Toxicological, cellular and gene expression responses in earthworms exposed to copper and cadmium. Comp Biochem Physiol 2004;138C:11–21.
[27] Galay-Burgos M, Winters C, Sturzenbaum SR, Randerson PF, Kille P, Morgan AJ. Cu and Cd effects on the earthworm *Lumbricus rubellus* in the laboratory: multivariate statistical analysis of relationships between exposure, biomarkers and ecologically relevant parameters. Environ Sci Technol 2005;39:1757–63.
[28] Homa J, Olchawa E, Sturzenbaum SR, Morgan AJ, Plytycz B. Early-phase immunodetection of metallothionein and heat shock proteins in extruded earthworm coelomocytes after dermal exposure to metal ions. Environ Pollut 2005;135:275–80.
[29] Wiesner L, Hahn ME, Karchner SI, Cooper EL, Kauschke E. Does an aryl hydrocarbon receptor (AHR)-like molecule exist in earthworms? Some implications for immunity. Pedobiologia 2003;47:646–50.

[30] Cooper EL, Roch P. Earthworm immunity: a model of immune competence. Pedobiologia 2003;47:676–88.
[31] Schmidt JV, Bradfield CA. Ah receptor signaling pathways. Annu Rev Cell Dev Biol 1996;12:55–89.
[32] Hahn ME, Karchner SI, Shapiro MA, Perera SA. Molecular evolution of two vertebrate Aryl Hydrocarbon (dioxin) Receptors (AHR1 and AHR2) and the PAS family. Proc Natl Acad Sci USA 1997;94:13743–8.
[33] Karchner SI, Kennedy SW, Trudeau S, Hahn ME. Towards molecular understanding of species differences in dioxin sensitivity: initial characterization of Ah receptor cDNAs in birds and amphibian. Mar Envion Res 2000;50:51–6.
[34] Hahn ME, Karchner SI. Evolutionary conservation of the vertebrate Ah (dioxin) receptor: amplification and sequencing of the PAS domain of a teleost Ah receptor cDNA. Biochem J 1995;310:383–7.
[35] Hahn ME, Woodin BR, Stegeman JJ, Tillitt DE. Aryl Hydrocarbon receptor function in early vertebrates: Inducibility of cytochrome P 450 1A in agnathan and elasmobranch fish. Comp Biochem Physiol 1998;120C:67–75.
[36] Kim EY, Hahn ME. cDNA cloning and characterization an aryl hydrocarbon receptor from the harbor seal (Phoca vitulina): a biomarker of dioxin susceptibility? Aquat Toxicol 2002;58:57–73.
[37] Jensen BA. Characterization of an Aryl Hydrocarbon Receptor from a cetacean: an approach for assessing contaminant susceptibility in protect species. Ph.D. thesis, p. 198; 2000.
[38] Abnet CC, Tanguay RL, Hahn ME, Heideman W, Peterson RE. Two forms of the Aryl Hydrocarbon Receptor type 2 in rainbow trout (*Oncorhynchus mykiss*). J Biol Chem 1999;274:15159–66.
[39] Hahn ME. The aryl hydrocarbon receptor: a comparative perspective. Comp Biochem Physiol 1998;121C:23–53.
[40] Hankinson O. The aryl hydrocarbon receptor complex. Annu Rev Pharmacol Toxicol 1995;35:307–40.
[41] Hahn ME, Poland A, Glover E, Stegeman JJ. Photoaffinity labeling of the Ah receptor: phylogenetic survey of diverse vertebrate and invertebrate species. Arch Biochem Biophys 1994;310:218–28.
[42] Brown DJ, Clarke GC, Clarke GC, Van Beneden RJ. Halogenated aromatic hydrocarbon-binding proteins identified in several invertebrate marine species. Aquat Toxicol 1997;37:71–8.
[43] Willett KL, Wilson C, Thomsen J, Porter W. Evidence for and against the presence of polynuclear aromatic hydrocarbon and 2, 3, 7, 8-tetrachloro-*p*-dioxin binding proteins in the marine mussels, *Bathymodiolus* and *Modiolus modiolus*. Aquat Toxicol 2000;48:51–64.
[44] Ville P, Roch P, Cooper EL, Masson P, Narbonne JF. PCBs increase molecular-related activities (lysozyme, antibacterial, hemolysis, proteases) but inhibit macrophage-related functions (phagocytosis, wound healing) in earthworms. J Invert Pathol 1995;65:217–24.
[45] Ville P, Roch P, Cooper EL, Narbonne JF. Immuno-modulator effects of carbaryl and 2,4D in the earthworm *Eiseina fetida andrei*. Environ Contam Toxicol 1997;32:291–7.
[46] Cikutovic MA, Fitzpatrick LC, Goven AJ, Giggelman MA, Cooper EL. Wound healing in earthworms *Lumbricus terrestris*: a cellular-based biomarker for assessing sublethal chemical toxicity. Bull Environ Contam Toxicol 1999;62:508–14.
[47] Komiyama K, Okaue M, Miki Y, Ohkubo M, Moro I, Cooper EL. Non-specific cellular function of *Eisenia fetida* regulated by polycyclic aromatic hydrocarbons. Pedobiologia 2003;47:717–23.
[48] Wiesner L, Wade HP, KarchnerSI, Franks DG, Cooper EL, Kauschke EKU, et al. cDNA cloning of the Aryl Hydrocarbon Receptor (AHR) homolog in zebra mussel (Dreissena polymorpha); submitted for publication.
[49] Dengg M, van Meel JC. *Caenorhabditis elegans* as model system for rapid toxicity assessment of pharmaceutical compounds. J Pharmacol Toxicol Methods 2004;50:209–14.
[50] Menzel R, Bogaert T, Achazi R. A systematic gene expression screen of *Caenorhabditis elegans* cytochrome P450 genes reveals CYP35 as strongly xenobiotic inducible. Arch Biochem Biophys 2001;395:158–68.
[51] Anderson SL, Wild GC. Linking genotoxic responses and reproductive success in ecotoxicology. Environ Health Perspect 1994;102:9–12.
[52] Guven K, Duce JA, de Pomerai DI. Calcium moderation of cadmium stress explored using a stress-inducible transgenic strain of *Caenorhabditis elegans*. Comp Biochem Physiol 1995;110C:61–70.
[53] Brdicka T, Kadlecek TA, Roose JP, Pastuszak AW, Weiss A. Intramolecular regulatory switch in ZAP-70: analogy with receptor tyrosine kinases. Mol Cell Biol 2005;25:4924–33.
[54] Castro JE, Prada CE, Loria O, Kamal A, Chen L, Burrows FJ, et al. ZAP-70 is a novel conditional heat shock protein 90 (Hsp90)-client protein: inhibition of Hsp90 leads to ZAP-70 degradation, apoptosis, impaired signaling in chronic lymphocytic, leukemia. Blood 2005;21. Epub ahead of print.
[55] Bartis D, Boldizsár F, Szabó M, Pálinkás L, Németh P, Berki T. Glucocorticoids induce rapid ZAP-70 tyrosine phosphorylation in Jurkat T-cells. J Biochem Mol Biol 2005 [in press].
[56] Zufferey R, Nagy D, Mandel RJ, Naldini L, Trono D. Multiply attenuated lentiviral vector achieves efficient gene delivery in vivo. Nat Biotechnol 1997;15:871–5.
[57] Bovia F, Salmon P, Matthes T, Kvell K, Nguyen TH, Werner-Favre C, et al. Efficient transduction of primary human B lymphocytes and nondividing myeloma B cells with HIV-1-derived lentiviral vectors. Blood 2003;101:1727–33.
[58] Kvell K, Nguyen TH, Salmon P, Glauser F, Werner-Favre C, Barnet M, et al. Transduction of CpG DNA-stimulated primary human B cells with bicistronic lentivectors. Mol Ther 2005. [Epub ahead of print].
[59] Engelmann P, Palinkas L, Cooper EL, Nemeth P. Monoclonal antibodies identify four distinct annelid leukocyte markers. Dev Comp Immunol 2005;29(7):599–614.
[60] Engelmann P, Molnar L, Palinkas L, Cooper EL, Nemeth P. Earthworm leukocyte populations specifically harbor lysosomal enzymes that may respond to bacterial challenge. Cell Tissue Res 2004.
[61] Engelmann P, Pál J, Berki T, Cooper EL, Németh P. Earthworm leukocytes reacted with different mammalian antigen specific monoclonal antibodies. Zoology 2002;105:257–65.
[62] Engelmann P, Cooper EL, Németh P. Comparative analysis of earthworms' immune system by phylogenetic aspects of cell surface and intracellular markers. In: Cooper EL, Beschin A, Bilej M, editors. A new model for analyzing antimicrobial peptides with biomedical applications. NATO Science Series: Life and Behavioral Sciences, 343. Amsterdam: IOS Press; 2002. p. 53–7.
[63] Takahashi T, Iwase T, Takenouchi N, Saito M, Kobayashi K, Moldoveanu Z, et al. The joining (J) chain is present in invertebrates that do not express in immunoglobulins. Proc Natl Acad Sci USA 1996;93:1886–91.

Immunobiology 219 (2014) 644–652

Contents lists available at ScienceDirect

Immunobiology

journal homepage: www.elsevier.com/locate/imbio

Active Wnt/beta-catenin signaling is required for embryonic thymic epithelial development and functionality *ex vivo*

Krisztian Kvell[a,*], Aniko V. Fejes[a], Sonia M. Parnell[b], Judit E. Pongracz[a,b]

[a] Department of Pharmacological Biotechnology, University of Pecs, Hungary
[b] Department of Anatomy, Division of Immunity and Infection, Institute for Biomedical Research, University of Birmingham, UK

ARTICLE INFO

Article history:
Received 13 July 2013
Accepted 25 March 2014
Available online 2 April 2014

Keywords:
Embryonic development
FoxN1
ICAT
Thymic epithelium
Wnt

ABSTRACT

The Wnt/beta-catenin signaling pathway plays an important role in the commitment and development of thymic epithelial precursors. Here we document similarities of thymic epithelial development during embryogenesis in human and mouse. We stained for thymic epithelial surface markers (EpCAM1, Ly51, K8) and ligand/receptor pair (Wnt4, Fz4). Our results confirm the relevance of using murine test systems to model human embryonic thymic epithelial cell development.

We have efficiently transduced murine embryonic epithelial cells using mock (GFP) and Wnt/beta-catenin-inhibiting (ICAT-encoding) recombinant adenoviral vectors. The effect of Wnt4 was assayed in the form of Wnt4-containing supernatant. Gene expressional changes were assessed by Q-PCR and also morphology using conventional and confocal fluorescent microscopy. Functional aberration caused by ICAT was assessed through evaluation of thymocyte maturation.

Our results demonstrate that ICAT and Wnt4 have reciprocal effects during embryonic thymic epithelial cell development. While Wnt4 is capable of increasing the expression level of characteristic intracellular (FoxN1), surface (MHCII) and secreted (IL7) molecules, Wnt/beta-catenin inhibition through ICAT can moderately decrease their expression. Morphological changes induced by ICAT resulted in the development of hollow, inflated thymic lobes with reduced epithelial cell numbers. The ICAT-treated thymic lobes also showed significant impairment in supporting thymocyte development and maturation.

© 2014 Elsevier GmbH. All rights reserved.

Introduction

Along with Notch and BMP, the abundantly secreted Wnt (wingless-related MMTV integration site) glycoproteins have been proposed to play an elementary role in the development, maintenance and functional integrity of the thymic stroma (Bleul and Boehm 2005; Pongracz et al. 2003; Osada et al. 2006; Anderson et al. 2001). The current article focuses on the evolutionarily conserved molecular family of secreted Wnt glycoproteins. The nineteen known Wnt glycoproteins signal through ten G-protein dependent receptors, called Frizzled receptors. For active signal transduction, Frizzled receptors need to form a complex with low density lipoprotein receptor-related proteins (LRP), as co-receptors. The actual constellation of the ligand, receptor and co-receptor defines Wnt-mediated effects in a context-dependent manner (Mikels and Nusse 2006; Gordon and Nusse 2006; Schweizer and Varmus 2003). Wnt4 is in spotlight of the current work being one of the most abundantly expressed non-canonical Wnt molecule secreted by the thymic epithelium during embryonic development, with expression levels progressively decreasing during postnatal development and aging (Kvell et al. 2010; Kvell and Pongracz 2011; Varecza et al. 2011). It is of note that FoxN1 (a key transcription factor that defines thymic epithelial identity) is an acknowledged target gene of Wnt4 in the thymic epithelial context (Balciunaite et al. 2002). ICAT (inhibitor of beta-catenin and TCF-4) is a polypeptide that inhibits Wnt/beta-catenin nuclear signaling by binding and competing its interaction with the transcription factor TCF (T cell factor) in the nucleus. Therefore ICAT is an intracellular negative regulator of the Wnt/beta-catenin pathway (Pongracz et al. 2006). Since the Wnt glycoproteins and Wnt4 in particular are key players of embryonic thymic epithelial development we examined the effect of both increased Wnt-effect (additional Wnt4 in the form of supernatant)

Abbreviations: BMP, bone morphogenic protein; EpCAM, epithelial cell adhesion molecule; FoxN1, forkhead box N1; Fz, frizzled; GFP, green fluorescent protein; ICAT, inhibitor of beta-catenin; IL7, interleukin 7; K, keratin; LRP, low density lipoprotein receptor-related proteins; MHCII, major histocompatibility complex II; TCF, T-cell factor; rAd, recombinant adeno-viruses; Wnt, wingless-related MMTV integration site.

* Corresponding author at: Department of Pharmacological Biotechnology, University of Pecs, 20 Ifjusag Street, H-7624 Pecs, Hungary. Tel.: +36 72 536 000/29250.
E-mail address: kvell.krisztian@pte.hu (K. Kvell).

http://dx.doi.org/10.1016/j.imbio.2014.03.017
0171-2985/© 2014 Elsevier GmbH. All rights reserved.

and decreased Wnt-effect (ICAT over-expression through adenoviral vectors) in embryonic thymic lobes *ex vivo*. In the mouse the thymus appears on day eleven (E11) of the total 21 days of embryonic development. The epithelial progenitors appear first followed by the quick colonization by T-cell progenitors from E12 onwards. By E15 the thymic epithelial medulla and cortex begin to form separate compartments required for the selection steps of developing thymocytes (Rezzani et al. 2008). In the human embryo the thymus appears on week 5 (W5) of the total 40 weeks of embryonic development. T-cell progenitors colonize the stromal niche from W7 (Hayward and Ezer 1974; Lobach and Haynes 1987). Despite obvious differences between murine and human embryonic thymic development concerning timing, numerous inter-species similarities exist in terms of function and immunological competence. The current article includes histological comparison of human and mouse embryonic thymic sections to identify similarities in staining patterns of cell surface and secreted proteins. Such similarities would highlight the utility of murine embryonic thymic test systems for their relevance in the context of human embryonic thymic epithelial development.

Materials and methods

Mouse and human thymic samples

Mice were bred in our animal facility. All animal work has been conducted according to relevant national and international guidelines following approval of ethics committee of the University of Pecs (ref. no. BA02/2000-3/2006). For *ex vivo* experiments we used thymic lobes from timed pregnancies at E12 and E15.

Human thymic sample originates from W15 aborted fetus. Abortion was initiated due to diagnosis of Patau-syndrome (chromosome 13 trisomy) that does not interfere with embryonic thymic development. The procedures were conducted according to relevant national and international guidelines following approval of ethics committee of the University of Pecs (ref. no. ad.8-2/2009-1018EKU).

Ex vivo experiments

Murine embryonic E12 and E15 thymic lobes were cultured in DMEM supplemented with 10% FCS, penicillin, streptomycin and beta-mercapto-ethanol (Lonza Walkersville). Recombinant adenoviral (rAd) preparations (prepared as published previously) that specifically transfect epithelial cells were added to the culture medium of murine thymic lobes that were further cultured for up to seven days (Hare et al. 2003). Flow-cytometric analysis of E12 murine thymic epithelial cells was performed 48 h following rAd transfection (E12 murine thymic lobes are devoid of thymocytes). E15 murine thymocytes were selectively liberated by mechanic dispersion then stained 168 h after rAd transfection (E15 murine thymic epithelial cells would require prolonged collagenase digestion for liberation). Murine thymocytes were stained with CD4-PE (clone H129.19 from BD Pharminden) and CD8-FITC (clone 53-6.7 from BioLegend) labeled antibodies. FACS Calibur cytometer and Cell Quest software were used for analysis (Becton Dickinson, USA).

The supernatant of mock and Wnt4-secreting transgenic TEP1 cells (murine thymic epithelial cell line model) were prepared as published previously (Kvell et al. 2010). (Recombinant Wnt proteins become inactivated during the process of purification, hence the use of supernatants instead). In order to exclude the thymocyte-mediated effects of secreted Wnt4 either E12 tmurine hymic lobes were used (practically devoid of thymocyte progenitors) or E15 murine thymic lobes were pre-treated with deoxiguanosine (at 2 mM final, Sigma) for five days prior to the ten-day supernatant treatment.

Histology

Cryostate sections (9 μm) of murine and human thymic lobes were fixed in cold acetone, then dried and blocked using 5% BSA in PBS for 20 min before staining with a-Ly51-PE (clone 6C3 from BD Pharmingen), a-EpCAM-FITC (clone G8.8, monoclonal antibody prepared in our lab), a-K8 (clone Ks8.7 from Santa Cruz Biotechnology), a-Wn4 (clone C-14 from Santa Cruz Biotechnology) or a-Fz4 (clone C-18 from Santa Cruz Biotechnology). Unlabeled antibodies were visualized using secondary antibodies of the Northern Light secondary antibody family (NL557 family, NL001: anti-goat, NL007: anti-mouse from R&D Systems). The sections were analyzed using Olympus BX61 system.

Cultured E12 murine thymic lobes were fixed in paraformaldehyde and stained in whole using the same reagents as above, but applying extended incubation period for fixation, wash and staining (~60 min each) to allow for antibodies to penetrate the miniature embryonic thymic lobes. Confocal fluorescent images were captured using the Olympus Fluoview-1000 system.

RNA isolation, cDNA preparation, Q-PCR analysis

Total RNA was isolated from the cultured murine thymic lobes using the RNAII kit (Macherey-Nagel), including a DNase digestion step. Then cDNA was synthesized using the high capacity RNA to cDNA kit (Life Technologies). For Q-PCR analysis, we used an AB7500 platform and SYBR green I chemistry (Life Technologies). Gene expression was normalized to beta-actin. The sequences/catalog numbers of mouse-specific primers are listed in Table 1. Primers were not designed to be exon-spanning, however, on column DNase digestion during RNA preparation eliminated genomic DNA residues.

Statistical analysis

All experiments were performed on three occasions, representative experiments are shown. Measures were obtained in triplicates; data are presented as mean ± 1 SD by error bars.

Results

Histological characterization of human embryonic thymus

Human embryonic thymic sections from W15 were stained for characteristic cell surface and secreted markers. Fig. 1A shows staining for EpCAM-1 and Ly-51 surface antigens. As expected EpCAM-1 is moderately expressed by all thymic epithelial cells with areas showing increased EpCAM-1 staining that correspond to epithelial cells of the medulla. Parallel Ly-51 staining identifies cortical epithelial cells. It appears that by W15 the thymic epithelial cells show distinct patterning to regions of the medulla and cortex, based on staining with these two markers. Fig. 1B shows co-localization of EpCAM-1 and cytokeratin8 following histological staining. Cytokeratin8 appears to stain broad epithelial areas of the human thymus, largely overlapping with EpCAM-1 staining. The staining patterns of the secreted Wnt4 molecule as well as its ligand Fz4 have also been assayed as demonstrated by Fig. 1C and D. As expected, Wnt4 is primarily expressed by the thymic epithelium as shown by the significantly overlapping staining pattern of Wnt4 and EpCAM-1. On the other hand, Fz4 expression shows only moderate co-localization with EpCAM-1, and indeed

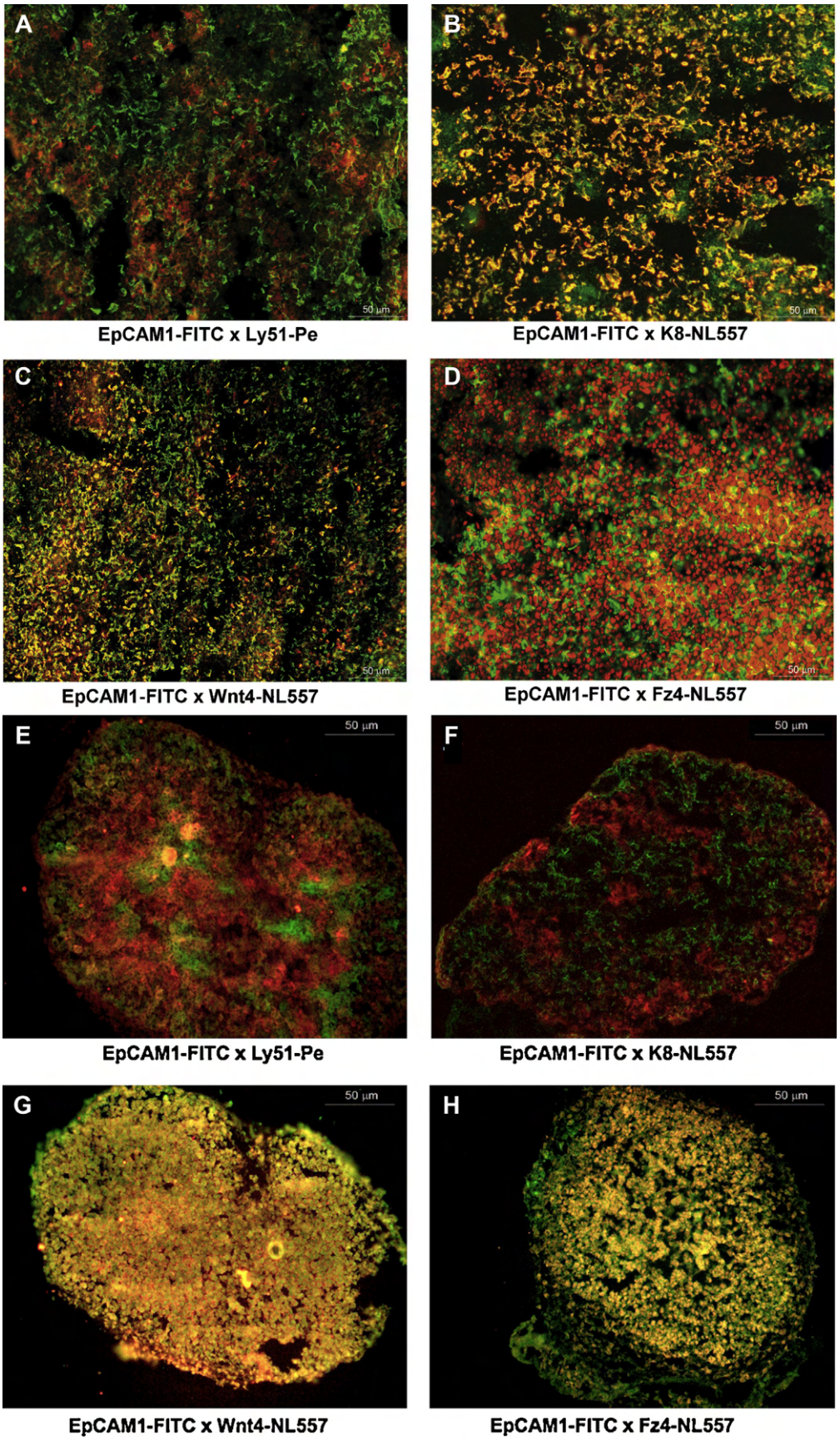

Fig. 1. Figure shows the histological characterization of the human embryonic thymus at 15w of age at 20× magnification using fluorescent microscopy. The figures portray co-localization patterns with EpCAM1 epithelial surface antigen. (A) Shows Ly51, (B) demonstrates cytokeratin8, (C) portrays Wnt4, while (D) depicts Fz4 staining pattern with respect to the thymic epithelial context. (A) Shows segregation of medullary (EpCAM1++) and cortical (Ly51+) epithelial cells. (B, C) Identify epithelial cells as the major source of K8 expression and Wnt4 secretion in this setting. As expected, (D) shows a distinct pattern as epithelial cells are not the only Fz4-bearing cells in thymus.

Table 1
List of gene specific PCR primers.

Gene	Forward primer	Reverse primer
Beta-actin	5′-TGG CGC TTT TGA CTC AGG A-3′	5′-GGG AGG GTG AGG GAC TTC C-3′
ICAT	5′-CGG AGG AGA TGT ACA TTC AAC AGA-3′	5′-TCA CTG GCG GTC AGG TTT G-3′
MHCII	5′-CTA GCC AAG TCC CTC CTA AGG-3′	5′-ATC TCA GAC TGA TCC TGG CAT-3′
IL7	5′-ACT ACA CCC ACC TCC CGC A-3′	5′-TCT CAG TAG TCT CTT TAG G-3′
FoxN1	Applied Biosystems TaqMan probe PN4351272 (Mm00477457_m1)	–

the vast population of non-epithelial cells including thymocytes are also known to be among Wnt4-binding cells.

Histological characterization of mouse embryonic thymus

Mouse embryonic thymic sections from E15 were also stained for the same, characteristic cell surface and secreted markers used above. Fig. 1E portrays staining for EpCAM-1 and Ly-51 surface antigens. As observed with the human sections, EpCAM-1 is expressed by all thymic epithelial cells with certain areas showing increased EpCAM-1 expression identifying epithelial cells of the medulla, while Ly-51 staining defines cortical epithelial cells. It seems that by the embryonic age E15 the thymic epithelial cells show differentiation toward either medullary or cortical phenotype, based on staining patterns. Fig. 1F shows staining with EpCAM-1 and cytokeratin8. The murine section shows expression with both surface markers, although the staining pattern is different from that of the human section showing significantly less overlap. The expression and staining pattern of the secreted Wnt4 molecule as well as its ligand Fz4 have also been tested as shown by Fig. 1G and H. Both Wnt4 and Fz4 are rather ubiquitously expressed in the mouse thymus and both show significant overlap with EpCAM-1. This co-localization is more significant in the mouse compared to the human section for both Wnt4 and Fz4.

Adenoviral transgene delivery to thymic epithelial cells

E12 murine thymic epithelial cells were transfected with recombinant adenoviral (rAd) vectors that specifically transfect epithelial cells and leave other cells unaffected. The vectors encoded either GFP marker gene alone (mock) or in combination with ICAT. Transfection efficiency was assayed by flow cytometry 48 h later and was found to be very high with the mock vector (91.49%) and high with the ICAT-encoding rAd vector (69.36%) based on GFP expression of transected cells (see Fig. 2A and B). Transgene expression was also verified at the mRNA level for ICAT by Q-PCR and was found to be efficiently over-expressed (∼10,000× or four magnitudes, see Fig. 2C) in the case of ICAT-encoding rAd compared to mock-transfection baseline, proving that rAd vectors are highly suitable vehicles for gene delivery into thymic epithelial cells.

Mouse E15 embryonic thymic lobes were transfected with rAd vectors encoding either GFP marker gene alone (mock) or combined with ICAT. In parallel, following thymocyte-depletion achieved by deoxiguanosine-treatment, further E15 murine thymic lobes were incubated in the presence of supernatants of either control or Wnt4-secreting transgenic TEP1 cells (thymic epithelial cell line model, method published previously (Beardsley et al. 1983). The effect of ICAT over-expression and additional Wnt4-treatment on gene expression was tested at the level mRNA by Q-PCR after seven days of incubation following treatment as shown on Fig. 3. Both treatments had their own controls (control supernatant for Wnt4-treatment and mock (GFP)-transfection for ICAT-transfection). Values corresponding to these controls were set as starting levels represented by value 1 of the vertical axis hence called relative gene expression. The assayed genes included surface (MHCII), intracellular (FoxN1) and secreted (IL7) molecules, conventionally associated with epithelial phenotype and function in the context of the thymus. Our results indicate that all the three assayed genes were up-regulated following increased Wnt4 exposure provided by Wnt4-containing supernatant compared to treatment with mock supernatant (MHCII: >2×, FoxN1: >3×, IL7: ∼6×). In parallel, the same read-out genes showed moderate, but consequent down-regulation following the over-expression of ICAT compared to mock-transfection baseline. Thus our data summarized by Fig. 3 indicate that increased Wnt4-exposure and the inhibition of the Wnt/beta-catenin pathway through ICAT have reciprocal effects on characteristic surface (MHCII), intracellular (FoxN1) and secreted (IL7) molecules conventionally associated with epithelial phenotype and function in the context of the thymus.

Morphological changes at the level of histology

Mouse embryonic thymic lobes from E12 (predominantly containing thymic epithelial progenitors) have been transfected with the above mock (GFP) and ICAT-encoding adenoviral vectors. Following an incubation period of seven days the thymic lobes were visualized in whole by conventional and confocal fluorescent microscopy following staining for EpCAM-1 to show thymic epithelial cells. Fig. 4A and B show mock-transfected and ICAT-transfected stained whole thymic lobes, respectively, by conventional fluorescent microscopy. The thymic lobe transfected with rAd ICAT appears to be larger in diameter compared to the mock-transfected thymic lobe (∼0.85 mm *vs.* ∼1.35 mm based on scale bar). However, if the same lobes are visualized using a confocal microscope combined with trans-white imaging, it becomes evident that the ICAT-transfected lobe is hollow compared to the mock-transfected thymic lobe (see Fig. 4C and D, respectively) harboring a large cavity without cells. It is also of note that the remaining epithelial cells reside adjacent to the inner lining of the internal cavity. (These phenomena are shown by the combination of confocal single-plane and conventional trans-white imaging used on Fig. 4C and D). Occasional thymic cysts were also observed with this combined imaging technique following ICAT-transfection (see Fig. 4D). Decreased cellularity despite increased lobe size was also supported by significantly lower RNA yield (∼0.3×) obtained with ICAT-transfected lobes compared to mock-transfected lobes (data not shown).

Figure portrays the histological characterization of the mouse embryonic thymus at E15 of age at 10× magnification using fluorescent microscopy. The figures show co-localization patterns with EpCAM1 epithelial surface antigen. (E) Demonstrates Ly51, (F) shows cytokeratin8, (G) depicts Wnt4, while (H) portrays Fz4 staining pattern with respect to the thymic epithelial context. According to (E) the medullary (EPCAM1++) and cortical (Ly51+) thymic epithelial regions show distinct patterns by E15. (F) Shows that K8 expression is different in the mouse as in the human, there is no significant overlap with EpCAM1-expression. (G) Shows similar ubiquitous expression of Wnt4 as seen in the human section. (H) Demonstrates that Fz4 expression is rather ubiquitous in the mouse setting compared to the human section.

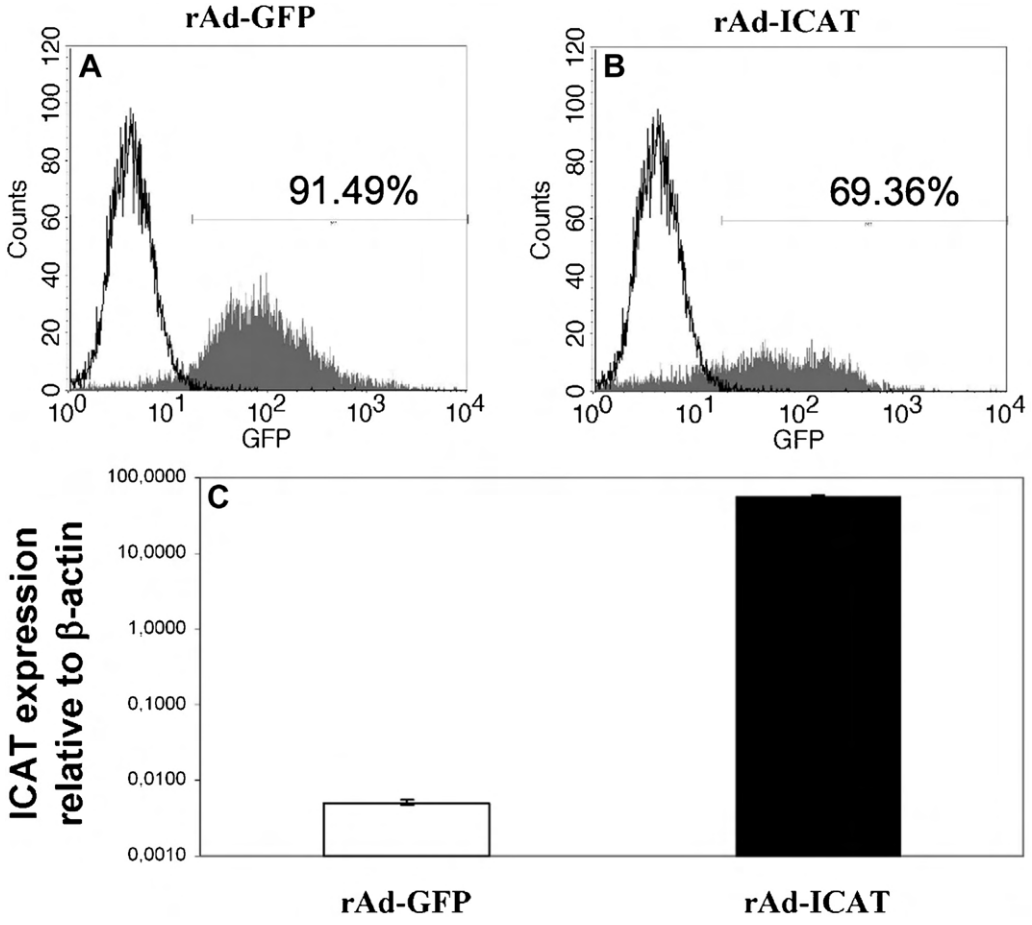

Fig. 2. Figure shows the flow-cytometric and Q-PCR characterization of transfection efficiency using recombinant adenoviral vectors to transfect E12 embryonic thymix epithelial cells. (A, B) Demonstrate GFP marker gene expression 48 h following GFP or ICAT transfection (shown by gray fill) compared to control cells (shown by black line). Transfection efficiencies were 91.49% for GFP(mock)- and 69.36% for ICAT-transfection, respectively. (C) Shows the increase of ICAT mRNA level obtained following transfection with ICAT-encoding recombinant adenoviral vector compared to vector encoding GFP alone. Please note that scale is exponential and hence shows increase of four magnitudes.

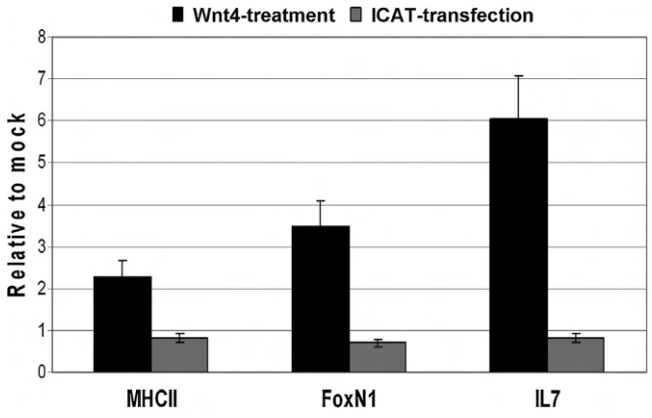

Fig. 3. Figure demonstrates gene expressional changes of characteristic epithelial cell surface (MHCII), intracellular (FoxN1) and secreted (IL7) in the embryonic thymic context measured by Q-PCR. The figure shows the effects of Wnt4-treatment (black boxes) and ICAT-transfection (gray boxes) on the mRNA levels of the assessed genes in E15 thymic lobes, error bars show ±1 S.D. Both Wnt4-treatment and ICAT-transfection had their own controls in the form of control-treatment and GFP(mock)-transfection, respectively. These provide control values represented by value 1 on the vertical axis (hence relative expression). Please note that Wnt4-treatment can reach all cells, whereas ICAT-transfection cannot.

Functional changes indicated by thymocyte maturation

Mouse embryonic thymic lobes from E15 (already colonized by thymocyte precursors) have also been transfected with the above mock (GFP)- and ICAT-encoding adenoviral vectors. Following an incubation period of seven days thymocytes were selectively liberated by mechanic dispersion then stained for CD4 and CD8 expression (E15 murine thymic epithelial cells would require prolonged collagenase digestion for liberation). During flow-cytometric evaluation viable cells (using morphological R1 gate, see Fig. 5A) were statistically analyzed for CD4/CD8 ratio (see Fig. 5B–D). A young adult (1 month old) female BALB/c mouse was sacrificed and the thymocytes were likewise liberated and stained for CD4/CD8 expression and ratio, serving as control (see Fig. 5B). The young adult thymus contains plenty of double positive thymocytes (46.6% CD4+, CD8+) and among single either CD4 or CD8 positive cells the helper T-cells dominate over cytotoxic T-cells (41.7% *vs.* 3.3%), as normally observed in young adult BALB/c mice. In comparison the mock (GFP)-transfected embryonic thymic lobe (Fig. 5C) shows a somewhat different ratio for CD4/CD8 expression. There are more double negative thymocytes (34.8% CD4−, CD8−) and less single either CD4 or CD8 positive T-cells (15% and 5.8%, respectively) with equal number of double positive thymocytes (44.4% CD4+, CD8+). Differences compared to young adult figures are likely due to the embryonic context of thymocyte development continued in an *ex vivo* setting. What is more striking,

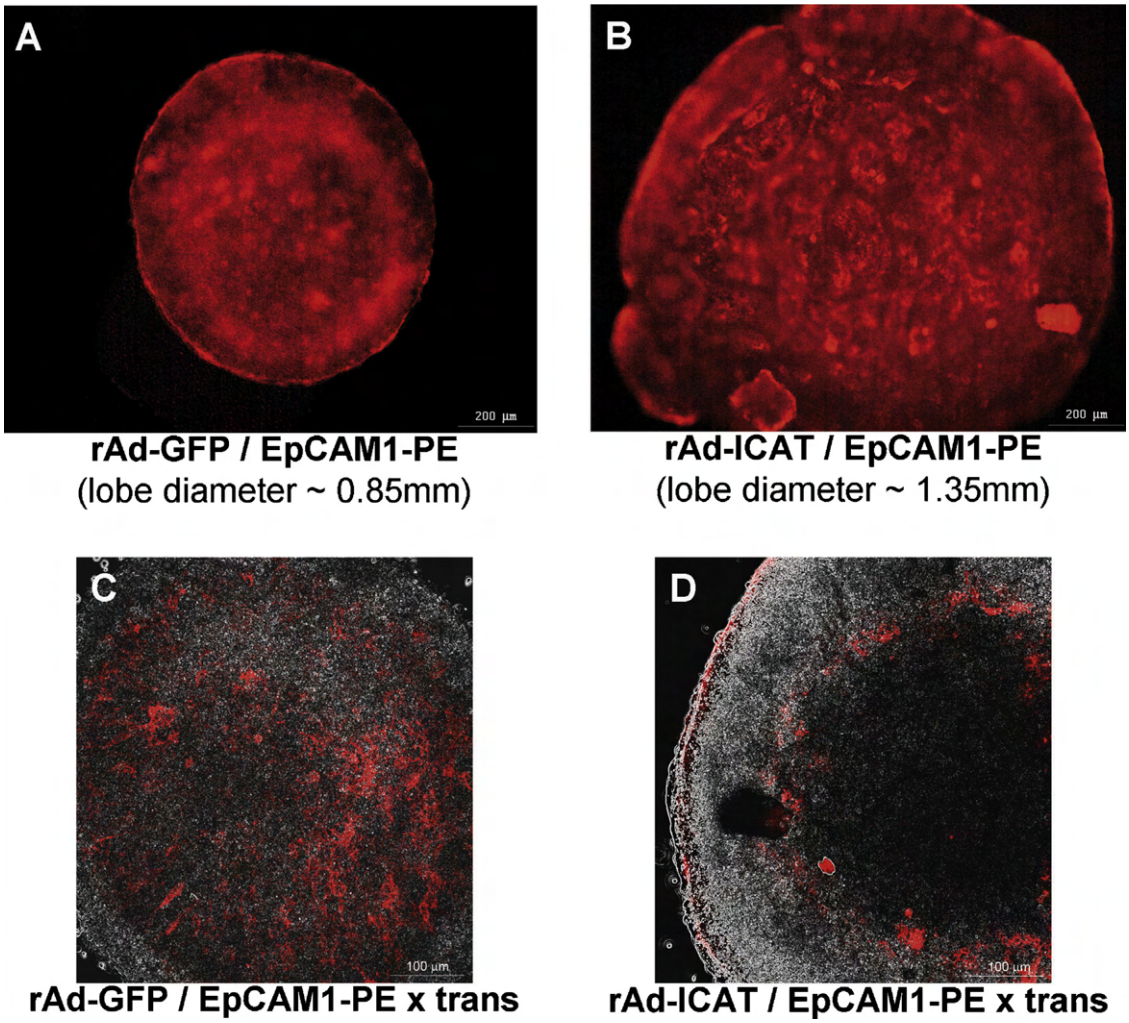

Fig. 4. Figure shows histological level morphological differences of mock and ICAT-transfected embryonic thymic lobes using fluorescent conventional and confocal microscopy. Epithelial cells were stained for their EpCAM1-expression on all four images. (A, B) Obtained with conventional fluorescent microscopy illustrates the size difference of GFP and ICAT-transfected lobes. The applied size marker (lower right corner) allows for approximate determination and comparison of lobe diameters. (C, D) Obtained with confocal microscopy allow for the visualization of internal lobe structure showing EpCAM1-staining cells in the examined plane (staining red) as well as the entire organ (trans-white image layer shown in gray). The lobe is significantly larger following ICAT-transfection as shown by Fig. 3(B and D). However, the lobe is inflated harboring a hollow cavity lined by epithelial cells following ICAT-transfection as shown by Fig. 3D. Occasional cysts are also observed (Fig. 3D).

however, is the degree of difference in CD4/CD8 ratio observed among thymocytes following ICAT-transfection (see Fig. 5D). There is a dominance of double negative thymocytes (80.9% CD4−, CD8−) with very few double positive thymocytes (8% CD4+, CD8+) and even less single either CD4 or CD8 positive T-cells (4.2% and 7%, respectively). The difference in CD4/8 ratio is striking not only compared to young adult, but also compared to mock-transfected E15 thymic lobes. Differences compared to mock-transfection can only be attributed to selective inhibition of Wnt/beta-catenin signaling through ICAT in mouse embryonic thymic epithelial cells selectively transfected by rAd vectors providing an altered niche for murine thymocyte development.

Discussion

Comparative histology

Human (W15) and mouse (E15) embryonic thymic sections were examined at the level of histology. The presence of characteristic cell surface markers (EpCAM-1, Ly-51, cytokeratin8) as well as a secreted protein and its ligand (Wnt4, Fz4) was assessed (Gill et al. 2002; Bennett et al. 2002; Klug et al. 2002). Both human and mouse sections stained positive for all the examined proteins. The thymic epithelial compartments of the medulla and the cortex showed signs of segregation in both the W15 human and the E15 mouse thymic sections. Staining patterns obtained with cytokeratin8 and Fz4 in particular showed differences between human and mouse. This, however, is not surprising as the examined embryonic stages (W15 for human and E15 for mouse) do not match exactly in terms of thymic developmental stage. Nevertheless it is reassuring that the same characteristic cell surface markers, secreted proteins and ligands are equally present during human and murine embryonic development emphasizing the human relevance of murine test systems therefore subsequent experiments were performed on murine cells.

Changes in gene expression related to Wnt/beta-catenin signaling

Reciprocal input signals were provided to murine embryonic thymic epithelial cells in terms of the Wnt/beta-catenin signaling pathway. Increased non-canonical Wnt-effect was modeled through providing additional Wnt4 in the form of supernatant. The opposite effect was achieved through rAd-mediated transfection of the ICAT transgene that inhibits the Wnt/beta-catenin signaling

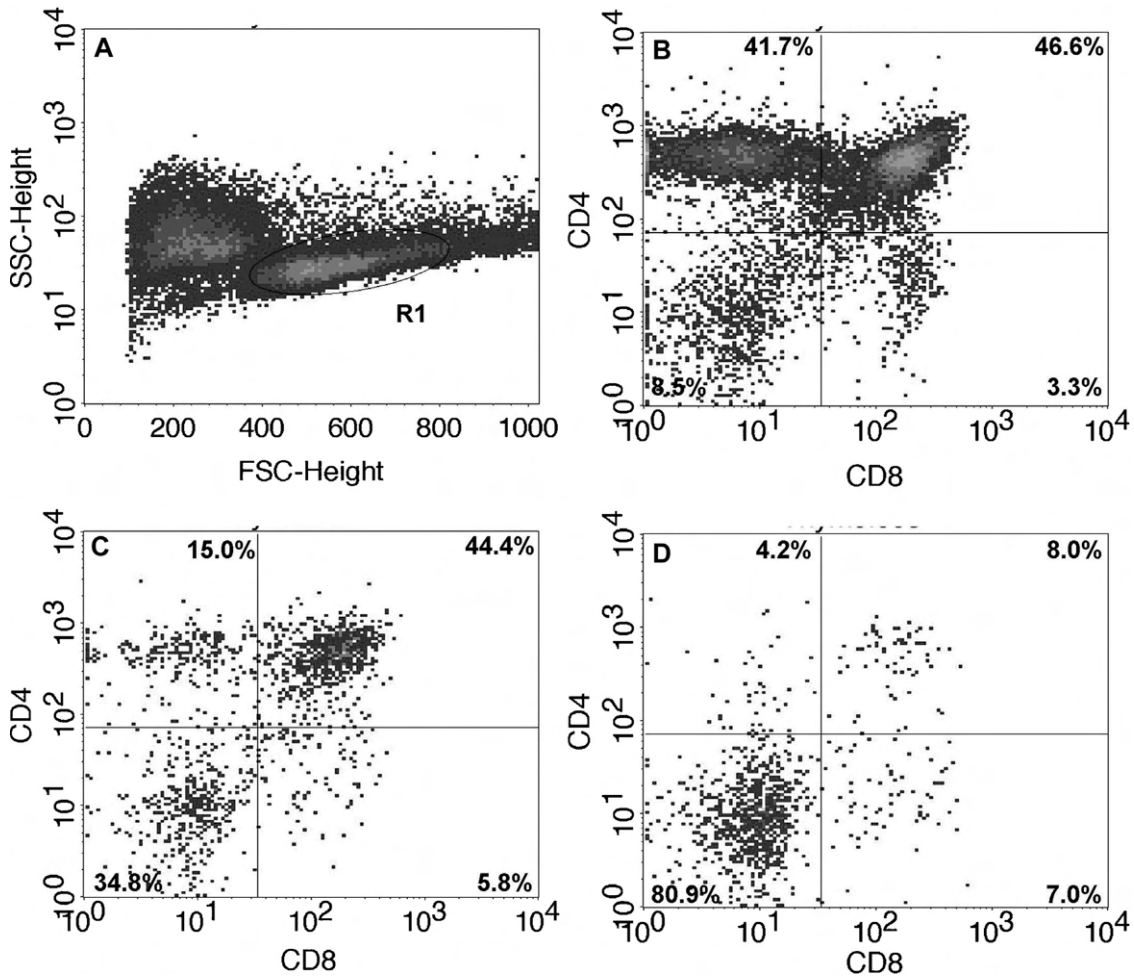

Fig. 5. Figure demonstrates flow-cytometric evaluation of epithelial functionality shown by thymocyte maturation. The thymic lobes were mechanically dispersed liberating the thymocytes. Viable cells were gated (R1) by morphology (A). Thymocytes were stained with CD4-PE and CD8-FITC. The ratio of CD4/CD8 expression is shown in viable thymocytes from young adult (B) control, and GFP-transfected (C) or ICAT-transfected (D) E15 thymic lobes after 7 days of *ex vivo* culture. Percentages of flow-cytometric statistics are shown in the corresponding quadrants. Representative flow-cytometric figures are shown. The young adult sample and the GFP(mock)-transfected sample show similarity in terms of thymocyte subpopulations. The CD4/CD8 double positive group shows equal representation, while double negative cells are more frequent and single positive cells are less frequent in the mock-transfected scenario compared to the young adult control, likely due continued *ex vivo* development in an embryonic setting. However, thymocyte subpopulation distribution is rather different following ICAT-transfection as there is a severe block in development shown by the accumulation of double negative cells and the loss of double positive and single positive cell groups.

pathway. Gene expression analysis of surface (MHCII), intracellular (FoxN1) and secreted (IL7) molecules, conventionally associated with epithelial phenotype and function in the context of the thymus showed that additional Wnt4 exposure could significantly increase the transcription of all three examined genes. It is of note that our data obtained *ex vivo* are in harmony with literature data suggesting that FoxN1 is a direct target gene of Wnt4 (Gill et al. 2002). In contrast, the over-expression of ICAT could consequently, though moderately down-regulate the transcription of all three examined genes.

The fact that decrease in gene expression achieved through ICAT-transfection was moderate is due to several factors. The Wnt4 supernatant affects all cells of the experimental system through a cell non-autonomous effect. In contrast, ICAT could only inhibit the Wnt/beta-catenin signaling pathway in transfected thymic epithelial cells due to its intracellular/cell-autonomous route of action. Also, gene expressional change following ICAT-mediated inhibition was compared to mock-transfection corresponding to basal level Wnt4 secretion that is low compared to additional Wnt4 supernatant. Currently there is no way in our experimental system for quantitative, balanced reciprocal Wnt4/ICAT treatment to affect epithelial cells with opposing signals of equal intensity.

Changes in morphology related to Wnt/beta-catenin signaling

We have performed mock-transfection and ICAT-transfection of E12 mouse embryonic thymic lobes followed by staining for EpCAM-1 and visualization in whole. Conventional fluorescent microscopy shows that the thymic lobes become significantly larger in diameter following ICAT-transfection compared to mock-transfection. However, confocal fluorescent microscopy (especially if combined with trans-white conventional image) shows that the ICAT-transfected lobe is rather empty compared to the mock-transfected thymic lobe containing a hollow cavity without cells. Also the overall number of epithelial cells appears to be lower and restricted to a spherical area surrounding the hollow cavity in this aberrant developmental scenario.

Changes in functionality related to Wnt/beta-catenin signaling

The indirect effect of Wnt4 on thymocyte development has already been thoroughly investigated by other groups (Heinonen et al. 2011). Therefore we focused on examining the indirect effect of selective Wnt/beta-catenin inhibition in murine thymic epithelial cells, thus altering the niche in which thymocytes develop.

At later stages (from E13 onwards) the mouse embryonic thymus contains thymocyte precursors that can undergo maturation processes *ex vivo*. We have performed mock (GFP)-transfection and ICAT-transfection of E15 mouse embryonic thymic lobes followed by flow-cytometric analysis of viable thymocytes for CD4/8 expression to demonstrate changes in the functionality of epithelial cells to support thymocyte maturation. During physiological maturation the developing thymocytes are first double negative (CD4−, CD8−) and then turn on the expression of both CD4 and CD8 to become double positive (CD4+, CD8+). This is followed by the single positive stage where either CD4 or CD8 expression is spared, while the other becomes muted, normally resulting in the dominance of helper T-cells (see Fig. 5B in young adult mouse).

The normal route of thymocyte development is somewhat slowed down in the mock (GFP)-transfected embryonic *ex vivo* cultured setting where we observe less single positive and more double negative thymocytes compared to the young adult mouse (see Fig. 5C). This is not surprising as we compare thymocyte maturation *ex vivo* in embryonic thymic lobes *vs.* thymocyte maturation *in vivo* in physiological young adult thymus. However, differences are much more striking following selective inhibition of Wnt/beta-catenin signaling in thymic epithelial cells by ICAT-encoding rAd vectors as shown by the dominance of the double negative maturation stage and the scarceness of single positive cells (see Fig. 5D). It is also observed that among the few single positive cells there are more CD8+ than CD4+ cells due to the fact that these two cell surface markers are not fully synchronized during transition from double negative to double positive stage, but CD4 up-regulation is a little delayed compared to CD8 (Jimenez et al. 2001; Pearse 2006).

Conclusion

Our data obtained in an *ex vivo* murine test system with human relevance prove that if the Wnt/beta-catenin signaling pathway is blocked in epithelial cells during crucial stages of thymic embryonic development, it seriously impairs normal developmental program resulting in the formation of aberrant thymic lobe morphology. This is also supported by changes recorded at the molecular level as we have observed the consequent, though moderate down-regulation of the examined characteristic genes encoding surface (MHCII), intracellular (FoxN1) and secreted (IL7) molecules. This is in contrast with the significant increase in expression level of the same genes following treatment with additional Wnt4.

Our results obtained during *ex vivo* experiments confirm that the Wnt/beta-catenin signaling pathway is a key player responsible for the proper differentiation and maintenance of thymic epithelial cells during embryonic development and potentially in postnatal life. Literature data also suggest that if *in vivo* the Wnt/b-catenin signaling pathway is either chronically suppressed or hyper-activated both may lead to abnormal tissue homeostasis due to insufficient proliferation signals of tissue stem cells (Wnt-suppression) or due to hyper-proliferating and thus exhausted tissue stem cell pools (Wnt-hyper-activation) (DeCarolis et al. 2008; Miller 2007; Liu et al. 2007). This proposes that the Wnt/b-catenin signaling pathway has a major role not only in development but also in tissue homeostasis.

It is also clearly indicated by our data that active Wnt/beta-catenin signaling is also required for normal embryonic thymic epithelial functionality and not only morphology as demonstrated by the severely impaired capacity to support thymocyte maturation following selective ICAT-transfection into thymic epithelial cells *ex vivo*. The simultaneously observed thymic cyst formation is an exciting phenomenon. It has been reported that following K14-restricted loss of FoxN1 expression, the development of the thymic structure is seriously impaired resulting in distant alveolar-like cystic structures suggesting potential trans-differentiation (Guo et al. 2011). Further studies, however, are required to study the exact mechanisms underlying the alternative developmental scenario resulting aberrant lobe morphology following the selective inhibition of the Wnt/beta-catenin pathway in thymic epithelial cells.

Acknowledgements

Research was supported by the following grants: 'Science Please' Research Team on Innovation grant No.: SROP-4.2.2/08/1/2008-0011 (grant holder: J.E.P.) and OTKA (Hungarian Scientific Research Fund) type: PD (post-doctoral) grant No.: 78310 (grant-holder: K.K.). The funders had no role in study design, data collection and analysis, decision to publish, or preparation of the manuscript. The authors are grateful to Bela Veszpremi MD, PhD (Department of Obstetrics and Gynecology) for providing us access to human embryonic samples and Gergely Berta MD (Department of Medical Biology) for the invaluable help provided during confocal microscopy imaging (confocal image station was purchased from grant no. GVOP-3.2.1-2004-04-0172/3.0). The authors claim that there is no conflict of interest for any of the authors.

References

Anderson, G., Pongracz, J., Parnell, S., Jenkinson, E.J., 2001. Notch ligand-bearing thymic epithelial cells initiate and sustain Notch signaling in thymocytes independently of T cell receptor signaling. Eur. J. Immunol. 31, 3349–3354.

Balciunaite, G., Keller, M., Balciunaite, E., Piali, L., Zuklys, S., Mathieu, Y.D., Gill, J., Boyd, R., Sussman, D.J., Holländer, G.A., 2002. Wnt glycoproteins regulate the expression of FoxN1, the gene defective in nude mice. Nat. Immunol. 3, 1102–1108.

Beardsley, T.R., Pierschbacher, M., Wetzel, G.D., Hays, E.F., 1983. Induction of T-cell maturation by a cloned line of thymic epithelium (TEPI). Proc. Natl. Acad. Sci. U.S.A. 80 (October (19)), 6005–6009.

Bennett, A.R., Farley, A., Blair, N.F., Gordon, J., Sharp, L., Blackburn, C.C., 2002. Identification and characterization of thymic epithelial progenitor cells. Immunity 16, 803–814.

Bleul, C., Boehm, T., 2005. BMP signaling is required for normal thymus development. J. Immunol. 175, 5213–5221.

DeCarolis, N.A., Wharton Jr., K.A., Eisch, A.J., 2008. Which way does the Wnt blow? Exploring the duality of canonical Wnt signaling on cellular aging. Bioessays 30 (February (2)), 102–106.

Gill, J., Malin, M., Hollander, G.A., Boyd, R., 2002. Generation of a complete thymic microenvironment by MTS24(+) thymic epithelial cells. Nat. Immunol. 3, 635–642.

Gordon, M.D., Nusse, R., 2006. Wnt signaling: multiple pathways, multiple receptors, and multiple transcription factors. J. Biol. Chem. 281, 22429–22433.

Guo, J., Rahman, M., Cheng, L., Zhang, S., Tvinnereim, A., Su, D.M., 2011. Morphogenesis and maintenance of the 3D thymic medulla and prevention of nude skin phenotype require FoxN1 in pre- and post-natal K14 epithelium. J. Mol. Med. (Berl.) 89 (March (3)), 263–277.

Hare, K., Pongracz, J., Jenkinson, E., Anderson, G., 2003. Modeling TCR signaling complex formation in positive selection. J. Immunol. 171 (6), 2825–2831.

Hayward, A.R., Ezer, G., 1974. Development of lymphocyte populations in the human foetal thymus and spleen. Clin. Exp. Immunol. 17 (May (1)), 169–178.

Heinonen, K.M., Vanegas, J.R., Brochu, S., Shan, J., Vainio, S.J., Perreault, C., 2011. Wnt4 regulates thymic cellularity through the expansion of thymic epithelial cells and early thymic progenitors. Blood 118 (19), 5163–5173.

Jimenez, E., Vicente, A., Sacedon, R., Muñoz, J.J., Weinmaster, G., Zapata, A.G., Varas, A., 2001. Distinct mechanisms contribute to generate and change the CD4:CD8 cell ratio during thymus development: a role for the Notch ligand, Jagged1. J. Immunol. 166, 5898–5908.

Klug, D.B., Carter, C., Gimenez-Conti, I.B., Richie, E.R., 2002. Cutting edge: thymocyte-independent and thymocyte-dependent phases of epithelial patterning in the fetal thymus. J. Immunol. 169, 2842–2845.

Kvell, K., Pongracz, J.E., 2011. Central immune senescence, reversal potentials. In: Nagata, T. (Ed.), Senescence. Publisher: INTECH, ISBN 978-953-308-28-6.

Kvell, K., Varecza, Z., Bartis, D., Hesse, S., Parnell, S., Anderson, G., Jenkinson, E.J., Pongracz, J.E., 2010. Wnt4 and LAP2alpha as pacemakers of thymic epithelial senescence. PLoS ONE 5 (5), e10701.

Liu, H., Fergusson, M.M., Castilho, R.M., Liu, J., et al., 2007. Augmented Wnt signaling in a mammalian model of accelerated aging. Science 317 (August (5839)), 803–806.

Lobach, D.F., Haynes, B.F., 1987. Ontogeny of the human thymus during fetal development. J. Clin. Immunol. 7 (March (2)), 81–97.

Mikels, A.J., Nusse, R., 2006. Wnts as ligands: processing, secretion and reception. Oncogene 25, 7461–7468.

Miller, R., 2007. Of aging mice and men. Science 318 (October (5849)), 390.

Osada, M., Ito, E., Fermin, H., Vazquez-Cintron, E., Venkatesh, T., Friedel, R.H., Pezzano, 2006. The Wnt signaling antagonist Kremen1 is required for development of thymic architecture. Clin. Dev. Immunol. 13, 299–319.

Pearse, G., 2006. Normal structure, function and histology of the thymus. Toxicol. Pathol. 34, 504–514.

Pongracz, J., Hare, K., Harman, B., Anderson, G., Jenkinson, E.J., 2003. Thymic epithelial cells provide Wnt signals. Eur. J. Immunol. 33, 1949–1956.

Pongracz, J.E., Parnell, S.M., Jones, T., Anderson, G., Jenkinson, E.J., 2006. Overexpression of ICAT highlights a role for catenin-mediated canonical Wnt signalling in early T cell development. Eur. J. Immunol. 36, 2376–2383.

Rezzani, R., Bonomini, F., Rodella, L.F., 2008. Histochemical and molecular overview of the thymus as site for T-cells development. Prog. Histochem. Cytochem. 43 (2), 73–120.

Schweizer, L., Varmus, H., 2003. Wnt/Wingless signaling through beta-catenin requires the function of both LRP/Arrow and frizzled classes of receptors. BMC Cell. Biol. 4, 4.

Varecza, Z., Kvell, K., Talaber, G., Miskei, G., Csongei, V., Bartis, D., Anderson, G., Jenkinson, E.J., Pongracz, J.E., 2011. Multiple suppression pathways of canonical Wnt signalling control thymic epithelial senescence. Mech. Ageing Dev. 132 (May (5)), 249–256.

frontiers in Physiology

ORIGINAL RESEARCH
published: 02 August 2021
doi: 10.3389/fphys.2021.658218

Physical Activity as a Preventive Lifestyle Intervention Acts Through Specific Exosomal miRNA Species—Evidence From Human Short- and Long-Term Pilot Studies

*Kitti Garai[1,2], Zoltan Adam[1,2], Robert Herczeg[3], Krisztina Banfai[1,2], Adam Gyebrovszki[4], Attila Gyenesei[3], Judit E. Pongracz[1,2], Marta Wilhelm[4] and Krisztian Kvell[1,2]**

[1] Department of Pharmaceutical Biotechnology, Faculty of Pharmacy, University of Pécs, Pécs, Hungary, [2] Wnt-Signaling Research Group, Szentagothai Research Center, University of Pécs, Pécs, Hungary, [3] Bioinformatics Research Group, Szentagothai Research Center, University of Pécs, Pécs, Hungary, [4] Faculty of Science, Institute of Sport Sciences and Physical Education, University of Pécs, Pécs, Hungary

Exercise initiates systemic adaptation to promote health and prevent various lifestyle-related chronic diseases. Emerging evidence suggests that circulating exosomes mediate some of the beneficial effects of exercise via the transfer of microRNAs between tissues. Yet to date, a comprehensive profile of the exosomal miRNA (exomiR) content released following short-term (0.5 year in this study) and long-term (25 + years in this study) regular bouts of exercise is still lacking. However, a better understanding of these miRNA species would assist in clarifying the role of regular exercise at the molecular level in the prevention of chronic diseases. In the present pilot studies we analyzed serum exomiR expression in healthy young, sedentary participants (n = 14; age: 23 ± 2 years) at baseline and following a half year-long moderate-intensity regular exercise training. We also analyzed serum exomiR expression in older, healthy trained participants (seniors, n = 11; age: 62 ± 6 years) who engaged in endurance activities for at least 25 years. Following the isolation and enrichment of serum exosomes using Total Exosome Isolation Reagent (TEI) their exomiR levels were determined using the amplification-free Nanostring platform. Hierarchical cluster analysis revealed that the majority of exomiRs overlap for short-term (0.5 year in this study) and long-term (25 + years in this study) regular bouts of exercise. The top 12 significantly altered exomiRs (let-7a-5p; let-7g-5p; miR-130a-3p; miR-142-3p; miR-150-5p; miR-15a-5p; miR-15b-5p; miR-199a-3p; miR-199b-3p; miR-223-3p; miR-23a-3p, and miR-451a-3p) were used for further evaluation. According to KEGG pathway analysis a large portion of the exomiRs target chronic diseases including cancer, neurodegenerative and metabolic diseases, and viral infections. Our results provide evidence that exosomal miRNA modulation is the molecular mechanism through which regular exercise prevents various chronic diseases. The possibility of using such exomiRs to target diseases is of great interest. While further validation is needed, our comprehensive exomiR study presents, for the first time, the disease-preventive molecular pattern of both short and long-term regular exercise.

Keywords: regular exercise, exosome, miRNA, chronic disease, prevention

OPEN ACCESS

Edited by:
Martin Burtscher,
University of Innsbruck, Austria

Reviewed by:
Shamila D. Alipoor,
National Institute for Genetic Engineering and Biotechnology, Iran
Sigrun Lange,
University of Westminster, United Kingdom

***Correspondence:**
Krisztian Kvell
kvell.krisztian@pte.hu

Specialty section:
This article was submitted to Exercise Physiology, a section of the journal Frontiers in Physiology

Received: *25 January 2021*
Accepted: *12 July 2021*
Published: *02 August 2021*

Citation:
Garai K, Adam Z, Herczeg R, Banfai K, Gyebrovszki A, Gyenesei A, Pongracz JE, Wilhelm M and Kvell K (2021) Physical Activity as a Preventive Lifestyle Intervention Acts Through Specific Exosomal miRNA Species—Evidence From Human Short- and Long-Term Pilot Studies. Front. Physiol. 12:658218. doi: 10.3389/fphys.2021.658218

INTRODUCTION

Regular exercise has been known as a major intervention tool not only to attenuate the risk of a multitude of disorders from metabolic disease and neurodegenerative disorders to cancer, but also to delay the occurrence of numerous age-related diseases (Brahmer et al., 2019). While most molecular mechanisms mediating the long-term beneficial effects of exercise remain unexplored, growing evidence suggests the involvement of tissue crosstalk via the release of exosomes following exercise (Frühbeis et al., 2015; Estébanez et al., 2021). Exosomes are small extracellular vesicles (sEVs) (30–150 nm) that are secreted by fusion of multivesicular bodies to the plasma membrane (Brennan et al., 2020). These vesicles transport a large variety of cargo molecules including miRNAs, DNA and proteins that may be taken up by distant cell types and alter the phenotype of these recipients (Kowal et al., 2014). Since miRNA species are well recognized for playing important roles in many physiological and pathological processes, they could also be involved in exercise-related benefits of disease prevention. Deciphering the contribution of miRNAs present in exercise-derived exosomes and their downstream targets is crucial for the better comprehension of how preventive lifestyle actually acts at the molecular level. According to a study, the expression of certain circulating miRNA species increases with age in plasma microvesicles (Rani et al., 2017). Of notable example, hsa-miR-223-3p, hsa-miR-23a-3p, hsa-let-7g-5p, hsa-miR-199a-5p, hsa-miR-15a-5p, and has-miR-142-3p show positive correlation with age and the development of specific chronic diseases (Rani et al., 2017). Recently it has been shown that healthy aging is also reflected by the profile of circulating exosomes, and exercise−induced beneficial effects may be related with the modulation of these exosomes (Bertoldi et al., 2018). There are reports indicating the changes of various miRNA species in exosomes following an acute of exercise (D'souza et al., 2018; Yin et al., 2019), however only a small number of studies examine exosomes in response to long-term training (Nederveen et al., 2021). Of note, in a mammalian study the levels of miR−19b, miR−148a, miR−150, miR−221, miR−361, and miR−486 were up-regulated during the first month of exercise, but returned to baseline by completion of a 4−month study period (Muroya et al., 2015). Regarding long-term human experiments, a significant increase in exosome release was shown after a single bout of flywheel exercise (Annibalini et al., 2019), whereas no change was found after a full year of rowing training (Hou et al., 2019). These conflicting results could potentially be attributed to the adaptation process that occurs with time. Additional research is crucial with various training modalities and durations to further understand the role of exosomes and their miRNA content in the prevention of chronic diseases induced by long-term exercise. In the present study first we investigated the effect of a 0.5 year-long, moderate intensity, personal trainer-supervised, concurrent resistance and aerobic training program on the overall circulating exomiRs expression profile of healthy, young, previously sedentary individuals. We also assessed whether exomiRs differentially expressed after a 0.5 year regular exercise in young adults were similarly present in healthy senior trained participants who have engaged in regular exercise activities for at least 25 years. The effect of short- and long-term regular exercise on the miRNA profile was determined by comparing baseline vs. 0.5 year, and baseline vs. 25 + years miRNA levels. As anticipated we found that the levels of the exomiRs are fairly consistent in comparison of the 0.5 year (short-term adaptation) and the 25 + years (long-term adaptation) active groups. Twelve exomiRs showed overlap for both study periods (baseline vs. 0.5 year and baseline vs. 25 + years). Of note, all of them were significantly down-regulated. Bioinformatics analysis was used to evaluate the interplay between biological signaling pathways offering insight into mechanisms linking exercise and chronic disease prevention. Our results prove that full miRNome analysis might be a useful tool to identify exomiRs acting on particular pathways that prevent the development of specific chronic diseases.

MATERIALS AND METHODS

Participants and Applied Training Protocol

Healthy young, sedentary (n = 14; age: 23 ± 2 years) and senior trained (n = 11; age: 62 ± 6 years) individuals were recruited. Participants were in good general health, defined as having no chronic diseases (e.g., metabolic disorders, cardiovascular disease, cancer, etc.). Main characteristics of the subjects are summarized in **Table 1** (see **Supplementary Material** for further details). Healthy, young sedentary individuals completed moderate-intensity, concurrent resistance and aerobic exercises regular exercise training three times a week for half a year (Garai et al., 2019). Our exercise bouts consisted of four parts: warm-up, resistance training, aerobic exercises and cool-down with stretching. The heart rate of the participants was measured continuously during exercise with a heart rate monitor (Polar Team System, Polar Electro, Finland). Age-predicted maximum heart rates were estimated with the following calculation: 220—age (years). Every trainings began with standardized, active warm-up protocol applying mobility and stability exercises, gymnastic exercises and moderate stretching. After warming-up resistance training was performed. During this part the heart rate of the subjects was allowed to reach 85% of individual heart rate maximum. Aerobic exercises included walking and jogging, if the subject's heart rate was lower than 65% of the individual heart rate maximum. The cool-down protocol included 2 min of slow walking and 8 min of static stretching exercises of all major muscle groups. Participants were asked to keep their diet and daily activity level unchanged during the 6 month-long lifestyle program. Training diary was prepared during the 6 months and compliance was calculated accordingly.

Senior trained subjects were engaged in regular exercise activities for at least 25 years. The exercise behavior of senior participants was assessed with the use of a general lifestyle questionnaire as well as with the International Physical Activity Questionnaire (IPAQ) (Craig et al., 2003). We obtained information on smoking-, alcohol consumption status and physical activity (frequency, type, duration). Senior trained

participants also performed both types of exercise (endurance and resistance training), including running, swimming, weightlifting, cycling, skating, adrenaline sports, walking, hiking and spinning. Over half (54%) of the senior participants performed physical activity on a daily basis, while the rest performed physical activity at least twice a week. For details please check the **Supplementary Material Section**. Each participant gave written informed consent before completing any data collection. The study was conducted according to the Declaration of Helsinki principles and approved by the Regional and Local Ethics Committee of Clinical Center, University of Pecs (ref. no.: 6439/2016 and 7755/2019).

Collection and Preparation of Human Serum Samples

Human blood samples were collected around 7:00 a.m. after a 12 h fasting in blood collection tubes (BD Vacutainer, SST: BD SST Tubes with Silica Clot Activator and Polymer Gel, Franklin Lakes, NJ, United States) at two time-points: at baseline and after the 0.5 year long training program from the young individuals and at one time-point from seniors. Participants were asked to avoid excessive exercise the day before each testing condition. Blood samples were clotted for approximately 30 min at room temperature. Samples were then centrifuged at 1,500 g for 10 min at room temperature. Serum samples were stored at −80°C until further analysis. The same procedure was carried out with the samples of seniors.

Exosome Isolation

In order for their samples to be processed participants had to show min. 85% compliance with regular exercise mandated by the program. Before exosome isolation, equal volumes of serum (100 μl each) from 14 healthy young participants and 11 seniors were pooled, separately (**Figure 1**). Prior to pooling we have carefully evaluated the participants for potential outliers based on the assessment of physiological and blood parameters. Only those participants' samples were pooled who constituted a homogenous population for the evaluated physiological and blood parameters (baseline, 0.5 year, 25 + years). Then, exosomes were isolated from the three pooled serum samples (baseline; n = 1, 0.5 year; n = 1 and 25 + years; n = 1 pooled samples) using TEI (from serum) (Invitrogen, Thermo Fisher Scientific, Waltham, MA, United States) following the manufacturer's protocol. TEI reagents contain volume-excluding polymers (e.g., polyethylene glycol, dextrans, or polyvinyls). According to Andreu et al. (2016) and Banfai et al. (2019), the use of precipitation reagents provide good reproducibility and are suitable for an easy and cost-efficient enrichment of serum exosomes for miRNA analyses. As a result TEI was chosen for studying exosomal miRNA content in our study.

NTA Measurement With Nanosight NS300

NTA Protocol

Exosome-enriched preparations were measured and quantified using Nanosight NS300 instrument (Malvern Panalytical Ltd., Malvern, United Kingdom). The camera level for each sample was manually adjusted to achieve optimal visualization of particles following the manufacturer's instructions. Samples were injected with a syringe pump (infuse = 50). Detection threshold was set for maximum sensitivity with a minimum of background noise. All measurements were performed in five replicates for each sample, collecting 60-s videos. Following capture, the videos were analyzed by the in-built NTA v3.2 software (Gardiner et al., 2013).

Particle Size and Concentration Analysis

The samples of 3 individuals were randomly chosen from each group (baseline, n = 3; 0.5 year, n = 3; and 25 + years, n = 3). All samples were diluted in PBS. Ideal measurement concentrations were achieved by pre-testing the ideal particle per frame value (40–100 particles/frame).

Single EV Direct Immunolabeling and NTA Evaluation

The following monoclonal antibodies were used for immune-labeling: anti-human-CD63-FITC (MEM-259) (Thermo Fisher Scientific) anti-human-CD81-PE/Cy7 (TAPA-1) (Sony Biotechnology). Particle concentrations were established for unlabeled EV sample prior to immune-labeling. The

TABLE 1 | Subject characteristics.

	Baseline	0.5 years	*p*	25 + years
Age (years)	23 ± 2	23.5 ± 2		62 ± 6
BMI	21.64 ± 1.57	21.46 ± 1.44	0.382	27.92 ± 2.95
Body weight (kg)	60.39 ± 5.42	59.55 ± 5.74	0.166	75.16 ± 7.18
Body fat percentage (%)	31.79 ± 3.39	31.49 ± 3.47	0.61	21.23 ± 6.03
VO_2 max (ml/kg/min)	36.41 ± 6.67	39.81 ± 6.20*	0.047	32.9 ± 6.99
LDL (mmol/L)	2.35 ± 0.9	2.44 ± 0.83	0.481	3.63 ± 1.19
HDL (mmol/L)	1.81 ± 0.55	2.13 ± 0.61*	0.002	1.68 ± 0.53
Glucose (mmol/L)	4.94 ± 0.39	4.63 ± 0.31 **	<0.001	5.67 ± 0.45
Systolic BP (Hgmm)	114.5 ± 14.18	108.07 ± 8.69	0.55	131.2 ± 19.42
Diastolic BP (Hgmm)	76.07 ± 9.19	72.93 ± 7.92	0.223	87.00 ± 9.25

*Values are expressed as mean ± SD. Paired t-test (*p < 0.05; **p < 0.001); p-values were calculated for baseline vs. 0.5 year as applicable; VO_2 max, maximal oxygen uptake (cardiorespiratory fitness); LDL, Low Density Lipoprotein; HDL, High Density Lipoprotein; BP, Blood Pressure.*

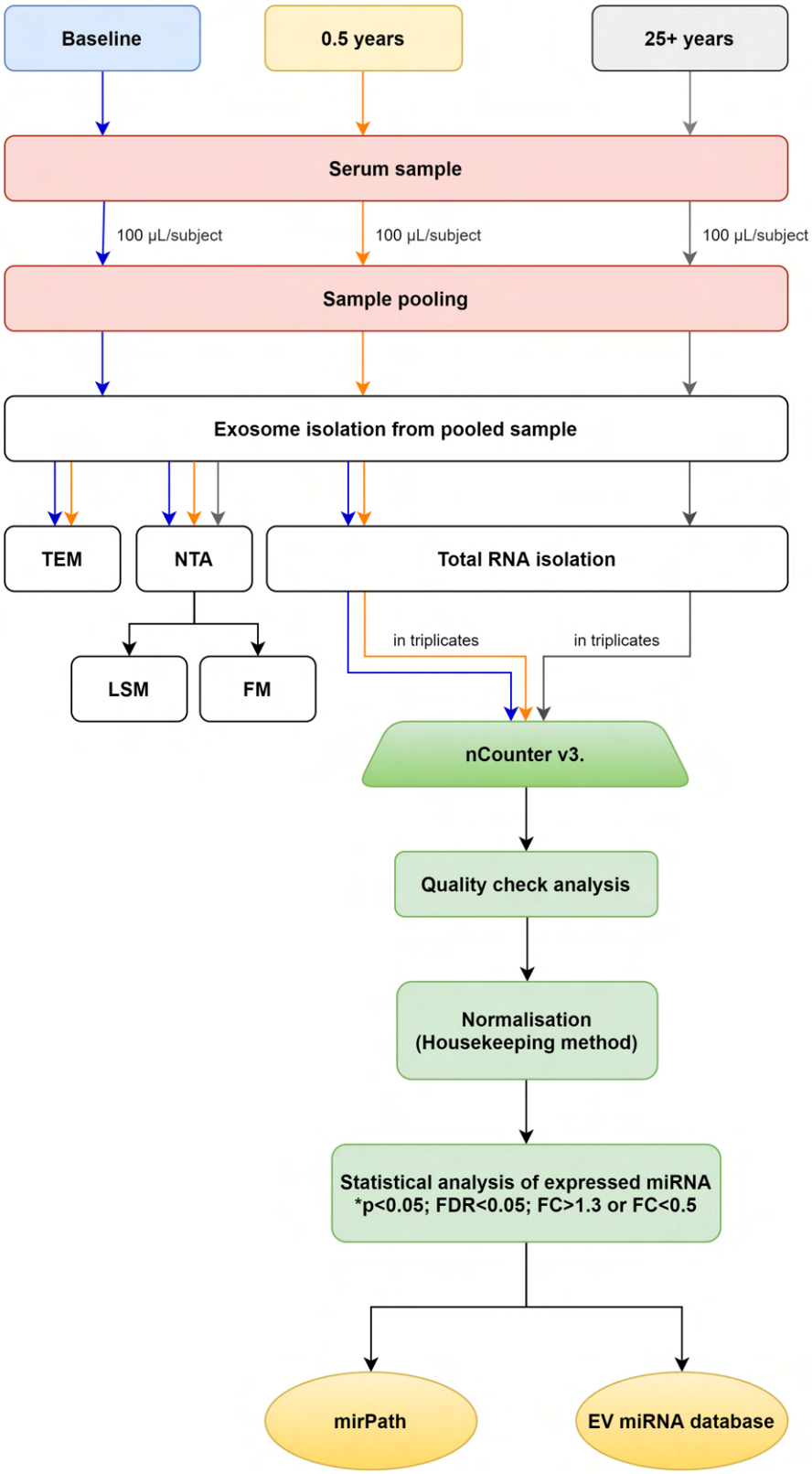

FIGURE 1 | Workflow. Flowchart representing the entire workflow.

concentration of the exosome stock solution was 3.17×10^{10} particles/ml (based on NTA). Sample aliquots were prepared to ensure equal dilution effects for each arm of the experiment. Varying concentration anti-CD63 and anti-CD81 antibodies was added to the 50 μl exosome stock solution to yield a volume of 100 μl and to determine an optimized antibody to exosome ratio for single-vesicle labeling. The samples (anti-CD63 labeled; $n = 1$ and anti-CD81 labeled; $n = 1$) were incubated in the dark for 1 h at room temperature. In order to minimize photobleaching during fluorescence mode (FM), all immune-labeled samples were evaluated first in FM, followed immediately by evaluation in light scatter mode (LSM). Then, the FM/LSM percentage was calculated (Thane et al., 2019).

Transmission Electron Microscopy (TEM)

Exosomes were visualized by transmission electron microscopy. Sample volume of 2.5 μl was placed onto a 300 mesh grid. The grid was left to air dry overnight. Then 5% uranyl-acetate and later 3% sodium-citrate were added to the grid. After 5 min incubation, the grid was allowed to air dry. Twenty four hours later the grid was analyzed using JEOL TEM 1,200 EX. The average diameter of the isolated exosomes was determined using three independent TEM preparations and ImageJ software.

Exosomal Total RNA Purification and Complete miRNome Profiling

Total RNA from exosomes was extracted using Total Exosome RNA and Protein Isolation Kit (Invitrogen, Thermo Fisher Scientific, Waltham, MA, United States) according to the manufacturer's protocol. ExomiR level profiling was performed using the Nanostring platform (NanoString Technologies, Seattle, WA) according to the manufacturer's instructions to analyze 800 human miRNAs. Since the extraction of exosomal miRNA yields low amounts of RNA, but amplification-free methods require high amounts, we adopted the standard method of using pooled samples to yield reproducible reads. Three technical replicates were run per sample (baseline; 0.5 year and 25 + years groups). Quality check confirmed the reliability of the run and also the validity and reproducibility of the miRNA screening protocol. nSolver software was used for data analysis and normalization. Normalization was performed using the Housekeeping method according to nCounter miRNA expression analysis in plasma and serum samples technote instructions. Briefly, NormFinder was used to identify putative housekeeping miRNAs. First, raw data (RCC files) were imported into nSolver and any sample which failed QC was removed. An experiment was built and background subtraction was set to the Mean + 1 SD of the NEG control probes. Of note, we kept normalization options turned off during this process. Data from the completed experiment were exported into an excel file derived from the normalized dataset. Using NormFinder background subtracted data were sorted by average counts across all samples, and all miRNAs expressed below 50 mean counts were deleted when averaged across all samples. NormFinder created a worksheet listing all the genes and a stability value for each of them. With the aid of NormFinder the potential housekeepers with the most stringent stability values were identified. After that we have applied normalization using the geometric mean of five stably expressed miRNAs (hsa-miR-495-3p; hsa-miR-302d-3p; hsa-miR-3144-3p; hsa-miR-612; hsa-miR-548ar-5p) (Andersen et al., 2004). Quality Control fulfilled all the requirements set by the manufacturer.

Statistical Analysis

All statistical analyses were performed with R (R Core Team, 2019). Paired *t*-tests (baseline vs. 0.5 year) and *t*-tests (baseline vs. 25 + years; 0.5 year vs. 25 + years) were used. We adjusted the *P*-values due to the multiple comparisons therefore False Discovery Rate (FDR) correction was also applied. Heatmap was created in R with the help of "heatmap.2" function from g-plots package (Bolker et al., 2020).

miRNA Target Prediction and Pathway Analysis

After identifying a dozen similarly expressed exomiRs in the active young and senior groups, miRNA—mRNA signaling pathway interaction analysis was performed. Briefly, online available software mirPath v.3 was used for this purpose (Vlachos et al., 2015). Human database of the mirPath v.3 and the TarBase v7.0 were used for mRNA target prediction. *P*-value and MicroT thresholds were kept as default, 0.05 and 0.8, respectively. False discovery rate (FDR) correction was applied.

ExomiRs as Biomarkers of Chronic Disease

The exomiR biomarkers related to certain types of chronic diseases were screened through the EVmiRNA database[1] (Liu et al., 2019). Studies were included if they were original research and evaluated the exomiR levels in a specific disease.

RESULTS

Anthropometric and Physiological Parameters

The study comprised 14 healthy, young, previously inactive and 11 senior trained participants. Healthy, young sedentary individuals completed moderate-intensity regular exercise training three times a week for half a year. Senior subjects have done regular exercise for at least 25 years. Participant parameters are listed in **Table 1**. After half a year of regular exercise, the previously inactive young individuals showed significant improvement in cardiorespiratory fitness (VO_2max), glucose and lipid metabolism. All physiological parameters of senior trained participants were within a normal range. For them, the VO_2max values were far better than the age-matched reference range (**Supplementary Material**).

Validation of Isolated Exosomes

Exosomes were isolated from blood serum samples and obtained from study participants, as described in section "Materials and

[1] http://bioinfo.life.hust.edu.cn/EVmiRNA

Methods." The purified exosomes were characterized using TEM, a gold-standard technique for nanoparticle validation (Kestens et al., 2017). Our TEM analysis showed typical exosomal round morphology (**Figure 2A**). Nanoparticle Tracking Analysis (NTA) allowed us to obtain the size distribution of EVs and estimate particle concentration. The mean size of particles (n = 9) was 143.2 ± 16.43 nm, which falls into the size range of exosomes (Brennan et al., 2020), confirming that the purified EVs contained exosomes (**Figure 2B**; see **Supplementary Material** for further details). Exosome concentrations in our preparations (n = 9) ranged from 1.97×10^{10} to 3.75×10^{10} particles/ml. For details please see the **Supplementary Material section**. Immune-labeled EV sample was evaluated using NTA in FM and LSM modes. The FM:LSM percentage was 83.87% for of CD63. With the CD81-labeled sample, the FM:LSM percentage was 76.95% (**Figure 2C**; please also refer **Supplementary Videos**).

The Expression Patterns of exomiRs After 0.5 Year of Regular Exercise

In order to study regular exercise-related changes in serum exomiR expression, we used amplification-free Nanostring technology. The effect of regular exercise on circulating exomiRs was assessed by comparing baseline (inactive status) and active status (after 0.5 year of regular exercise) expression levels. After analyzing and normalizing raw data, we identified 54 exomiRs (**Figure 3**). Then, we applied filtering criteria to differentiate baseline vs. 0.5 year results ($^*p < 0.05$; #FDR < 0.05; FC > 1.3 or FC < 0.5). Through this analysis, we have observed significant differences in exomiR abundance for several exomiRs (let-7a-5p, $p < 0.05$; let-7g-5p, $p < 0.05$; miR-130a-3p, FDR < 0.05; miR-142-3p, $p < 0.05$; miR-150-5p, $p < 0.05$; miR-15a-5p, $p < 0.05$; miR-15b-5p, FDR < 0.05; miR-199a-3p, FDR < 0.05; miR-199b-3p, FDR < 0.05; miR-223-3p, FDR < 0.05; miR-23a-3p, FDR < 0.05; miR-451a-3p, FDR < 0.05; miR-126-3p, $p < 0.05$; miR-199a-5p, $p < 0.05$; miR-21-5p, FDR < 0.05; miR-25-3p, $p < 0.05$; miR-374a-5p, $p < 0.05$) (for further details please refer to **Supplementary Material**) (ArrayExpress accession number: **E-MTAB-10067**).

ExomiR Overlap of the 0.5 Year- and the 25 + Years of Exercise Groups

Going further we then wished to assess whether exomiRs differentially expressed after 0.5 year of regular exercise were similarly expressed in healthy senior trained participants who engaged in endurance activities for at least 25 years. Therefore, using Nanostring technology we examined the miRNA copy numbers in 11 trained senior individuals focusing on the levels of serum exomiRs. Then, we utilized a hierarchical clustering method to compare circulating exomiR profiles at baseline, after 0.5 year and 25 + years of exercise. As shown by **Figure 3**, the 0.5 year and 25 + years group share an exomiR expression profile that is completely different from that of the sedentary group. In contrast, the 0.5 year and 25 + years active groups showed a highly similar exomiR expression pattern. In addition, 12 exomiRs (let-7a-5p; let-7g-5p; miR-130a-3p; miR-142-3p; miR-150-5p; miR-15a-5p; miR-15b-5p; miR-199a-3p; miR-199b-3p; miR-223-3p; miR-23a-3p, and miR-451a-3p) showed overlap between the two tested signatures (baseline vs. 0.5 year and baseline vs. 25 + years) (**Supplementary Material**). Notably, all 12 exomiRs were significantly down-regulated both in the 0.5 year and the 25 + years trained groups as compared to the sedentary group. Having performed a detailed comparison of the 0.5 year vs. 25 + years trained group profiles, miR-411-5p ($p < 0.05$; FC = 0.879) and miR-144-3p (FC = 1.322)

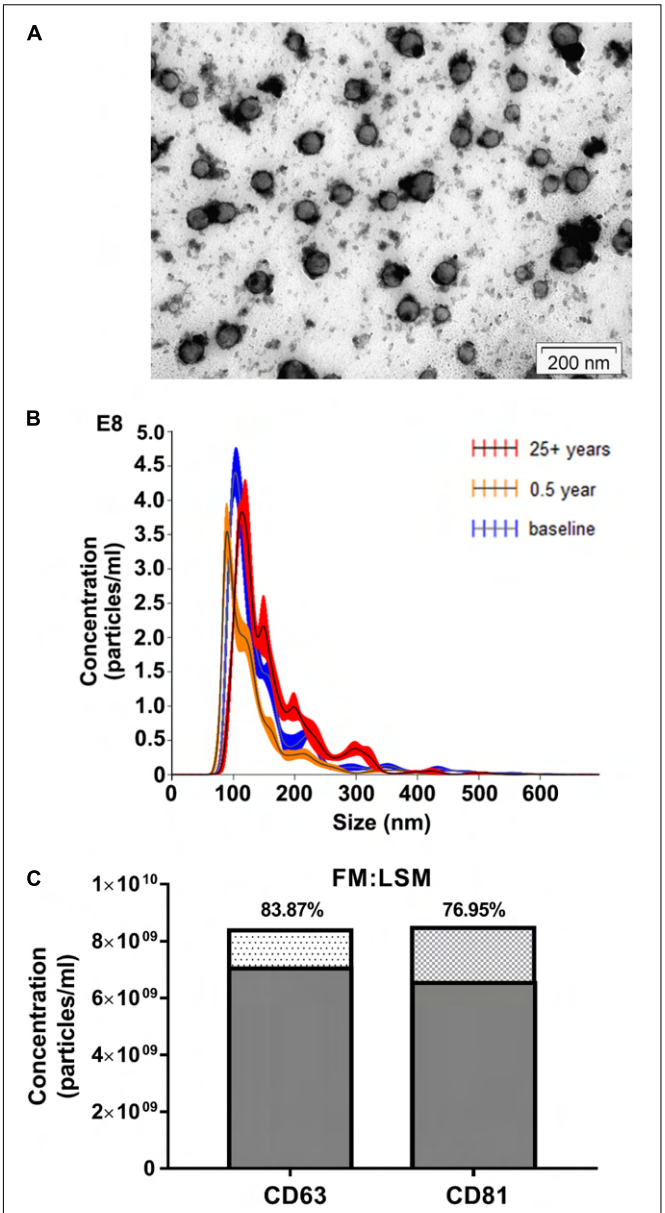

FIGURE 2 | Characterization of exosome-enriched preparations isolated from human serum. **(A)** Transmission electron microscope (TEM) image of exosomes purified from human serum samples (Scale bar: 200 nm). **(B)** Analysis of EV size distribution and concentration in exosome-enriched preparations using a NanoSight NS300 instrument. **(C)** Evaluation of CD63 and CD81 surface expression abundance in exosome-enriched preparations using a NanoSight NS300 instrument.

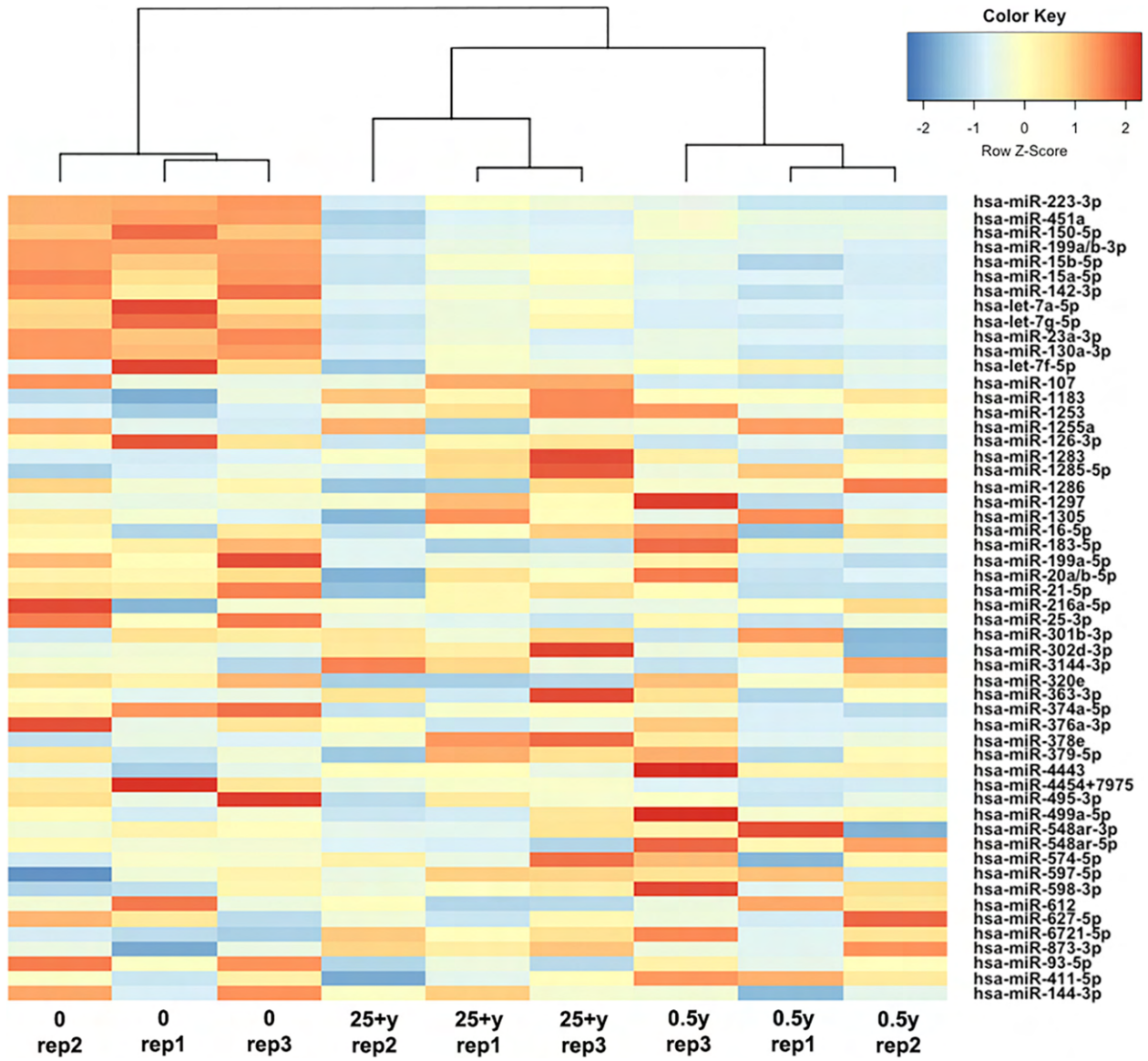

FIGURE 3 | Differential expression of circulating exomiRs. Heatmap with dendrogram shows clustering results for 54 exomiRs at baseline (0), after 0.5 year and 25 + years of regular exercise. Colors represent the level of exomiR expression; red: high expression; blue: low expression.

showed remarkably different expression. Specifically, miR-411-5p was significantly down-regulated, while miR-144-3p was up-regulated in the 25 + years trained group.

Pathway Analysis

To better understand how these exomiRs may contribute to the health benefits of exercise, we examined the mRNA targets of the 12 similarly expressed exomiRs of the 0.5 year and 25 + year trained groups. Then, to reveal the top targeted pathways associated with each exomiRs, KEGG database analysis was used. We found that 38 KEGG signaling pathways were significantly affected by the 12 selected exomiRs (**Figure 4B**). Of these Pathways in cancer (hsa05200) had the largest number of targeted mRNAs (148 genes) (**Figure 4A**). The 148 genes were targeted by four differentially expressed exomiRs (let-7a-5p; let-7g-5p; miR-15b-5p; miR-23a-3p). These findings are consistent with the fact that regular exercise is associated with reduced risk of cancer development. Going further, most exomiRs targeted proteoglycans in cancer pathways (nine exomiRs) and let-7g-5p appeared to affect the most pathways (26 pathways) (for details see **Supplementary Material 2**).

ExomiRs as Biomarkers of Chronic Diseases

exomiR biomarkers related to specific diseases were evaluated using an EVmiRNA database. It is the first concise database

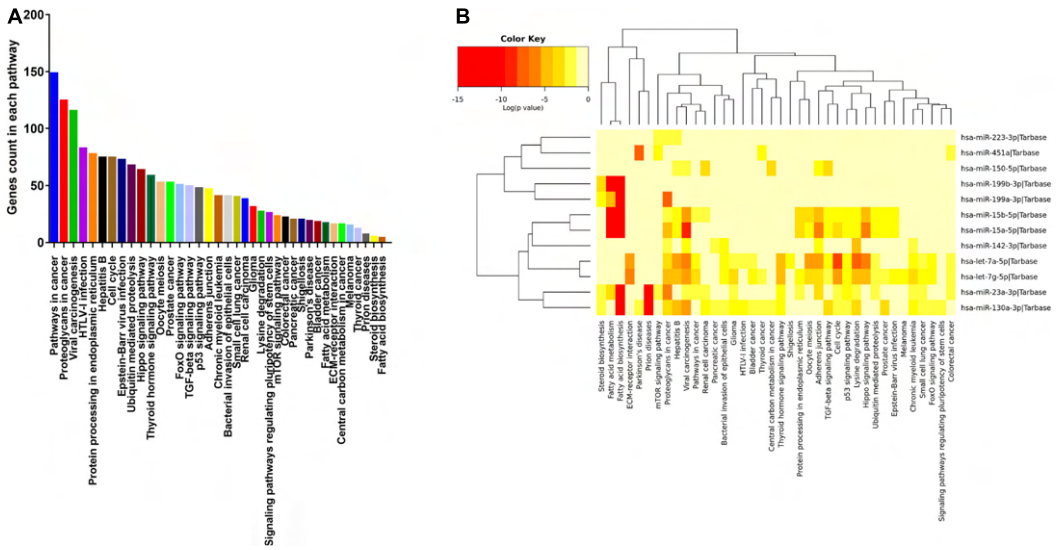

FIGURE 4 | Pathways targeted by the 12 similarly expressed exomiRs in the active young and active senior group. **(A)** Number of genes targeted within each pathways ranked based on high to low. **(B)** The 12 similarly expressed exomiRs in the active young and active senior group regulate 38 signaling pathways in total.

focusing on miRNA expression profiles in EVs (Liu et al., 2019). Several studies have reported the aberrant expression of the 12 identified exomiRs in various chronic diseases (as summarized by **Table 2**).

DISCUSSION

Regular exercise has a beneficial role in preventing a number of chronic diseases. This is primarily due to the fact that regular exercise acts at a systemic level (Anderson and Durstine, 2019). However, a gap remains between identifying in detail the molecular mechanisms induced by exercise and the observed potential benefits in health (Sanford et al., 2020). A better understanding of these biological processes and pathways could allow for the development of targeted exercise intervention and also provide basis for developing exercise-mimetic molecular level interventions (Sanford et al., 2020).

Therefore, in the present study we examined, for the first time, the effect of short-term (0.5 year in this study) and long-term (25 + years in this study) regular exercise on global circulating exomiR profile. To the best of our knowledge, this is the first study to use an amplification-free platform (Nanostring) to determine the miRNA expression profile of exercise-derived exosomes as most studies of the field evaluate specific miRNA species by amplification-based RT-qPCR (Estébanez et al., 2021). The technology applied in the current study is not only amplification-free, but also a sensitive, robust and reproducible state-of-the-art method (Hong et al., 2021). Exosomal miRNA analysis showed a significant number of differentially expressed exosomal miRNAs in all group comparisons. Comparing the miRNAs enriched or depleted in both groups (0.5 year and 25 + years), we have identified 12 similarly regulated exomiRs in the young and senior trained groups as compared to the sedentary group as shown by **Figure 3** (for details please refer to **Supplementary Material**). The KEGG pathway analysis of similarly expressed serum-derived exomiRs confirmed their involvement in pathways related to cancer development affecting TGF-beta, p53 and mTOR signaling. In support of our observations, physical activity has been shown to be associated with lower cancer risks (Li et al., 2020). Moreover, the overall cancer incidence is lower in athletes than in the general population (Sormunen et al., 2014). Recently, a number of studies have indicated that certain exosomal miRNA species (**Table 2**), can be used as biomarkers of cancer and other chronic diseases (references of the studies are listed in **Table 2**).

An elevated expression level of miR-23a has been identified in the serum of various types of human cancer, including breast, gastric, pancreatic, and esophageal squamous cell carcinoma (Wang et al., 2019). Further analysis showed that miR-23a travels as exosomal cargo, and circulating exosomal miR-23a is up-regulated in the serum of early stage colorectal cancer patients (Yong et al., 2013). As a robust cellular regulator of gene expression, miR-23a targets a broad range of mRNA species in cancer cells by directly binding to their three prime untranslated regions (3'-UTR), which in turn suppresses gene expression (Wang et al., 2019). For example, the up-regulation of miR-23a in gastric cancer promotes cell proliferation and inhibits apoptosis (Hua et al., 2018). Zhu et al. (2010) suggested that miR-23a can target IL6R in gastric adenocarcinoma thus encouraging the proliferation of tumor cells. Based on literature data, the inhibition of miR-23a by antisense oligonucleotide inhibits proliferation and promotes the apoptosis of gastric adenocarcinoma cells (Liu et al., 2014). Its biological functions encompass drug resistance, metastasis formation and cancer

TABLE 2 | Summary of exomiR biomarkers related to certain diseases according to EVmiRNA database.

miRNA species	Affected age-related chronic disease, autoimmune condition or infection	References
hsa-let-7a-5p	Colorectal-, renal-, prostate-, ovarian-, breast-, lung-, pancreas-, gastric-, esophageal-, thyriod cancer, Ewing's and Kaposi's sarcoma, glioblastoma, AML and MML; metastasis formation; cell cycle control; inflammation; diabetes; cardiovascular disease; hepatitis B infection	Iliopoulos et al., 2009; Trang et al., 2010; Lee et al., 2011
hsa-let-7g-5p	Breast-, esophageal-, lung cancer, glioblastoma, AML and CML; graft-vs.-host disease; inflammation; autoimmune thyroid disease; cell cycle control; diabetes; cardiovascular disease; metabolic syndrome; hepatitis B and influenza A infection	Arora et al., 2011; Wang et al., 2013; Biamonte et al., 2019
hsa-miR-130a-3p	Lung-, liver-, prostate-, ovarian-, breast-, cervical-, nasopharyngeal-, prostate cancer, myeloma, CML and glioblastoma; cardiovascular disease; fibrosis; inflammation; autophagy; diabetes; Crohn's disease; hepatitis C infection; cardiac arrhythmia; renal GBM disease; UV damage	Osbourne et al., 2014; Huang et al., 2015; Eichelmann et al., 2018
hsa-miR-142-3p	Liver-, lung-, colorectal-, breast-, cervical-, esophageal cancer, osteosarcoma, prolactinoma, ALL, AML, CLL and MALT lymphoma; graft rejection; Hashimoto's thyroiditis; multiple sclerosis; cardiovascular disease; inflammation; rotavirus infection; Alzheimer's disease; fibrosis	Ma et al., 2016; Sukma Dewi et al., 2017; Wang et al., 2017
hsa-miR-150-5p	Colorectal-, lung-, liver-, prostate-, cervical-, pancreas-, breast-, ovarian-, esophageal cancer, osteosarcoma, glioblastoma, melanoma; Burkitt lymphoma, ALL and MML; inflammation; cardiovascular disease; fibrosis; irritable bowel syndrome; myasthenia; diabetes; SLE; psoriasis	Roderburg et al., 2013; Qu et al., 2014; Yu et al., 2015
hsa-miR-15a-5p	Gastric-, colorectal-, lung-, breast-, liver-, ovarian-, prostate cancer, melanoma, osteosarcoma, neuroblastoma, pheochromocytoma, AML, CLL and multiple myeloma; inflammation; cell cycle control; apoptosis induction; autophagy; multiple sclerosis; hepatitis B infection; fibrosis; diabetes	Xia et al., 2008; Bandi et al., 2009; Sun et al., 2013
hsa-miR-15b-5p	Liver-, gastric-, lung-, liver-, pancreas-, ovarian-, squamous cell cancer, glioblastoma, melanoma, CLL and thymoma; apoptosis induction; metastasis formation; angiogenesis; fibrosis; bipolar disorder; insulin-resistance; skin photoaging; multiple sclerosis; diabetes	Zhang et al., 2015; Li et al., 2016; MacLean et al., 2016
hsa-miR-199a/b-3p	Liver-, gastric-, lung-, renal cell-, ovarian-, pancreas-, colorectal, liver-, breast-, testicular germ cell-, thyroid-, colorectal cancer, endometriosis, glioblastoma, CLL, melanoma, chondrosarcoma and osteosarcoma; osteoarthritis; COPD; autophagy; angiogenesis; HCV infection; inflammation	Li et al., 2015
hsa-miR-223-3p	Ovarian-, gastric-, colorectal-, prostate-, pancreas-, lung-, liver cancer, CLL, AML, ALL, glioblastoma and osteosarcoma; metastasis formation graft rejection; inflammation; osteoarthritis; lipid metabolism; obesity; rheumatoid arthritis; psoriasis; cardiovascular disease; diabetes; COPD; Alzheimer's disease	Wong et al., 2008; Filková et al., 2014; Lunavat et al., 2015
hsa-miR-23a-3p	Gastric-, colorectal-, esophageal-, liver-, renal-, breast-, prostate-, pancreas-, lung-, laryngeal-, lung cancer, CML, AML, Burkitt lymhoma, melanoma, osteosarcoma and endometriosis; retinal degeneration; UV damage; apoptosis induction; autophagy; progeria; osteoarthritis; obesity	Wang et al., 2014; Yang et al., 2014; Zheng et al., 2014
hsa-miR-451a	Lung-, colorectal-, breast-, skin-, bladder-, gastric-, renal-, esophageal-, thyroid-, liver cancer, T-ALL, AML, CML, multiple myeloma, endometriosis, prolactinoma, osteosarcoma and glioblastoma; drug transporters; cell cycle; metastasis formation; angiogenesis; rheumatoid arthritis; cardiomyopathy	Lopotová et al., 2011; Song et al., 2014; Riquelme et al., 2016

progression, suggesting its potential role as an emerging targetable entity in cancer treatment (Wang et al., 2019). Of note, miR23a shows natural correlation with age, partly explaining the correlation of the above cancers with senior age (Rani et al., 2017).

Exosomal miR-451a was highly expressed in non-small-cell lung carcinoma patients (NSCLC) compared to healthy individuals. This miRNA was strongly associated with tumor progression, recurrence, and poor prognosis in NSCLC patients. According to literature data, it may serve as a potential predictive biomarker for NSCLC (Kanaoka et al., 2018). Zhu et al. (2014) also found that miR-451 levels were consistently elevated in the plasma of patients with gastric cancer providing high diagnostic accuracy for early stage gastric adenocarcinoma. To date, numerous genes have been confirmed as actual targets of miR-451, covering multiple biological signaling pathways including apoptosis, cell invasion and migration, cell proliferation and angiogenesis. Taken together, an accumulating body of evidence indicates that miR-451 is a potential biomarker for cancer diagnosis and prognosis, possibly a treatment target in combination with established drugs (Bai and Wu, 2019).

Exosomal miR-223-3p level in the serum of patients with breast cancer was significantly higher in comparison with healthy controls (Yoshikawa et al., 2018). Its expression was tightly associated with the malignancy of breast cancer, suggesting that exosomal miR-223-3p might be a useful biomarker for the early detection of invasive breast cancer. Of further note, miR223-3p also shows correlation with the advance of age, and these cancers are known to emerge at senior age (Rani et al., 2017).

Elevated expression of miR-150-5p has been shown in breast cancer (BC), described as a good prognostic biomarker for patients with HER2-positive BC (Ozawa et al., 2020).

Exercise was shown to modulate the expression of several miRNA species that in turn are protective against cancer (Li et al., 2020; Pulliero et al., 2020). In our report we demonstrate this modulation observed after both short-term (0.5 year) and long-term (25 + years) regular exercise since our miR-23a, 451a, 223-3p, and miR-150-5p were all suppressed emphasizing the role of exercise in the prevention of several cancer entities. Nevertheless, data on exercise-derived exosomal miRNA species in modulating cancer prevention is still in its infancy (Pulliero et al., 2020). Therefore, elaborate research effort

is required to reveal the role of exosomal miRNA species in this particular field.

The deregulation of miRNA species described in conjunction with other chronic diseases has also been observed in our study. According to our results, regular exercise altered the levels of miR-15a and miR-142 in the opposite direction as observed in patients with diabetes and neurodegenerative disease, supporting that regular exercise (either short- or long-term) reduces the risk of developing such chronic diseases. In more detail, miR-15a was shown to be elevated in the plasma of diabetic patients also showing correlation with disease severity (Kamalden et al., 2017). Xiong et al. (2020) demonstrated that miR-15a-3p is up-regulated in exosomes of diabetic patients, and impairs wound healing. When miR-15a-3p was knocked down and such exosomes were utilized later on, their negative effects on the metabolism and wound healing in particular were partially reversed both *in vitro* and *in vivo* (Xiong et al., 2020).

Barbagallo et al. (2020) isolated exosomal miRNA from the serum of 30 Parkinson disease (PD) patients and compared it with that of 30 healthy controls. The expression levels of ex-miR-23a; ex-miR-142-3p were significantly elevated in the serum of PD patients, unlike in our study where miR-142 showed a decrease in expression compared to healthy, but sedentary state (Barbagallo et al., 2020). Previous studies have also reported the benefits of physical exercise in improving the symptoms in individuals with PD (Da Silva et al., 2021). Taken together these reports suggest the protective role of miR-142-3p in PD, though further studies are required.

Taken together, the miRNAs that we have observed to be modulated by both short and long-term exercise are mostly involved in cancer prevention mechanisms including tumor suppression (miR-223-3p; miR-451a; miR-15a/b-5p; let-7a/7g-5p) (Wang et al., 2016; Gao et al., 2011), aging (miR-223-3p; miR-451a; miR-15a/b-5p; miR-23a-3p) (Mercken et al., 2013; Teteloshvili et al., 2015), induction of apoptosis (miR-150-5p; miR-15a/b-5p; miR-130a-3p) (Xu et al., 2014; Wang et al., 2015) and reduction of inflammation (miR-199a/b-3p; miR-142-3p) (Cai et al., 2012). In addition, the inverse deregulation of miR-15a characteristic to diabetes, and miR-142 featured in Parkinson's disease has also been recorded in our study. Potential applications target these miRNA species to prevent the development of cancer, diabetes and neurodegenerative disease or to be used as adjuvant therapy in established diseases. However, to date no such experiments exist supporting that exercise-derived exomiRs could prevent or treat chronic diseases.

So, beyond the utility of serum-derived exomiRs as potential biomarkers of physical fitness or chronic diseases, our work suggests their key role in essential pathways, potentially preventing the development of multiple chronic diseases. In the future the evaluation of physical activity level may be used to predict the risk of developing various chronic diseases. Furthermore, this study is important as a starting point to understand the global pattern of regular exercise-related exomiRs and their target pathways in health and disease. However, the present study must be seen as an exploratory study. Our current pilot-study is limited by the number of biological replicates. Therefore, further studies are required with larger sample size to comprehensively examine the effect of regular exercise on circulating exomiR profile.

CONCLUSION

Both short- (0.5 year) and long-term (25 + years) regular exercise significantly alters the serum miRNA profile in healthy individuals, potentially reducing the risk of a number of malignant, metabolic and neurodegenerative diseases. Combining an amplification-free miRNome profiling platform and bioinformatics analysis, our study revealed that numerous disease-associated exomiRs show differential expression toward a more beneficial pattern. Physiological relevance is also supported by the large number of genes targeted by these miRNAs. Future work lies ahead in determining the exact mechanism of action and the potential use of exomiRs as therapeutic tools to efficiently prevent or successfully treat age-related diseases.

DATA AVAILABILITY STATEMENT

The datasets presented in this study can be found in online repositories. The names of the repository/repositories and accession number(s) can be found below: EBI ArrayExpress, accession no: E-MTAB-10067.

ETHICS STATEMENT

The studies involving human participants were reviewed and approved by the Regional and Local Ethics Committee of Clinical Centre, University of Pecs (ref. no.: 6439/2016 and 7755/2019). The patients/participants provided their written informed consent to participate in this study.

AUTHOR CONTRIBUTIONS

KG, KK, and MW designed the study. KG, ZA, KB, and AdG recruited participants, collected samples and performed the experiments. RH and AtG analyzed the data. KG and ZA interpreted data and drafted the manuscript. JP, MW, and KK critically revised the manuscript. All authors contributed to the article and approved the submitted version.

FUNDING

The project was supported by the ÚNKP-19-3-I 2019/2020 new national excellence program of the ministry for innovation and technology to KG and KB. Scientific research support was provided by GINOP -2.3.2.-15-2016-00047 to MW. The Janos Bolyai Scholarship of the Hungarian Academy of Sciences and Bolyai + 2019/2020 (UNKP-19-4 or 2019/2020 new national excellence program of the ministry of human capacities) also

supported KK. JP was supported by the EFOP-3.6.1-16-2016-00004; 2020-4.1.1/TKP2020 'Biomedical Engineering', and GINOP-2.3.2.-15-2016-00022. The publication process has been supported by PTE Internal grant PoC to KK.

ACKNOWLEDGMENTS

We wish to thank Prof. Hajnalka Abraham MD, Ph.D. (Central Electron Microscope Laboratory, University of Pecs, Hungary) for the technical aid in taking transmission electron microscope images. The research was performed in collaboration with the Genomics and Bioinformatics Core Facility at the Szentágothai Research Center of the University of Pecs. We are also grateful for Prof. Mary Keen (Faculty of Pharmacy, University of Birmingham, United Kingdom) having performed careful and critical revision on key parts of the manuscript as a native English speaker.

SUPPLEMENTARY MATERIAL

The Supplementary Material for this article can be found online at: https://www.frontiersin.org/articles/10.3389/fphys.2021.658218/full#supplementary-material

REFERENCES

Andersen, C. L., Jensen, J. L., and Ørntoft, T. F. (2004). Normalization of real-time quantitative reverse transcription-PCR data: A model-based variance estimation approach to identify genes suited for normalization, applied to bladder and colon cancer data sets. *Cancer Res.* 64, 5245–5250. doi: 10.1158/0008-5472.CAN-04-0496

Anderson, E., and Durstine, J. L. (2019). Physical activity, exercise, and chronic diseases: A brief review. *Sports Med. Health Sci.* 1, 3–10. doi: 10.1016/j.smhs.2019.08.006

Andreu, Z., Rivas, E., Sanguino-Pascual, A., Lamana, A., Marazuela, M., González-Alvaro, I., et al. (2016). Comparative analysis of EV isolation procedures for miRNAs detection in serum samples. *J. Extracell. Vesicl.* 5, 1–10. doi: 10.3402/jev.v5.31655

Annibalini, G., Contarelli, S., Lucertini, F., Guescini, M., Maggio, S., Ceccaroli, P., et al. (2019). Muscle and systemic molecular responses to a single flywheel based iso-inertial training session in resistance-trained men. *Front. Physiol.* 10:1–10. doi: 10.3389/fphys.2019.00554

Arora, H., Qureshi, R., Jin, S., Park, A. K., and Park, W. Y. (2011). MiR-9 and let-7g enhance the sensitivity to ionizing radiation by suppression of NFκB1. *Exp. Mol. Med.* 43, 298–304. doi: 10.3858/emm.2011.43.5.031

Bai, H., and Wu, S. (2019). Mir-451: A novel biomarker and potential therapeutic target for cancer. *OncoTargets Ther.* 12, 11069–11082. doi: 10.2147/OTT.S230963

Bandi, N., Zbinden, S., Gugger, M., Arnold, M., Kocher, V., Hasan, L., et al. (2009). miR-15a and miR-16 are implicated in cell cycle regulation in a Rb-dependent manner and are frequently deleted or down-regulated in non-small cell lung cancer. *Cancer Res.* 2009:4277. doi: 10.1158/0008-5472.CAN-08-4277

Banfai, K., Garai, K., Ernszt, D., Pongracz, J. E., and Kvell, K. (2019). Transgenic exosomes for thymus regeneration. *Front. Immunol.* 10:1–9. doi: 10.3389/fimmu.2019.00862

Barbagallo, C., Mostile, G., Baglieri, G., Giunta, F., Luca, A., Raciti, L., et al. (2020). Specific Signatures of Serum miRNAs as Potential Biomarkers to Discriminate Clinically Similar Neurodegenerative and Vascular-Related Diseases. *Cell. Mol. Neurobiol.* 40, 531–546. doi: 10.1007/s10571-019-00751-y

Bertoldi, K., Cechinel, L. R., Schallenberger, B., Corssac, G. B., Davies, S., Guerreiro, I. C. K., et al. (2018). Circulating extracellular vesicles in the aging process: impact of aerobic exercise. *Mol. Cell. Biochem.* 440, 115–125. doi: 10.1007/s11010-017-3160-4

Biamonte, F., Santamaria, G., Sacco, A., Perrone, F. M., Di Cello, A., Battaglia, A. M., et al. (2019). MicroRNA let-7g acts as tumor suppressor and predictive biomarker for chemoresistance in human epithelial ovarian cancer. *Sci. Rep.* 9:5668. doi: 10.1038/s41598-019-42221-x

Bolker, B., Huber, W., Lumley, T., Maechler, M., Magnusson, A., and Moeller, S. (2020). *Package 'gplots' R topics documented*. Vienna: R Core Team.

Brahmer, A., Neuberger, E., Esch-Heisser, L., Haller, N., Jorgensen, M. M., Baek, R., et al. (2019). Platelets, endothelial cells and leukocytes contribute to the exercise-triggered release of extracellular vesicles into the circulation. *J. Extracell. Vesicl.* 8:1615820. doi: 10.1080/20013078.2019.1615820

Brennan, K., Martin, K., FitzGerald, S. P., O'Sullivan, J., Wu, Y., Blanco, A., et al. (2020). A comparison of methods for the isolation and separation of extracellular vesicles from protein and lipid particles in human serum. *Sci. Rep.* 10, 1–13. doi: 10.1038/s41598-020-57497-7

Cai, Z. G., Zhang, S. M., Zhang, Y., Zhou, Y. Y., Wu, H. B., and Xu, X. P. (2012). MicroRNAs are dynamically regulated and play an important role in LPS-induced lung injury. *Canad. J. Physiol. Pharmacol.* 90, 37–43. doi: 10.1139/Y11-095

Craig, C. L., Marshall, A. L., Sjöström, M., Bauman, A. E., Booth, M. L., Ainsworth, B. E., et al. (2003). International physical activity questionnaire: 12-Country reliability and validity. *Med. Sci. Sports Exerc.* 35, 1381–1395. doi: 10.1249/01.MSS.0000078924.61453.FB

D'souza, R. F., Woodhead, J. S. T., Zeng, N., Blenkiron, C., Merry, T. L., Cameron-Smith, D., et al. (2018). Circulatory exosomal miRNA following intense exercise is unrelated to muscle and plasma miRNA abundances. *Am. J. Physiol. Endocrinol. Metabol.* 315, E723–E733. doi: 10.1152/ajpendo.00138.2018

Da Silva, F., Rode, M., Vietta, G., Iop, R., Creczynski-Pasa, T., Martin, A., et al. (2021). Expression levels of specific microRNAs are increased after exercise and are associated with cognitive improvement in Parkinson's disease. *Mol. Med. Rep.* 24, 1–10. doi: 10.3892/mmr.2021.12257

Eichelmann, A. K., Matuszcak, C., Lindner, K., Haier, J., Hussey, D. J., and Hummel, R. (2018). Complex role of miR-130a-3p and miR-148a-3p balance on drug resistance and tumor biology in esophageal squamous cell carcinoma. *Sci. Rep.* 8:17553. doi: 10.1038/s41598-018-35799-1

Estébanez, B., Jiménez-Pavón, D., Huang, C. J., Cuevas, M. J., and González-Gallego, J. (2021). Effects of exercise on exosome release and cargo in in vivo and ex vivo models: A systematic review. *J. Cell. Physiol.* 236, 3336–3353. doi: 10.1002/jcp.30094

Filková, M., Aradi, B., Šenolt, L., Ospelt, C., Vettori, S., Mann, H., et al. (2014). Association of circulating miR-223 and miR-16 with disease activity in patients with early rheumatoid arthritis. *Ann. Rheumat. Dis.* 2014:202815. doi: 10.1136/annrheumdis-2012-202815

Frühbeis, C., Helmig, S., Tug, S., Simon, P., and Krämer-Albers, E. M. (2015). Physical exercise induces rapid release of small extracellular vesicles into the circulation. *J. Extracell. Vesicl.* 4, 1–11. doi: 10.3402/jev.v4.28239

Gao, S. M., Xing, C. Y., Chen, C. Q., Lin, S. S., Dong, P. H., and Yu, F. J. (2011). MiR-15a and miR-16-1 inhibit the proliferation of leukemic cells by down-regulating WT1 protein level. *J. Exp. Clin. Cancer Res.* 30, 1–9. doi: 10.1186/1756-9966-30-110

Garai, K., Adam, Z., Herczeg, R., Katai, E., Nagy, T., Pal, S., et al. (2019). Artificial Neural Network Correlation and Biostatistics Evaluation of Physiological and Molecular Parameters in Healthy Young Individuals Performing Regular Exercise. *Front. Physiol.* 10:01242. doi: 10.3389/fphys.2019.01242

Gardiner, C., Ferreira, Y. J., Dragovic, R. A., Redman, C. W. G., and Sargent, I. L. (2013). Extracellular vesicle sizing and enumeration by nanoparticle tracking analysis. *J. Extracell. Vesicl.* 2:19671. doi: 10.3402/jev.v2i0.19671

Hong, L. Z., Zhou, L., Zou, R., Khoo, C. M., Chew, A. L. S., Chin, C. L., et al. (2021). Systematic evaluation of multiple qPCR platforms, NanoString and miRNA-Seq for microRNA biomarker discovery in human biofluids. *Sci. Rep.* 11, 1–11. doi: 10.1038/s41598-021-83365-z

Hou, Z., Qin, X., Hu, Y., Zhang, X., Li, G., Wu, J., et al. (2019). Longterm Exercise-Derived Exosomal miR-342-5p: A Novel Exerkine for Cardioprotection. *Circulat. Res.* 124, 1386–1400. doi: 10.1161/CIRCRESAHA.118.314635

Hua, K., Chen, Y. T., Chen, C. F., Tang, Y. S., Huang, T. T., Lin, Y. C., et al. (2018). Microrna-23a/27a/24-2 cluster promotes gastric cancer cell proliferation synergistically. *Oncol. Lett.* 16, 2319–2325. doi: 10.3892/ol.2018.8924

Huang, J. Y., Chou, S. F., Lee, J. W., Chen, H. L., Chen, C. M., Tao, M. H., et al. (2015). MicroRNA-130a can inhibit hepatitis B virus replication via targeting PGC1α and PPARγ. *RNA* 2015, 114. doi: 10.1261/rna.048744.114

Iliopoulos, D., Hirsch, H. A., and Struhl, K. (2009). An Epigenetic Switch Involving NF-κB, Lin28, Let-7 MicroRNA, and IL6 Links Inflammation to Cell Transformation. *Cell* 2009:014. doi: 10.1016/j.cell.2009.10.014

Kamalden, T. A., Macgregor-Das, A. M., Kannan, S. M., Dunkerly-Eyring, B., Khaliddin, N., Xu, Z., et al. (2017). Exosomal MicroRNA-15a Transfer from the Pancreas Augments Diabetic Complications by Inducing Oxidative Stress. *Antioxid. Redox Signal.* 27, 913–930. doi: 10.1089/ars.2016.6844

Kanaoka, R., Iinuma, H., Dejima, H., Sakai, T., Uehara, H., Matsutani, N., et al. (2018). Usefulness of Plasma Exosomal MicroRNA-451a as a Noninvasive Biomarker for Early Prediction of Recurrence and Prognosis of Non-Small Cell Lung Cancer. *Oncology* 94, 311–323. doi: 10.1159/000487006

Kestens, V., Bozatzidis, V., De Temmerman, P. J., Ramaye, Y., and Roebben, G. (2017). Validation of a particle tracking analysis method for the size determination of nano- and microparticles. *J. Nanopart. Res.* 19:271. doi: 10.1007/s11051-017-3966-8

Kowal, J., Tkach, M., and Théry, C. (2014). Biogenesis and secretion of exosomes. *Curr. Opin. Cell Biol.* 29, 116–125. doi: 10.1016/j.ceb.2014.05.004

Lee, S. T., Chu, K., Oh, H. J., Im, W. S., Lim, J. Y., Kim, S. K., et al. (2011). Let-7 microRNA inhibits the proliferation of human glioblastoma cells. *J. Neuro Oncol.* 102, 19–24. doi: 10.1007/s11060-010-0286-6

Li, F., Bai, M., Xu, J., Zhu, L., Liu, C., and Duan, R. (2020). Long-Term Exercise Alters the Profiles of Circulating Micro-RNAs in the Plasma of Young Women. *Front. Physiol.* 11:1–10. doi: 10.3389/fphys.2020.00372

Li, J., Chen, Y., Guo, X., Zhou, L., Jia, Z., Tang, Y., et al. (2016). Inhibition of miR-15b decreases cell migration and metastasis in colorectal cancer. *Tumor Biol.* 2016, 8765–8773. doi: 10.1007/s13277-015-4396-9

Li, S. Q., Wang, Z. H., Mi, X. G., Liu, L., and Tan, Y. (2015). MiR-199a/b-3p suppresses migration and invasion of breast cancer cells by downregulating PAK4/MEK/ERK signaling pathway. *IUBMB Life* 2015:1433. doi: 10.1002/iub.1433

Liu, T., Zhang, Q., Zhang, J., Li, C., Miao, Y. R., Lei, Q., et al. (2019). EVmiRNA: A database of miRNA profiling in extracellular vesicles. *Nucleic Acids Res.* 47, D89–D93. doi: 10.1093/nar/gky985

Liu, X., Liu, Q., Fan, Y., Wang, S., Liu, X., Zhu, L., et al. (2014). Downregulation of PPP2R5E expression by miR-23a suppresses apoptosis to facilitate the growth of gastric cancer cells. *FEBS Lett.* 588, 3160–3169. doi: 10.1016/j.febslet.2014.05.068

Lopotová, T., Žáèková, M., Klamová, H., and Moravcová, J. (2011). MicroRNA-451 in chronic myeloid leukemia: MiR-451-BCR-ABL regulatory loop? *Leukemia Res.* 2011:029. doi: 10.1016/j.leukres.2011.03.029

Lunavat, T. R., Cheng, L., Kim, D. K., Bhadury, J., Jang, S. C., Lässer, C., et al. (2015). Small RNA deep sequencing discriminates subsets of extracellular vesicles released by melanoma cells – Evidence of unique microRNA cargos. *RNA Biol.* 2015:1056975. doi: 10.1080/15476286.2015.1056975

Ma, Z., Liu, T., Huang, W., Liu, H., Zhang, H. M., Li, Q., et al. (2016). MicroRNA regulatory pathway analysis identifies miR-142-5p as a negative regulator of TGF-ß pathway via targeting SMAD3. *Oncotarget* 2016:12229. doi: 10.18632/oncotarget.12229

MacLean, J. A., King, M. L., Okuda, H., and Hayashi, K. (2016). WNT7A regulation by miR-15b in ovarian cancer. *PLoS One* 2016:0156109. doi: 10.1371/journal.pone.0156109

Mercken, E. M., Majounie, E., Ding, J., Guo, R., Kim, J., Bernier, M., et al. (2013). Age-associated miRNA alterations in skeletal muscle from rhesus monkeys reversed by caloric restriction. *Aging* 5, 692–703. doi: 10.18632/aging.100598

Muroya, S., Ogasawara, H., and Hojito, M. (2015). Grazing affects exosomal Circulating microRNAs in cattle. *PLoS One* 10:1–19. doi: 10.1371/journal.pone.0136475

Nederveen, J. P., Warnier, G., Di Carlo, A., Nilsson, M. I., and Tarnopolsky, M. A. (2021). Extracellular Vesicles and Exosomes: Insights From Exercise Science. *Front. Physiol.* 11:604274. doi: 10.3389/fphys.2020.604274

Osbourne, A., Calway, T., Broman, M., McSharry, S., Earley, J., and Kim, G. H. (2014). Downregulation of connexin43 by microRNA-130a in cardiomyocytes results in cardiac arrhythmias. *J. Mol. Cell. Cardiol.* 2014:024. doi: 10.1016/j.yjmcc.2014.04.024

Ozawa, P. M. M., Vieira, E., Lemos, D. S., Souza, I. L. M., Zanata, S. M., Pankievicz, V. C., et al. (2020). Identification of miRNAs enriched in extracellular vesicles derived from serum samples of breast cancer patients. *Biomolecules* 10:biom10010150. doi: 10.3390/biom10010150

Pulliero, A., You, M., Chaluvally-Raghavan, P., Marengo, B., Domenicotti, C., Banelli, B., et al. (2020). Anticancer effect of physical activity is mediated by modulation of extracellular microRNA in blood. *Oncotarget* 11, 2106–2119. doi: 10.18632/oncotarget.27609

Qu, Z., Li, W., and Fu, B. (2014). MicroRNAs in autoimmune diseases. *BioMed Res. Int.* 2014:527895. doi: 10.1155/2014/527895

R Core Team (2019). *A Language and Environment for Statistical Computing*. Vienna: R Foundation for Statistical Computing.

Rani, A., O'Shea, A., Ianov, L., Cohen, R. A., Woods, A. J., and Foster, T. C. (2017). miRNA in circulating microvesicles as biomarkers for age-related cognitive decline. *Front. Aging Neurosci.* 9:1–10. doi: 10.3389/fnagi.2017.00323

Riquelme, I., Tapia, O., Leal, P., Sandoval, A., Varga, M. G., Letelier, P., et al. (2016). miR-101-2, miR-125b-2 and miR-451a act as potential tumor suppressors in gastric cancer through regulation of the PI3K/AKT/mTOR pathway. *Cell. Oncol.* 39, 23–33. doi: 10.1007/s13402-015-0247-3

Roderburg, C., Luedde, M., Vargas Cardenas, D., Vucur, M., Scholten, D., Frey, N., et al. (2013). Circulating MicroRNA-150 Serum Levels Predict Survival in Patients with Critical Illness and Sepsis. *PLoS One* 2013:0054612. doi: 10.1371/journal.pone.0054612

Sanford, J. A., Nogiec, C. D., Lindholm, M. E., Adkins, J. N., Amar, D., Dasari, S., et al. (2020). Molecular Transducers of Physical Activity Consortium (MoTrPAC): Mapping the Dynamic Responses to Exercise. *Cell* 181, 1464–1474. doi: 10.1016/j.cell.2020.06.004

Song, L., Su, M., Wang, S., Zou, Y., Wang, X., Wang, Y., et al. (2014). MiR-451 is decreased in hypertrophic cardiomyopathy and regulates autophagy by targeting TSC1. *J. Cell. Mol. Med.* 2014:12380. doi: 10.1111/jcmm.12380

Sormunen, J., Bäckmand, H. M., Sarna, S., Kujala, U. M., Kaprio, J., Dyba, T., et al. (2014). Lifetime physical activity and cancer incidence-A cohort study of male former elite athletes in Finland. *J. Sci. Med. Sport* 17, 479–484. doi: 10.1016/j.jsams.2013.10.239

Sukma Dewi, I., Hollander, Z., Lam, K. K., McManus, J. W., Tebbutt, S. J., Ng, R. T., et al. (2017). Association of serum MiR-142-3p and MiR-101-3p levels with acute cellular rejection after heart transplantation. *PLoS One* 2017:0170842. doi: 10.1371/journal.pone.0170842

Sun, C. Y., She, X. M., Qin, Y., Chu, Z. B., Chen, L., Ai, L. S., et al. (2013). miR-15a and miR-16 affect the angiogenesis of multiple myeloma by targeting VEGF. *Carcinogenesis* 2013:bgs333. doi: 10.1093/carcin/bgs333

Teteloshvili, N., Kluiver, J., Van Der Geest, K. S. M., Van Der Lei, R. J., Jellema, P., Pawelec, G., et al. (2015). Age-associated differences in MiRNA signatures are restricted to CD45RO negative T cells and are associated with changes in the cellular composition, activation and cellular ageing. *PLoS One* 10:1–13. doi: 10.1371/journal.pone.0137556

Thane, K. E., Davis, A. M., and Hoffman, A. M. (2019). Improved methods for fluorescent labeling and detection of single extracellular vesicles using nanoparticle tracking analysis. *Sci. Rep.* 9, 1–13. doi: 10.1038/s41598-019-48181-6

Trang, P., Medina, P. P., Wiggins, J. F., Ruffino, L., Kelnar, K., Omotola, M., et al. (2010). Regression of murine lung tumors by the let-7 microRNA. *Oncogene* 2010:445. doi: 10.1038/onc.2009.445

Vlachos, I. S., Zagganas, K., Paraskevopoulou, M. D., Georgakilas, G., Karagkouni, D., Vergoulis, T., et al. (2015). DIANA-miRPath v3.0: Deciphering microRNA function with experimental support. *Nucleic Acids Res.* 43, W460–W466. doi: 10.1093/nar/gkv403

Wang, F., Ren, X., and Zhang, X. (2015). Role of microRNA-150 in solid tumors (review). *Oncol. Lett.* 10, 11–16. doi: 10.3892/ol.2015.3170

Wang, J., Zhao, X., Shi, J., Pan, Y., Chen, Q., Leng, P., et al. (2016). MIR 451 suppresses bladder cancer cell migration and invasion via

directly targeting c-Myc. *Oncol. Rep.* 36, 2049–2058. doi: 10.3892/or.2016.5040

Wang, N., Tan, H. Y., Feng, Y. G., Zhang, C., Chen, F., and Feng, Y. (2019). microRNA-23a in human cancer: Its roles, mechanisms and therapeutic relevance. *Cancers* 11, 1–22. doi: 10.3390/cancers11010007

Wang, W. L., Yang, C., Han, X. L., Wang, R., Huang, Y., Zi, Y. M., et al. (2014). MicroRNA-23a expression in paraffin-embedded specimen correlates with overall survival of diffuse large B-cell lymphoma. *Med. Oncol.* 31:919. doi: 10.1007/s12032-014-0919-2

Wang, Y. T., Tsai, P. C., Liao, Y. C., Hsu, C. Y., and Juo, S. H. H. (2013). Circulating microRNAs have a sex-specific association with metabolic syndrome. *J. Biomed. Sci.* 2013:72. doi: 10.1186/1423-0127-20-72

Wang, Z., Liu, Z., Fang, X., and Yang, H. (2017). MiR-142-5p Suppresses Tumorigenesis by Targeting PIK3CA in Non-Small Cell Lung Cancer. *Cell. Physiol. Biochem.* 2017:000484459. doi: 10.1159/000484459

Wong, Q. W. L., Lung, R. W. M., Law, P. T. Y., Lai, P. B. S., Chan, K. Y. Y., To, K. F., et al. (2008). MicroRNA-223 Is Commonly Repressed in Hepatocellular Carcinoma and Potentiates Expression of Stathmin1. *Gastroenterology* 2008:003. doi: 10.1053/j.gastro.2008.04.003

Xia, L., Zhang, D., Du, R., Pan, Y., Zhao, L., Sun, S., et al. (2008). miR-15b and miR-16 modulate multidrug resistance by targeting BCL2 in human gastric cancer cells. *Int. J. Cancer* 2008:23501. doi: 10.1002/ijc.23501

Xiong, Y., Chen, L., Yu, T., Yan, C., Zhou, W., Cao, F., et al. (2020). Inhibition of circulating exosomal microRNA-15a-3p accelerates diabetic wound repair. *Aging* 12, 8968–8986. doi: 10.18632/aging.103143

Xu, Q., Meng, S., Liu, B., Li, M. Q., Li, Y., Fang, L., et al. (2014). MicroRNA-130a regulates autophagy of endothelial progenitor cells through Runx3. *Clin. Exp. Pharmacol. Physiol.* 41, 351–357. doi: 10.1111/1440-1681.12227

Yang, Z., Chen, H., Si, H., Li, X., Ding, X., Sheng, Q., et al. (2014). Serum miR-23a, a potential biomarker for diagnosis of pre-diabetes and type 2 diabetes. *Acta Diabetol.* 51, 823–831. doi: 10.1007/s00592-014-0617-8

Yin, X., Zhao, Y., Zheng, Y. L., Wang, J. Z., Li, W., Lu, Q. J., et al. (2019). Time-Course Responses of Muscle-Specific MicroRNAs Following Acute Uphill or Downhill Exercise in Sprague-Dawley Rats. *Front. Physiol.* 10:01275. doi: 10.3389/fphys.2019.01275

Yong, F. L., Law, C. W., and Wang, C. W. (2013). Potentiality of a triple microRNA classifier: MiR-193a-3p, miR-23a and miR-338-5p for early detection of colorectal cancer. *BMC Cancer* 13:280. doi: 10.1186/1471-2407-13-280

Yoshikawa, M., Iinuma, H., Umemoto, Y., Yanagisawa, T., Matsumoto, A., and Jinno, H. (2018). Exosome-encapsulated microRNA-223-3p as a minimally invasive biomarker for the early detection of invasive breast cancer. *Oncol. Lett.* 15, 9584–9592. doi: 10.3892/ol.2018.8457

Yu, F., Lu, Z., Chen, B., Dong, P., and Zheng, J. (2015). microRNA-150: A promising novel biomarker for hepatitis B virus-related hepatocellular carcinoma. *Diagnost. Pathol.* 10:129. doi: 10.1186/s13000-015-0369-y

Zhang, Y., Huang, F., Wang, J., Peng, L., and Luo, H. (2015). MiR-15b mediates liver cancer cells proliferation through targeting BCL-2. *Int. J. Clin. Exp. Pathol.* 8, 15677–15683.

Zheng, H., Li, W., Wang, Y., Xie, T., Cai, Y., Wang, Z., et al. (2014). miR-23a inhibits E-cadherin expression and is regulated by AP-1 and NFAT4 complex during Fas-induced EMT in gastrointestinal cancer. *Carcinogenesis* 2014:bgt274. doi: 10.1093/carcin/bgt274

Zhu, C., Ren, C., Han, J., Ding, Y., Du, J., Dai, N., et al. (2014). A five-microRNA panel in plasma was identified as potential biomarker for early detection of gastric cancer. *Br. J. Cancer* 110, 2291–2299. doi: 10.1038/bjc.2014.119

Zhu, L. H., Liu, T., Tang, H., Tian, R. Q., Su, C., Liu, M., et al. (2010). MicroRNA-23a promotes the growth of gastric adenocarcinoma cell line MGC803 and downregulates interleukin-6 receptor. *FEBS J.* 277, 3726–3734. doi: 10.1111/j.1742-4658.2010.07773.x

Conflict of Interest: The authors declare that the research was conducted in the absence of any commercial or financial relationships that could be construed as a potential conflict of interest.

Publisher's Note: All claims expressed in this article are solely those of the authors and do not necessarily represent those of their affiliated organizations, or those of the publisher, the editors and the reviewers. Any product that may be evaluated in this article, or claim that may be made by its manufacturer, is not guaranteed or endorsed by the publisher.

Copyright © 2021 Garai, Adam, Herczeg, Banfai, Gyebrovszki, Gyenesei, Pongracz, Wilhelm and Kvell. This is an open-access article distributed under the terms of the Creative Commons Attribution License (CC BY). The use, distribution or reproduction in other forums is permitted, provided the original author(s) and the copyright owner(s) are credited and that the original publication in this journal is cited, in accordance with accepted academic practice. No use, distribution or reproduction is permitted which does not comply with these terms.